N°d'ordre NNT : xxx

PHD THESIS of the UNIVERSITY OF LYON

Jointly awarded at:
INSA of Lyon
Ecole Doctorale N° 162
Mécanique, Energétique, Génie Civil, Acoustique (MEGA)
Spécialité : Mécanique

And at:
"La Sapienza" University of Rome
Dottorato di ricerca in Meccanica Teorica e Applicatta XXXI ciclo

Publicly defended on the 10/12/2018, by:

Multiscale poroelastic modeling of bone

PROVISIONARY VERSION

In front of the PhD commitee composed of:

CHABRAND Patrick	Professeur	Université Aix-Marseille	Reviewer
SANSALONE Vittorio	Professeur	Université Paris-Est	Reviewer
CICONE Traian	Profesorul	Universitatea Politehnica Bucureşti	Examiner
MEZIANE Anissa	Maître de Conférences	Université de Bordeaux	Examiner
BOU-SAÏD Benyebka	Professeur	INSA-LYON	PhD director
MASSI Francesco	Professore Associato	Università di Roma "La Sapienza"	PhD director

Département FEDORA – INSA Lyon - Ecoles Doctorales – Quinquennal 2016-2020

SIGLE	ECOLE DOCTORALE	NOM ET COORDONNEES DU RESPONSABLE
CHIMIE	**CHIMIE DE LYON** http://www.edchimie-lyon.fr Sec. : Renée EL MELHEM Bât. Blaise PASCAL, 3e étage secretariat@edchimie-lyon.fr INSA : R. GOURDON	M. Stéphane DANIELE Institut de recherches sur la catalyse et l'environnement de Lyon IRCELYON-UMR 5256 Équipe CDFA 2 Avenue Albert EINSTEIN 69 626 Villeurbanne CEDEX directeur@edchimie-lyon.fr
E.E.A.	**ÉLECTRONIQUE, ÉLECTROTECHNIQUE, AUTOMATIQUE** http://edeea.ec-lyon.fr Sec. : M.C. HAVGOUDOUKIAN ecole-doctorale.eea@ec-lyon.fr	M. Gérard SCORLETTI École Centrale de Lyon 36 Avenue Guy DE COLLONGUE 69 134 Écully Tél : 04.72.18.60.97 Fax 04.78.43.37.17 gerard.scorletti@ec-lyon.fr
E2M2	**ÉVOLUTION, ÉCOSYSTÈME, MICROBIOLOGIE, MODÉLISATION** http://e2m2.universite-lyon.fr Sec. : Sylvie ROBERJOT Bât. Atrium, UCB Lyon 1 Tél : 04.72.44.83.62 INSA : H. CHARLES secretariat.e2m2@univ-lyon1.fr	M. Philippe NORMAND UMR 5557 Lab. d'Ecologie Microbienne Université Claude Bernard Lyon 1 Bâtiment Mendel 43, boulevard du 11 Novembre 1918 69 622 Villeurbanne CEDEX philippe.normand@univ-lyon1.fr
EDISS	**INTERDISCIPLINAIRE SCIENCES-SANTÉ** http://www.ediss-lyon.fr Sec. : Sylvie ROBERJOT Bât. Atrium, UCB Lyon 1 Tél : 04.72.44.83.62 INSA : M. LAGARDE secretariat.ediss@univ-lyon1.fr	Mme Emmanuelle CANET-SOULAS INSERM U1060, CarMeN lab, Univ. Lyon 1 Bâtiment IMBL 11 Avenue Jean CAPELLE INSA de Lyon 69 621 Villeurbanne Tél : 04.72.68.49.09 Fax : 04.72.68.49.16 emmanuelle.canet@univ-lyon1.fr
INFOMATHS	**INFORMATIQUE ET MATHÉMATIQUES** http://edinfomaths.universite-lyon.fr Sec. : Renée EL MELHEM Bât. Blaise PASCAL, 3e étage Tél : 04.72.43.80.46 Fax : 04.72.43.16.87 infomaths@univ-lyon1.fr	M. Luca ZAMBONI Bât. Braconnier 43 Boulevard du 11 novembre 1918 69 622 Villeurbanne CEDEX Tél : 04.26.23.45.52 zamboni@maths.univ-lyon1.fr
Matériaux	**MATÉRIAUX DE LYON** http://ed34.universite-lyon.fr Sec. : Marion COMBE Tél : 04.72.43.71.70 Fax : 04.72.43.87.12 Bât. Direction ed.materiaux@insa-lyon.fr	M. Jean-Yves BUFFIÈRE INSA de Lyon MATEIS - Bât. Saint-Exupéry 7 Avenue Jean CAPELLE 69 621 Villeurbanne CEDEX Tél : 04.72.43.71.70 Fax : 04.72.43.85.28 jean-yves.buffiere@insa-lyon.fr
MEGA	**MÉCANIQUE, ÉNERGÉTIQUE, GÉNIE CIVIL, ACOUSTIQUE** http://edmega.universite-lyon.fr Sec. : Marion COMBE Tél : 04.72.43.71.70 Fax : 04.72.43.87.12 Bât. Direction mega@insa-lyon.fr	M. Jocelyn BONJOUR INSA de Lyon Laboratoire CETHIL Bâtiment Sadi-Carnot 9, rue de la Physique 69 621 Villeurbanne CEDEX jocelyn.bonjour@insa-lyon.fr
ScSo	**ScSo*** http://ed483.univ-lyon2.fr Sec. : Viviane POLSINELLI Brigitte DUBOIS INSA : J.Y. TOUSSAINT Tél : 04.78.69.72.76 viviane.polsinelli@univ-lyon2.fr	M. Christian MONTES Université Lyon 2 86 Rue Pasteur 69 365 Lyon CEDEX 07 christian.montes@univ-lyon2.fr

*ScSo : Histoire, Géographie, Aménagement, Urbanisme, Archéologie, Science politique, Sociologie, Anthropologie

CONVENZIONE PER UNA CO-TUTELA DI TESI DI DOTTORATO DI RICERCA

L'Università degli Studi di Roma "La Sapienza" con sede in Roma (Italia), Piazzale Aldo Moro, 5 rappresentata dal Rettore Prof. Eugenio GAUDIO, che opera in virtù dei poteri che gli sono conferiti, da una parte

e

L'INSA di Lione rappresentata dal Direttore Eric MAURINCOMME, direttore dello stabilimento, che opera in virtù dei poteri che gli sono conferiti, dall'altra parte

Per la parte italiana:
- VISTA la Legge 210 del 3 luglio 1998 art. 4 – dottorato di ricerca;
- VISTO il D.M. 224/99 recante norme in materia di dottorato di ricerca
- VISTO il D.M. 509/99 recante norme concernenti l'autonomia didattica degli Atenei;
- VISTO il Regolamento di Ateneo in materia di dottorato di ricerca;
- VISTA la delibera del Senato Accademico del 2 ottobre 2003;

e

Visti, per la parte francese,
- La delibera del 6 gennaio 2005 relativo alla procedura internazionale per la cotutela di tesi (Francia);
- La delibera del 7 agosto 2006 relativo al dottorato (Francia);
- La convenzione franco-italiana tra la Conférence des Présidents d'Université (CPU) e la Conferenza dei Rettori delle Università Italiane (CRUI) sul riconoscimento dei diplomi e della validità dei titoli universitari siglata in data 18 gennaio 1996;
- La convenzione franco-italiana tra la Conférence des Présidents d'Université (CPU) e la Conferenza dei Rettori delle Università Italiane (CRUI) sulla cotutela di tesi siglata li 13 febbraio 1998;

nell'intento di contribuire ad instaurare e/o sviluppare la cooperazione scientifica tra équipe di ricerca italiana e straniere attraverso la mobilità dei dottorandi

convengono e stipulano quanto segue

Parte prima – Modalità amministrative

Art. 1 – L'Università degli Studi di Roma "La Sapienza" e L'INSA di Lione denominati qui di seguito "Istituzioni" concordano, nel rispetto delle leggi e dei regolamenti in vigore in ciascun Paese e/o Istituzione, di organizzare congiuntamente una co-tutela di tesi di dottorato a beneficio del dottorando sottoindicato:
nome e cognome: Eléonore PERRIN
iscritto al corso di Dottorato di Ricerca in Meccanica Teorica e Applicata presso l'Università La Sapienza di Roma e in "Mecanique" presso l' "ecole doctorale MEGA".
Soggetto di tesi: **Sviluppo di modelli multiscala per rimodellamento osseo.**

L'obiettivo del progetto di tesi di dottorato è quello di sviluppare modelli multi-scala delle diverse fasi di rimodellamento osseo; i modelli saranno alimentati dai dati sperimentali sulle proprietà meccaniche degli elementi presenti. Tali esperimenti saranno eseguiti al LaMCoS

dell'INSA di Lione. Questi modelli multi-scala dovranno essere in grado di riprodurre fenomeni locali di meccano-trasduzione e tradurli in informazioni di tipo globale per un approccio di omogeneizzazione. Anche la scala temporale ha una importanza fondamentale in questo contesto, ed i modelli selezionati dovranno essere pertinenti. Particolare attenzione sarà rivolta alla ricerca di parametri critici di rimodellamento osseo che favoriscano l'emergere del fenomeno di "squeaking".

A termine, il modello virtuale verrà validato attraverso confronti clinici e potrà essere messo a disposizione di medici su una piattaforma digitale dedicata che permetterà, da una radiografia o risonanza magnetica di un paziente, di eseguire analisi personalizzate, aiutandoli nella diagnostica.

I principi e le modalità amministrative e didattiche di tale co-tutela sono definiti dalla presente convenzione.

Art.2 - La durata per la preparazione della tesi è di 3 anni, a partire dall'anno accademico 2015/2016.

Art.3 - La preparazione della tesi si effettuerà in periodi alterni, pressoché equivalenti, in ciascuna delle due Istituzioni. La durata di tali periodi sarà fissata in comune accordo dai due Direttori di tesi.

Art.4 – Il dott.ssa Eléonore PERRIN sarà iscritta in entrambe le Istituzioni. Corrisponderà i regolari diritti di iscrizione all'INSA di Lione e sarà esonerato dal pagamento delle tasse presso l' Università "La Sapienza" di Roma, presso cui corrisponderà annualmente solo i diritti di segreteria.

Art.5 - Per tutto il periodo di preparazione della tesi il dott. Eléonore PERRIN beneficerà di quanto disposto dalla delibera del 7 Agosto 2006 e della carta dei tesisti de l'INSA de Lyon.

Art.6 - Per la durata della sua iscrizione, il dott. Eléonore PERRIN dovrà fornire giustificazione relativamente alle sue risorse, alla sua copertura sanitaria così come alla sua assicurazione sugli incidenti di lavoro, in ognuno dei paesi.

Parte seconda – Modalità didattiche

Art.1 – Il dott. preparerà la tesi sotto la direzione comune dei professori:
- Benyebka BOU-SAID (Docente presso il Laboratorio di Meccanica dei Contatti e delle Strutture), direttore di tesi all'INSA di Lione
- Francesco MASSI (Docente presso il Dipartimento di Ingegneria Meccanica e Aerospaziale), direttore di tesi a l'Università di Roma "La Sapienza")

che si impegnano ad esercitare pienamente la funzione di tutori del dottorando e si impegnano a valutarne, ciascuno con propria relazione scritta, la tesi di Dottorato.

Il giudizio positivo di entrambi i Direttori di Tesi è condizione necessaria per l'ammissione all'esame finale.

Art. 2 - La discussione della tesi, unica e riconosciuta dalle due istituzioni, avrà luogo presso l'INSA di Lione. La Commissione giudicatrice, nominata dai Rettori delle due Università, sarà composta da un numero pari di studiosi appartenenti alle due Istituzioni e designati congiuntamente da esse, oltre a membri esterni alle due Istituzioni. Essa dovrà essere

composta da un minimo di quattro membri ed un massimo di otto, appartenenti ai settori scientifico-disciplinari del Dottorato, tra cui, a meno di derogazioni, i due direttori di tesi.

Art. 3 – La tesi sarà redatta e discussa in inglese; un riassunto sostanziale sarà redatto ·in lingua francese ed in lingua italiana.

Art. 4 – Ognuna delle due Istituzioni si impegna a conferire il titolo di dottore di ricerca per la stessa tesi, in seguito ad una relazione favorevole della Commissione giudicatrice.
L'Università degli Studi di Roma "La Sapienza" conferirà il titolo di dottore di ricerca in Meccanica Teorica e Applicata.
L'INSA di Lione conferirà il titolo di dottore di ricerca in Meccanica.

Art. 5- In caso il dottorando dovesse convalidare le formazioni complementari (scientifiche o mirate alla sua inserzione professionale), le Istituzioni (l'Ecole Doctorale MEGA pour l'INSA) specificheranno le modalità di riconoscimento reciproco di queste formazioni, in accordo con i direttori di tesi ed il dottorando.

Parte terza – Conclusione

Art. 1 – Il dottorando dovrà rispettare i regolamenti e le consuetudini dell'Istituzione ospitante.

Art. 2 – Le Istituzioni contraenti, attraverso l'intermediazione dei rispettivi direttori di tesi, si impegnano a comunicarsi rispettivamente tutte le informazioni e la documentazione utile per l'organizzazione della co-tutela di tesi oggetto della presente convenzione.

Art. 3 – Le modalità di presentazione, di deposito e riproduzione della tesi saranno effettuati in ogni paese secondo i regolamenti in vigore.
La protezione dell'oggetto della tesi, così come la pubblicazione, lo sfruttamento e la protezione dei risultati ottenuti con lo studio di ricerca del dottorando nelle Istituzioni contraenti saranno assoggettati alla normativa in vigore e assicurati conformemente alle procedure specifiche di ciascun Paese coinvolto nella co-tutela.
Qualora richiesto, le disposizioni relative alla protezione dei diritti di proprietà intellettuale potranno costituire oggetto di protocolli o documenti specifici.

Art. 4 – La presente convenzione entra in vigore dalla data di firma del rappresentante legale di ciascuna Istituzione contraente e sarà valida fino alla fine dell'anno accademico nel corso del quale la tesi o lo studio saranno discussi. Nel caso in cui il dottorando non fosse iscritto in una e/o l'altra delle Istituzioni contraenti, oppure rinunciasse per iscritto a proseguire, oppure, in virtù della decisione di almeno uno dei due direttori di tesi, non fosse autorizzato a proseguire la preparazione della tesi in co-tutela, le Istituzioni contraenti porranno fine, congiuntamente e senza ritardo, alle disposizioni del presente accordo.

Art. 5 – La presente convenzione è redatta in quattro esemplari originali, di cui due in lingua italiana e due in lingua francese, aventi valore legale.

Roma, li _____   Villeurbanne, li __ **03 DEC. 2013** __

Per il Rettore dell'Università   Per il Direttore dell'INSA de Lyon
di Roma "La Sapienza"   DR Marie Christine BAIETTO

Addetta alla Direzione della Ricerca
E degli Studi di Dottorato

Il Responsabile del Dottorato di Ricerca
Carlo Massimo CASCIOLA

Il Responsabile del Dottorato di Ricerca
Philippe BOISSE

Il Direttore del laboratorio
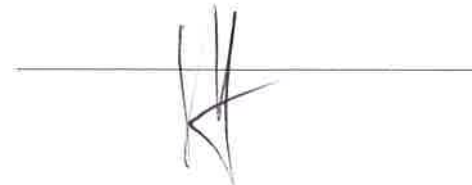David DUREISSEIX

·Co-direttore di tesi
Francesco MASSI

Co-direttore di tesi
Benyebka BOU-SAID

Il Dottorando
Eléonore PERRIN

ACCORD DE COOPÉRATION POUR LA MISE EN ŒUVRE D'UNE COTUTELLE DE THESE

L'Université de Rome "La Sapienza" ayant son siège à Rome (Italie), Piazzale Aldo Moro 5, représentée par son Recteur Professeur Eugenio GAUDIO agissant en-qualité et en vertu des pouvoirs qui lui sont conférés d'une part

ET

L'INSA de LYON, représenté par Monsieur Eric MAURINCOMME, Directeur de l'établissement, agissant en-qualités et en vertu des pouvoirs qui lui sont conférés, d'autre part

Pour la partie italienne :
-   Vue la Loi n. 210 du 3 juillet 1998 art. 4 – doctorat de recherche ;
-   Vu le D.M. 224/99 relatif aux normes en matière de doctorat de recherche ;
-   Vu le D.M. 509/99 relatif aux normes en matière d'autonomie didactique des Universités ;
-   Vu le Règlement de l'Université en matière de doctorat de recherche ;
-   Vue la délibération du Sénat Académique du 2 octobre 2003 ;

ET

Vu pour la part française :
-   L'arrêté du 6 janvier 2005 relatif à la procédure de cotutelle internationale de thèse (France);
-   L'arrêté du 7 août 2006 relatif aux études doctorales (France);
-   La convention cadre franco-italienne entre la Conférence des Présidents d'Université (CPU) et la Conferenza dei Rettori delle Università Italiane (CRUI) sur la reconnaissance des diplômes et validation des titres universitaires signée en date 18 janvier 1996;
-   La convention cadre franco-italienne entre la Conférence des Présidents d'Université (CPU) e la Conferenza dei Rettori delle Università Italiane (CRUI) sur la co-tutelle de thèse signée le 13 février 1998;

désireux (désireuses) de contribuer à l'instauration et/ou au développement de la coopération scientifique entre équipes de recherche italiennes et étrangères en favorisant la mobilité des doctorants

sont convenu(e)s des dispositions suivantes

Titre I – Modalités administratives

Art. 1 – L'Université de Rome "La Sapienza" et L'INSA de Lyon désignées ci-après "les établissements", décident dans le respect des lois et des règlements en vigueur dans chacun des pays et/ou établissements, d'organiser conjointement une cotutelle de thèse au bénéfice de l'étudiante désigné ci-après:
Prénom et nom : Eléonore PERRIN
Spécialité : Ingenieur Mecanique – Doctorat en Meccanica Teorica ed Applicata
Sujet de thèse : **Développement de modèles multi-échelles pour le remodelage osseux**

L'objectif de ce projet est de développer des modèles multi-échelles des différentes phases du remodelage osseux, modèles qui seront alimentés par des données expérimentales sur les

propriétés mécaniques des éléments en présence. Ces expérimentations seront effectuées au sein du LaMCoS. Ces modèles multi-échelles seront capables de capter les phénomènes locaux de mécano-transduction et de les transcrire en informations globales par une approche de type homogénéisation. L'échelle de temps dans ce contexte a aussi toute son importance et les modèles choisis devront être pertinents à cet effet. Une attention particulière sera portée sur la recherche des paramètres critiques du remodelage osseux favorisant l'apparition du phénomène de « squeaking ».

Ce modèle virtuel sera validé grâce à des confrontations cliniques et sera mis à disposition aux cliniciens sur une plateforme numérique dédiée, qui pourront à partir d'une radiographie ou IRM d'un patient, réaliser une analyse personnalisée, analyse qui pourra les aider dans leurs diagnostiques.

Les principes et les modalités administratives et pédagogiques de cette cotutelle sont définis par le présent accord.

Art. 2 - La durée prévue pour la préparation de la thèse en cotutelle est de 3 ans, à partir de l'année scolaire 2015/2016

Art. 3 - La préparation de la thèse s'effectue par périodes alternées, à peu près équivalentes, dans chacun des deux établissements partenaires. La durée de ces périodes sera déterminée de commun accord par les deux directeurs de thèse.

Art. 4 – L'étudiante Eléonore PERRIN est tenue à s'inscrire régulièrement dans les deux établissements. L'étudiante paiera les droits d'inscriptions à l'INSA de Lyon et en sera dispensée à l'Università La Sapienza di Roma, auprès de laquelle l'étudiante paiera annuellement uniquement les charges de secrétariat.

Art. 5 –Pour les périodes d'études effectuées en France et pour la soutenance, la doctorante bénéficie de l'ensemble des dispositions de l'arrêté du 7 août 2006 susvisé, et de la charte des thèses de l'INSA de Lyon.

Art.6 –Lors de son inscription, la doctorante devra fournir les justificatifs relatifs à ses ressources, à sa couverture sociale ainsi qu'à son assurance relative aux accidents du travail, dans chacun des pays.

Titre II – Modalités pédagogiques

Art. 1 – Le travail de thèse de l'étudiante sera réalisé sous la supervision commune de deux directeurs de thèse :
- Francesco MASSI (Professeur au Dipartimento di Ingegneria Meccanica e Aerospaziale), directeur de thèse à l'Université "La Sapienza" ;
- Benyebka BOU-SAID (Professeur au Laboratoire de Mécanique des Contacts et des Structures), directeur de thèse à l' INSA de Lyon ;

qui s'engagent à exercer pleinement la fonction de tuteurs de la candidate ainsi qu'à formuler chacun un avis écrit sur la thèse de Doctorat.

L'avis favorable des deux Directeurs de Thèse est une condition nécessaire à l'admission à l'examen final.

Art. 2- La thèse donnera lieu à une soutenance unique, reconnue par les deux établissements concernés. La soutenance aura lieu à l'INSA de Lyon. Le jury de soutenance est composé sur la base d'une proportion équilibrée de membres de chaque établissement désignés

conjointement par les établissements contractants et comprend, en outre, des personnalités extérieures à ces établissements.

Il comprendra au moins quatre membres et au maximum huit membres, dont, sauf dérogation, les deux directeurs de thèse.

Art. 3 - La thèse sera rédigée et discutée en Anglais. Elle comportera un résumé substantiel rédigé en Français et en Italien.

Art. 4 – En cas de rapport favorable du Jury, chacun des deux établissements s'engage à conférer le titre de docteur de recherche pour la même thèse.

L'Université de Rome "La Sapienza" s'engage à conférer le grade de docteur de recherche en en Meccanica Teorica e Applicata.

L'INSA de Lyon s'engage à conférer le grade de docteur de recherche en Mécanique.

Art. 5-Lorsque la doctorante doit valider des formations complémentaires (scientifiques ou visant à son insertion professionnelle), les établissements (l'Ecole Doctorale MEGA pour l'INSA) préciseront les modalités de reconnaissance mutuelle de ces formations, en accord avec les directeurs de thèse et la doctorante.

Titre III – Conclusions

Art. 1 – L'étudiante est tenue de respecter les règlements et les usages de l'établissement d'accueil.

Art. 2 – Par l'intermédiaire de leurs directeurs de thèses respectifs, les établissements signataires s'engagent à se communiquer toutes les informations et la documentation utiles à l'organisation de la cotutelle de thèse faisant l'objet du présent accord.

Art. 3 – Les modalités de présentation, de dépôt et de reproduction de la thèse seront établies dans chaque pays dans le respect de la réglementation en vigueur.

La protection du sujet de thèse, ainsi que la publication, l'exploitation et la protection des résultats issus des travaux de recherche du doctorant dans les deux établissements signataires seront assujetties à la réglementation en vigueur et assurées conformément aux procédures spécifiques à chacun des pays impliqués dans la cotutelle.

Sur demande, les dispositions concernant la protection des droits de propriété intellectuelle pourront faire l'objet de protocoles ou de documents spécifiques.

Art. 4 – Le présent accord entre en vigueur à partir de la date de signature du représentant légal de chaque établissement signataire et le reste jusqu'à la fin de l'année universitaire au cours de laquelle la thèse ou les travaux seront soutenus. Dans le cas où l'étudiante ne serait pas inscrite dans l'un et/ou l'autre des établissements signataires, ou bien renoncerait par écrit à poursuivre, ou bien n'est pas autorisée à poursuivre la préparation de sa thèse en vertu de la décision de l'un au moins des deux directeurs de thèse, les deux établissements signataires mettront fin conjointement et sans délai, aux dispositions du présent accord.

Art. 5 – Le présent accord est rédigé en quatre exemplaires originaux, dont deux en italien et deux en française, faisant également foi.

Roma, li _____   Villeurbanne, li _____ **0 3 DEC. 2013**

Pour le Recteur de l'Université   Pour le directeur de l'INSA de Lyon

La Sapienza de Rome

Il Coordinatore del Dottorato di Ricerca
Carlo Massimo CASCIOLA

Il Co-direttore di tesi
Francesco MASSI

La Doctorante
Eléonore PERRIN

DR Marie Christine BAIETTO
Directrice Adjoint de la Recherche
Et des Etudes Doctorales

Le Responsable de l'Ecole Doctorale
Philippe BOISSE

Le Directeur du laboratoire
David DUREISSEIX

Co-directeur (s) de thèse
Benyebka BOU-SAID

Abstract

Total Hip Arthroplasty is nowadays one of the most performed orthopedic surgery and is representing a major health and economic issue. Therefore, it is essential to provide a better understanding of bone mechanical behavior and its reaction to the implantation of a device such as a hip prosthesis. Numerical simulation can play a key role on this challenge, allowing for the reproduction, interpretation and analysis of the bone response to the external stimuli.

Bone is a complex material showing a hierarchical and porous structure, but also a natural ability to remodel itself thanks to specific cells, which are sensitive to fluid flows. Based on these characteristics, a multiscale numerical model has been developed within this thesis in order to simulate the bone response under external mechanical solicitations. The developed model relies on the homogenization technique for periodic structures based on an asymptotic expansion. It simulates cortical bone as a homogeneous structure. It is constituted of a porous microstructure with a 5% saturated with bone fluid, which, in the considered conditions, follows the Darcy's law.

The first application of the developed model is a case study, consisting in the loading of a finite volume of bone, allowing for the determination of an equivalent poroelastic stiffness. Focusing on two extreme fluid boundary conditions (impermeable walls and atmospheric pressure), the analysis of the corresponding structural response provides an overview of the fluid contribution to the poroelastic behavior, impacting the equiva-

lent stiffness of the considered material. This parameter is either reduced (when the fluid can flow out of the structure) or increased (when the fluid is kept inside the structure) and quantified through the developed model. To validate the developed model, both numerical and experimental validation are proposed. The numerical validation consists in the estimation of the model accuracy when varying parameters such as material properties or boundary conditions. Then, an experimental validation is set up in order to attest the reliability of the numerical model. As a reference case, a previous work on a cubic trabecular bone sample, extracted from a human hip and put under a compressive load, has been used. Increasing the load applied on the top of the bone specimen, the displacement is extracted, allowing the computation of the equivalent strain-stress curve. The equivalent stiffness of the bone specimen, calculated numerically by the developed numerical tool, is then compared with the one from the experiments. A good agreement between the curves attests the validity of the developed numerical model, accounting for both the solid matrix and fluid contributions.

The presented poroelastic numerical model, accounting for the bone fluid contribution, is here developed in the perspective of providing a bio-reliable model of bones, to determine the critical parameters that might impact bone remodeling. Towards the design and manufacturing of new generation of prosthesis, this bone model shows both accuracy and ease of computation, which will be required for its application as a preoperative or design tool.

Riassunto in italiano

L'artroplastica totale dell'anca rappresenta l'operazioni più praticata nel campo dell'ortopedia. Dato l'invecchiamento generale della popolazione e il progresso sia tecnico che medico, il numero di operazioni praticate annualmente tende ad aumentare. La ricerca di prospettive di miglioramento su questo argomento è quindi una questione socioeconomica importante.

L'interesse principale è garantire che i pazienti interessati ritornino ad una qualità della vita prevista da questo tipo di intervento. Ciò consiste nel limitare i rischi di allentamento della protesi (a causa di una scarsa integrazione dell'impianto nell'osso) e dei dolori associati, aumentando, se possibile, la durata delle protesi. Questo scopo è conseguito da due attori principali: il clinico, che si prende cura del paziente, dalla prima consultazione al seguito post-operatorio, e il produttore della protesi, che proporrà dispositivi biocompatibili che soddisfino i requisiti strutturali del corpo umano.

Tuttavia, l'osso è un materiale complesso, con molte caratteristiche che gli conferiscono eccezionali proprietà meccaniche. Ciò rende il suo studio impegnativo ed è al momento oggetto di molte ricerche. In particolare, un fattore di discussione è la risposta del tessuto osseo dopo l'inserimento dell'impianto, che è l'elemento che condizionerà la corretta evoluzione della rieducazione del paziente e quantificherà direttamente il successo dell'operazione. È quindi naturale che la sfida di questo progetto risieda in questa interfaccia tra medico e industriale, al fine proporre strumenti

numerici su cui tutte le parti possano fare affidamento.

È quindi necessario concentrarsi sulla ricostruzione ossea attorno all' impianto, come evidenziato da numerosi studi su questo argomento. È stato evidenziato in letteratura che questa ricostruzione avviene attraverso una ricca attività cellulare, naturalmente presente in tutte le ossa sane, che consente all'osso di ripararsi dopo una frattura: è il rimodellamento osseo. È anche noto che questa attività cellulare è principalmente condizionata dagli stress meccanici applicati all'osso. Tuttavia, non esiste attualmente alcun collegamento tra questo fenomeno biologico naturale e la risposta post-impianto dell'osso.

Il ruolo concreto che la protesi può svolgere, così come il modo in cui viene impiantata, deve essere analizzato. In definitiva, l'obiettivo della tesi è creare uno strumento numerico di previsione digitale per la ricostruzione ossea attorno a un impianto. L'approccio numerico sviluppato in questa tesi potrebbe essere usato come strumento per la progettazione di protesi nell'industria biomedica, nella scelta del suo design e del suo materiale, o come ausilio alla preparazione chirurgica durante lo studio clinico preoperatorio, in modo che il posizionamento del dispositivo sia completamente previsto per la ricostruzione ossea ottimizzata.

Inizialmente, per la scelta delle metodologie ed ipotesi di modellazione adeguate, particolare attenzione è stata rivolta all'intera problematica, sia nel funzionamento biologico e nella modellazione numerica delle ossa, che nei bisogni concreti dei produttori e medici. Il nostro posizionamento, all'interfaccia tra industria e clinica, richiede una conoscenza globale delle diverse problematiche presenti su entrambi i lati, per proporre un compromesso essenziale per un'applicabilità realistica, senza trascurare tuttavia elementi chiave.

Queste considerazioni sono alla base delle due nozioni su cui si basa il lavoro di ricerca qui presentato:

- L'aspetto multi-scala dell'osso e della sua ricostruzione: gli eventi che definiscono il rimodellamento osseo accadono su scala a livello cellulare (microscopica), mentre la scal di interesse per la modellazione è quello della protesi (macroscopica).

- Il rimodellamento osseo dipende principalmente dai movimenti dei

fluidi nelle porosità dell'osso, che attivano le cellule ossee.

Per tenere conto di questi criteri, che sono considerati i più importanti in base all'attuazione del progetto, viene sviluppato un modello numerico basato su queste principali ipotesi. Si è scelto di considerare l'osso come un materiale poroelastico, cioè composto da una matrice solida con comportamento elastico, all'interno del quale circola un fluido.

Per questo, è stato adottato un metodo di omogeneizzazione. Il suo interesse è di separare le eterogeneità della scala microscopica (qui i pori e flussi di fluido) e la scala macroscopica, in cui il materiale viene considerato omogeneo nonostante la sua particolare microstruttura. Attraverso una descrizione delle variabili di omogeneizzazione, che coinvolgono il rapporto di scala, il complesso problema meccanico è più facilmente modellabile. Tale approccio comporta anche uno studio specifico del flusso di fluido che è stato implementato, in modo che la sua inclusione nell'aspetto poroelastico sia la più biologicamente realistica.

L'algoritmo sviluppato, e implementato in un software di calcolo, è riassunto in 1.

Al fine di convalidare il modello numerico, uno studio in due fasi è stato proposto nella tesi.
Innanzitutto, una validazione numerica, per stimare la pertinenza dei primi risultati del modello sottoposto a diversi casi di simulazione, variando le proprietà materiali o le condizioni al contorno. I risultati ottenuti, in qualità di rigidezza equivalente (Fig. 2) e distribuzione di stress e pressione (Fig. 3 e Fig. 4) sono stati confrontati e discussi con un solido elastico equivalente, validando la corretta implementazione della modellazione multiscala.

In una seconda fase, il modello ha richiesto una validazione sperimentale per giudicare la pertinenza e la precisione dei risultati ottenuti. Ciò è stato possibile grazie ad una collaborazione con un gruppo di ricerca dell'università Sapienza di Roma, dove sono già stati condotti numerosi studi sperimentali sul comportamento meccanico dell'osso. Un campione di osso, estratto da un femore umano, è stato sottoposto ad una forza di compressione. La rigidezza equivalente sperimentale è stata ottenuta dalla curva sforzo-deformazione risultante dal test, che è stata poi con-

frontata con quella ottenuta numericamente (Fig. 5 e 6). Sembra che affinché i risultati siano coerenti, un particolare interesse deve essere posto sulla scelta delle proprietà del materiale che alimentano il modello. Questi possono essere difficili da determinare a seconda del tipo di osso, della sua posizione nello scheletro e in particolare della sua qualità. La nozione di qualità dell'osso è essenziale per determinare le proprietà meccaniche dell'osso ed è oggetto di molte ricerche con le tecniche dell' imaging medicale.

Mentre il progetto di tesi pone le basi per l'introduzione del rimodellamento osseo nel modello sviluppato e convalidato, le prospettive per rispondere al problema indicato in precedenza possono essere considerate in molte forme. Tra le differenti prospettive, sarebbe necessario essere in grado di stimare con precisione lo stress meccanico indotto dal chirurgo durante l'impianto o di valutare l'influenza dei parametri di impianto (orientamento, profondità della protesi) sulla ricostruzione ossea. L'obiettivo finale è quello di fornire un semplice strumento numerico, per l'analisi preoperatoria da parte del clinico, cosicché per ogni paziente ed il suo specifico scheletro ed identità ossea, sia possibile determinare la protesi più appropriata e lo scenario di impianto ottimale. Ciò limiterebbe il rischio di allentamento e aumenterebbe notevolmente le probabilità che il paziente riacquisti una qualità della vita ottimale, dimenticando la presenza della protesi nella sua vita quotidiana.
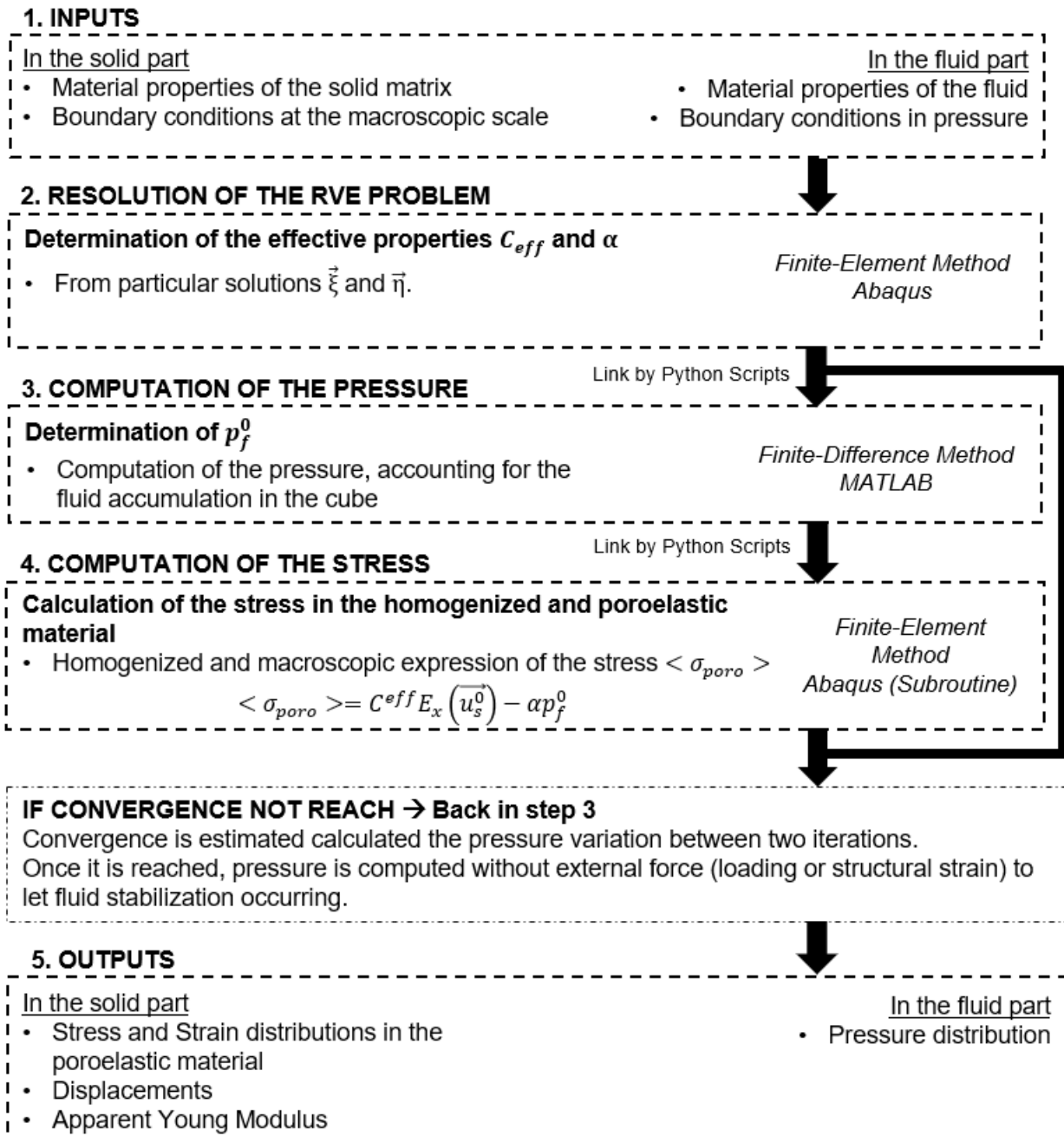
1. INPUTS

In the solid part
- Material properties of the solid matrix
- Boundary conditions at the macroscopic scale

In the fluid part
- Material properties of the fluid
- Boundary conditions in pressure

2. RESOLUTION OF THE RVE PROBLEM

Determination of the effective properties C_{eff} and α

- From particular solutions $\vec{\xi}$ and $\vec{\eta}$.

Finite-Element Method
Abaqus

Link by Python Scripts

3. COMPUTATION OF THE PRESSURE

Determination of p_f^0

- Computation of the pressure, accounting for the fluid accumulation in the cube

Finite-Difference Method
MATLAB

Link by Python Scripts

4. COMPUTATION OF THE STRESS

Calculation of the stress in the homogenized and poroelastic material

- Homogenized and macroscopic expression of the stress $< \sigma_{poro} >$

$$< \sigma_{poro} >= C^{eff} E_x \left(\vec{u_s^0} \right) - \alpha p_f^0$$

Finite-Element
Method
Abaqus (Subroutine)

IF CONVERGENCE NOT REACH → Back in step 3
Convergence is estimated calculated the pressure variation between two iterations.
Once it is reached, pressure is computed without external force (loading or structural strain) to let fluid stabilization occurring.

5. OUTPUTS

In the solid part
- Stress and Strain distributions in the poroelastic material
- Displacements
- Apparent Young Modulus

In the fluid part
- Pressure distribution

Figure 1: **Diagramma dell'algoritmo sviluppato per lo studio numerico multi-scala di un materiale poroelastico.**
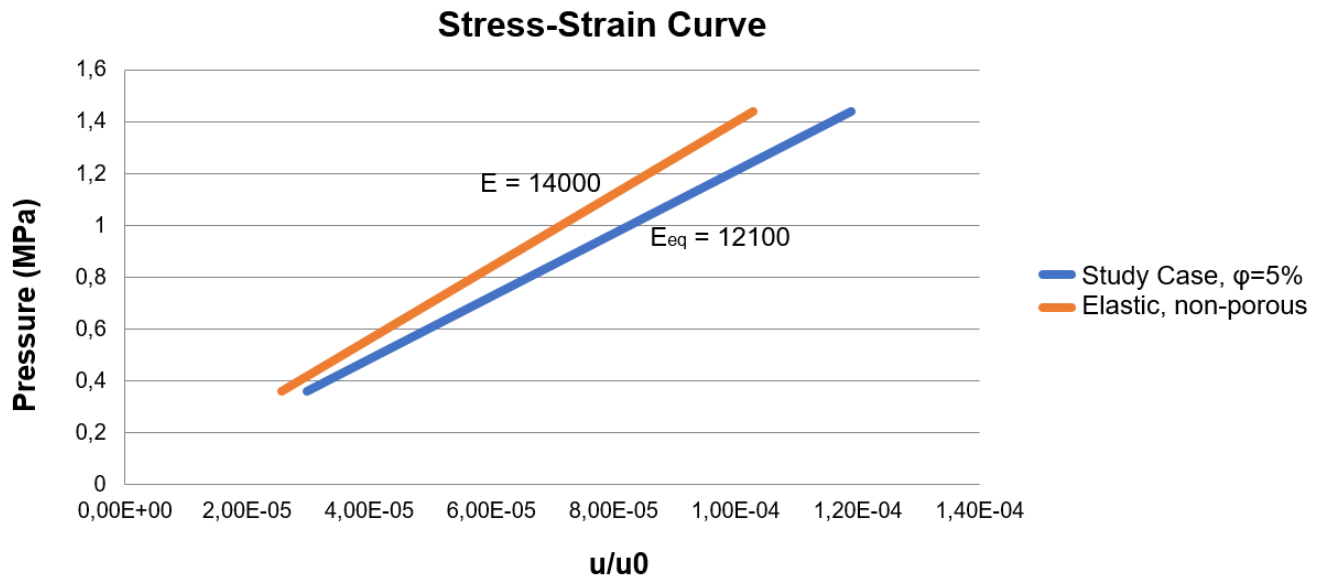
Figure 2: **Curva di sforzo-deformazione per il caso di studio (E è in MPa).**
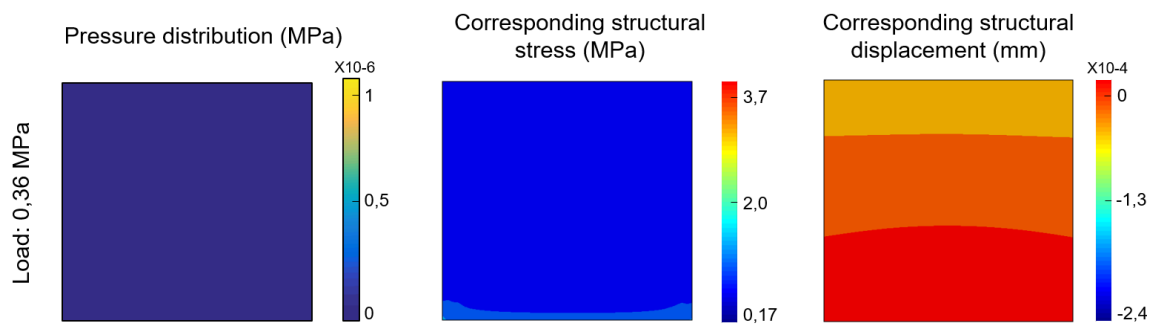
Figure 3: **Distribuzione della pressione (in MPa), corrispondente stress strutturale (in MPa) e corrispondente spostamento strutturale (mm) sotto una pressione di 0,36 MPa.**
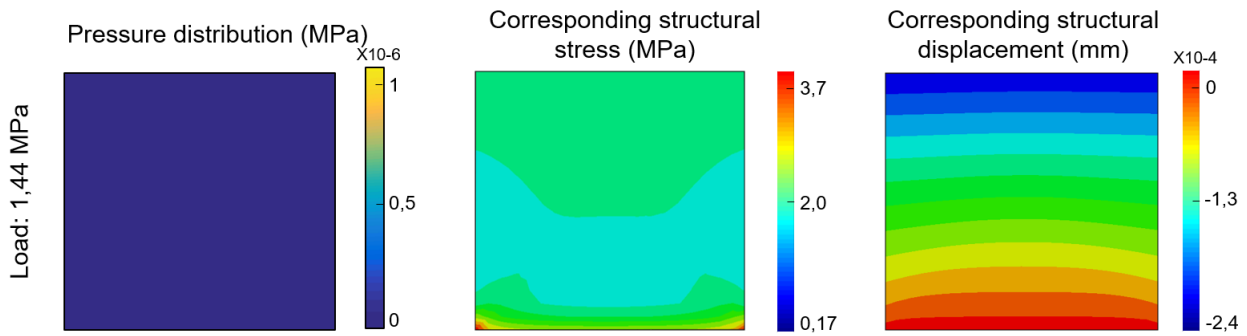
Figure 4: **Distribuzione della pressione (in MPa), corrispondente stress strutturale (in MPa) e corrispondente spostamento strutturale (mm) sotto una pressione di 1.44 MPa.**
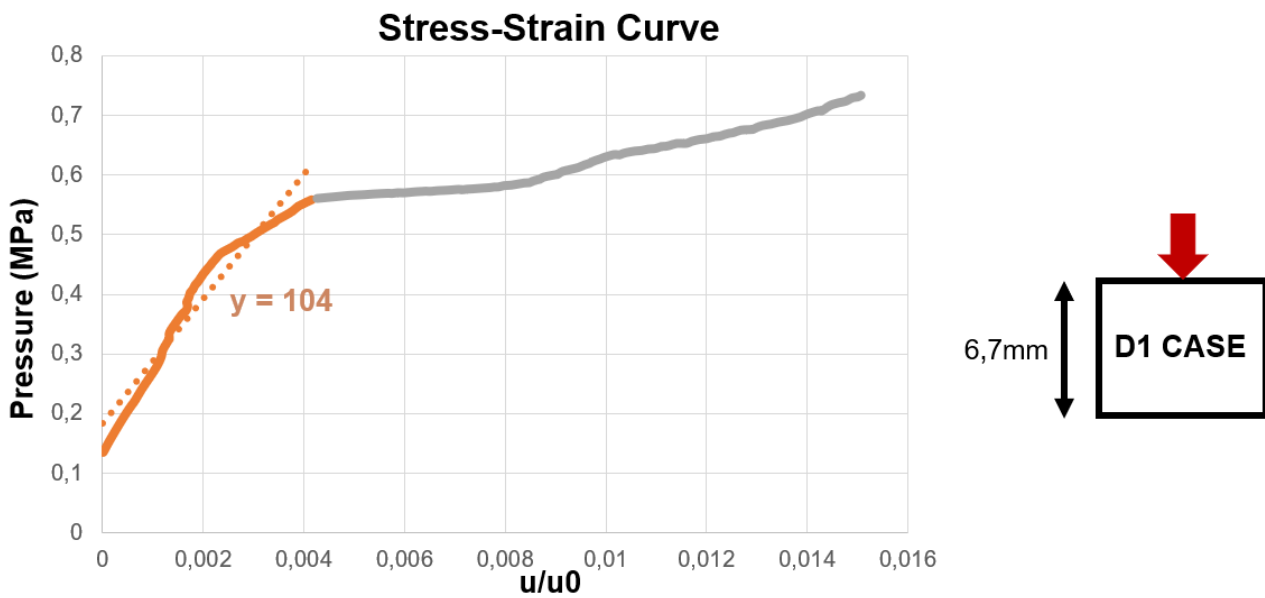
Figure 5: **Curva di sforzo-deformazione per il caso D1.**
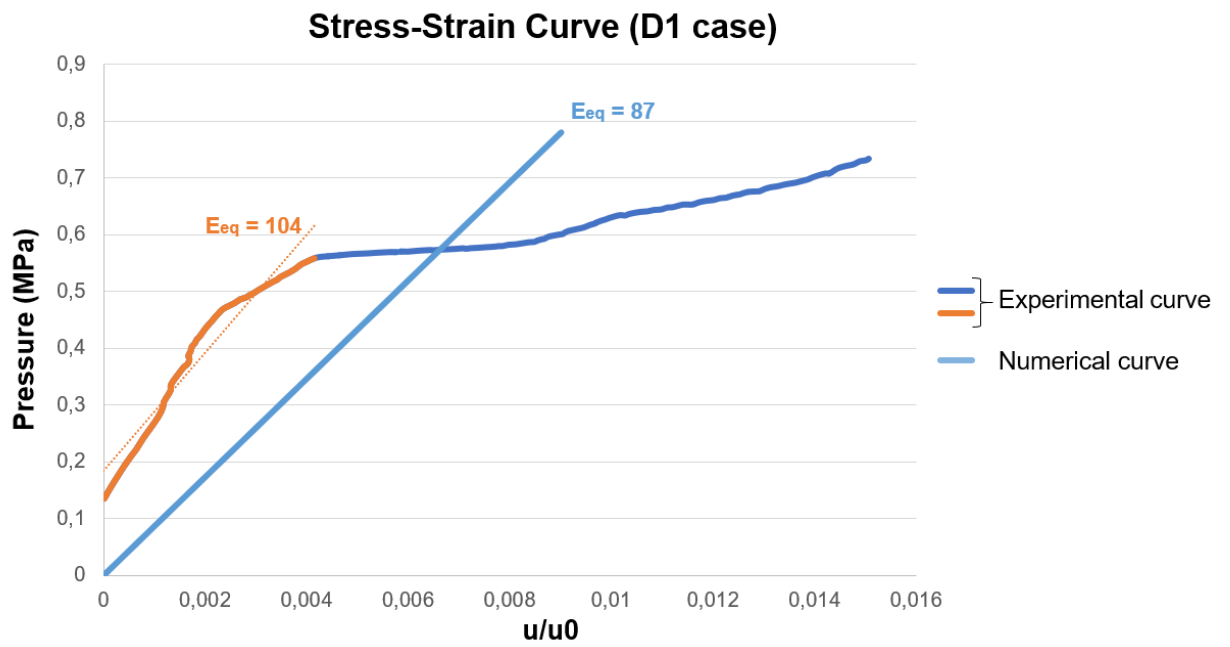
Figure 6: **Confronto delle curve di sforzo-deformazione per il caso D1.**

Résumé en français

Les poses de prothèse de hanche sont les opérations les plus pratiquée dans le domaine de l'orthopédie. Compte tenu du vieillissement global de la population et des progrès à la fois techniques et médicaux, ce nombre tend à augmenter. La recherche des perspectives d'amélioration sur ce sujet constitue donc un enjeu socio-économique majeur. L'intérêt capital est d'assurer aux patients concernés le retour à une qualité de vie attendue de ce type d'intervention. Cela consiste à limiter les risques de descellement de la prothèse (dus à une mauvaise intégration de l'implant dans l'os) et les douleurs associées, et augmenter si possible la durée de vie des prothèses. Cette démarche est conduite par deux acteurs principaux : le clinicien, qui va assurer la prise en charge du patient, de la première consultation jusqu'au suivi post-opératoire, et le fabricant de prothèse, qui va proposer des dispositifs biocompatibles répondant aux exigences structurelles du corps humain.

Or, l'os est un matériau complexe, avec de nombreuses caractéristiques qui lui confèrent des propriétés mécaniques hors du commun. Cela rend son étude exigeante et il est l'objet d'un grand nombre de recherches à l'heure actuelle. On peut notamment s'interroger sur la réponse du tissu osseux suite à l'insertion d'un implant, qui est l'élément qui va conditionner le bon déroulé de la rééducation du patient et directement quantifier le succès de l'opération. C'est donc naturellement que l'enjeu de ce projet de thèse se situe à cette interface entre clinicien et industriel, afin de rassembler les savoirs et de les synthétiser, et de proposer des outils

numériques sur lesquels toutes les parties peuvent s'appuyer.

Il est donc nécessaire de s'intéresser à la reconstruction osseuse autour de l'implant, comme en attestent les nombreuses études à ce sujet. Il a alors été mis en avant que cette reconstruction se fait par le biais d'une activité cellulaire riche, présente naturellement dans tous les os sains, qui permet à l'os de se réparer après une fracture : c'est le remodelage osseux. On sait également que cette activité cellulaire est principalement conditionnée par les sollicitations mécaniques appliquées à l'os.

Toutefois, il manque à l'heure actuelle un lien entre ce phénomène biologique naturel et la réaction post-implantation de l'os. Le rôle concret que peut jouer aussi bien la prothèse et la manière dont celle-ci est implantée est à estimer. A terme, le but de ce projet est de créer un outil de prédiction numérique de reconstruction osseuse autour d'un implant. Cet outil serait utilisable soit en tant qu'instrument lors de la conception de prothèse dans l'industrie biomédicale, dans le choix de son design et de son matériau ; soit en tant qu'aide à la préparation à la chirurgie lors de l'étude pré-opératoire du clinicien pour que le positionnement du dispositif soit pleinement anticipé pour reconstruction osseuse optimisée.

Dans un premier temps, un intérêt particulier a été porté à l'ensemble de la problématique aussi bien au niveau du fonctionnement biologique et de la modélisation numérique de l'os, que des besoins concrets des industriels et des cliniciens. Le positionnement des objectifs de cette thèse, à l'interface entre industrie et clinique, nécessite une connaissance globale des différents verrous présents de part et d'autre afin de proposer un compromis essentiel pour une applicabilité réaliste, sans pour autant négliger les éléments clés.

Ces considérations sont à la base des deux notions sur lesquelles repose le travail de recherche ici présenté :

- L'aspect multi-échelle de l'os et de sa reconstruction, dont les événements déterminants se passent à l'échelle cellulaire (microscopique) alors que notre échelle d'intérêt est celle de la prothèse (macroscopique).

- Le remodelage osseux est principalement tributaire des mouvements de fluides dans les porosités de l'os, qui vont activer les cellules osseuses.

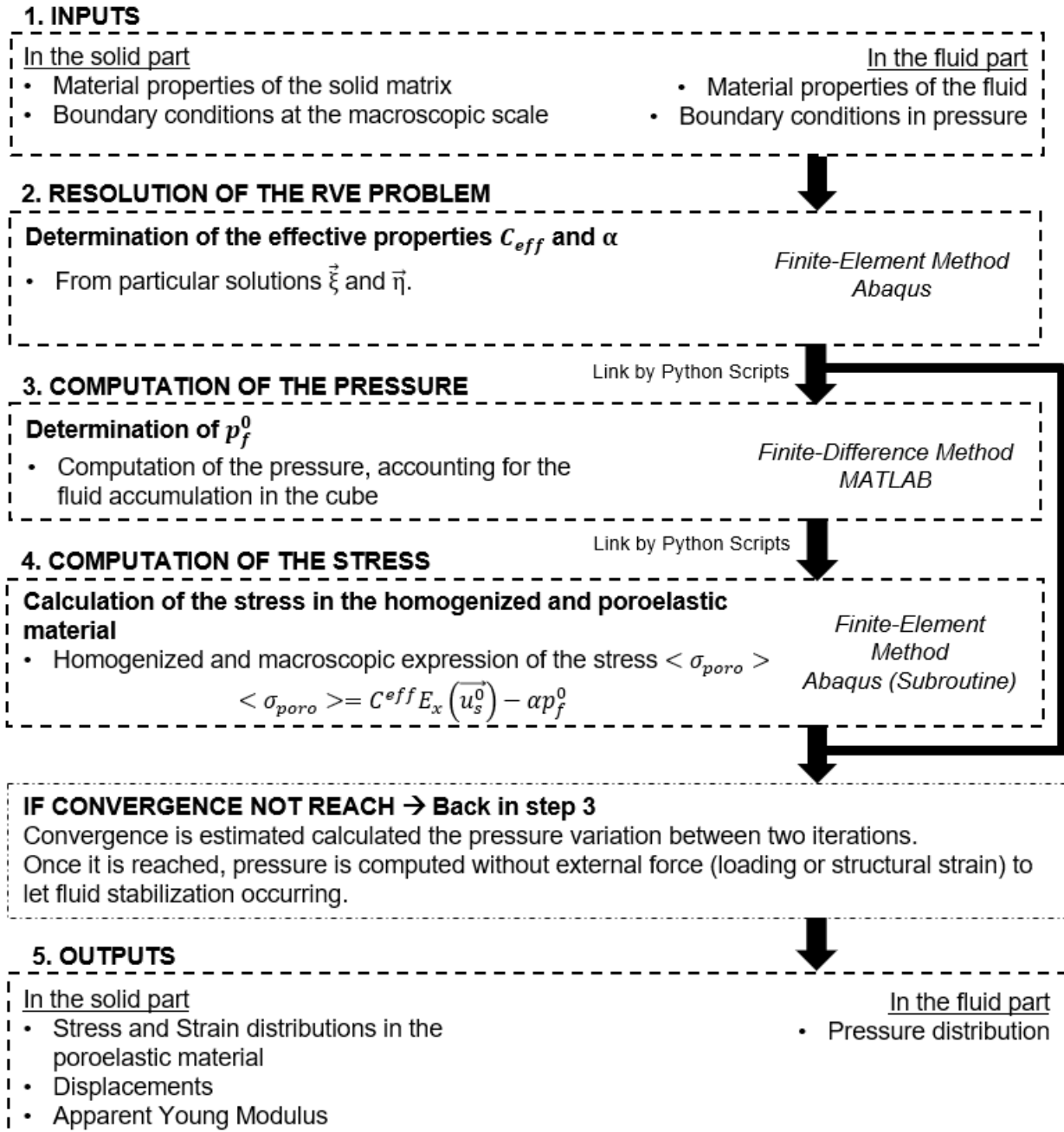L'algorithme développé et implémenté dans un logiciel de calcul est résumé dans la Figure 7.

1. INPUTS

In the solid part
- Material properties of the solid matrix
- Boundary conditions at the macroscopic scale

In the fluid part
- Material properties of the fluid
- Boundary conditions in pressure

2. RESOLUTION OF THE RVE PROBLEM

Determination of the effective properties C_{eff} and α

- From particular solutions $\vec{\xi}$ and $\vec{\eta}$.

Finite-Element Method
Abaqus

Link by Python Scripts

3. COMPUTATION OF THE PRESSURE

Determination of p_f^0

- Computation of the pressure, accounting for the fluid accumulation in the cube

Finite-Difference Method
MATLAB

Link by Python Scripts

4. COMPUTATION OF THE STRESS

Calculation of the stress in the homogenized and poroelastic material

- Homogenized and macroscopic expression of the stress $< \sigma_{poro} >$

$$< \sigma_{poro} >= C^{eff} E_x \left(\vec{u_s^0} \right) - \alpha p_f^0$$

Finite-Element Method
Abaqus (Subroutine)

IF CONVERGENCE NOT REACH → Back in step 3
Convergence is estimated calculated the pressure variation between two iterations.
Once it is reached, pressure is computed without external force (loading or structural strain) to let fluid stabilization occurring.

5. OUTPUTS

In the solid part
- Stress and Strain distributions in the poroelastic material
- Displacements
- Apparent Young Modulus

In the fluid part
- Pressure distribution

*Figure 7: **Diagramme de l'algorithme développé pour l'étude numérique de l'os comme un matériau multiéchelles et poroélastique.***

Afin de prendre en compte ces critères, que l'on estime les plus importants selon la mise en application du projet, un modèle numérique basé sur ces principales hypothèses a été développé. Le choix a été fait de considérer l'os comme un matériau poroélastique c'est-à-dire composé d'une matrice solide au comportement élastique, à l'intérieur de laquelle circule un fluide. Pour cela, une méthode d'homogénéisation est utilisée. Son intérêt est de séparer l'échelle des hétérogénéités (ici celle des pores et des écoulements de fluide) de l'échelle globale, à laquelle le matériau est considéré homogène malgré sa microstructure particulière. Au moyen d'une description des variables considérées faisant intervenir le rapport d'échelle, le problème mécanique complexe est plus facilement modélisable. Il implique par ailleurs une étude spécifique de l'écoulement du fluide qui a été mise en œuvre pour que sa prise en compte dans l'aspect poroélastique soit la plus réaliste biologiquement.

Dans le but de valider le modèle numérique, une étude en deux temps est proposée. Dans un premier temps, une validation numérique visant à estimer la pertinence des premiers résultats du modèle soumis à différents cas de simulation, variant en termes de propriétés matériaux ou des conditions aux limites. Les résultats obtenus, en tant que rigidité équivalente (Fig 8) et distribution des contraintes et des pressions (Fig. 9 et Fig. 10), ont été comparés et discutés avec un solide élastique équivalent, validant la mise en œuvre correcte de la modélisation multi-échelles.

Dans un deuxième temps, le modèle requiert également une validation expérimentale afin de juger de la pertinence et de la précision des résultats obtenus. Cela a pu être effectué par le biais d'une collaboration avec une équipe de recherches de La Sapienza (université basée à Rome), où a déjà été réalisé un certain nombre d'études expérimentales sur le comportement mécanique de l'os. Un échantillon d'os, extrait d'un fémur humain, est soumis à une force de compression. La rigidité équivalente expérimentale est obtenue à partir de la courbe contrainte-déformation issue de l'essai , qui est alors confrontée à celle obtenue numériquement (Fig. 11 et 12). Il apparaît que pour que les résultats concordent, un intérêt particulier doit être porté au choix des propriétés matériaux qui alimentent le modèle. Celles-ci peuvent être difficiles à déterminer selon le type d'os, sa localisation dans le squelette, et surtout sa qualité. La

Stress-Strain Curve

E = 14000

E_{eq} = 12100

Study Case, φ=5%
Elastic, non-porous

Pressure (MPa)

u/u0
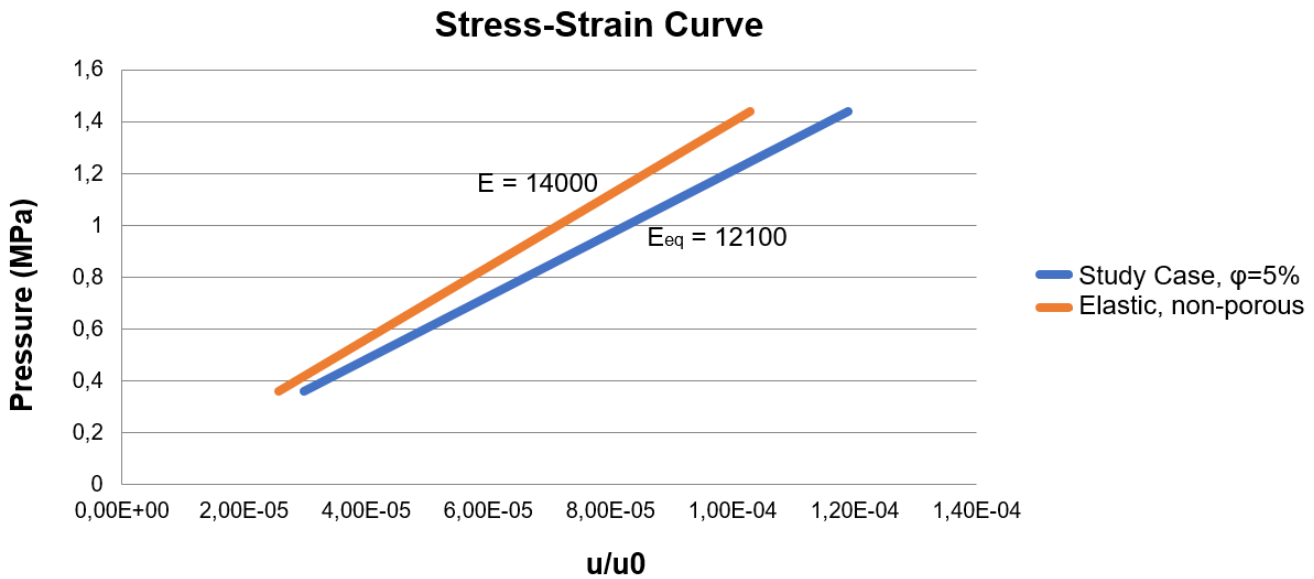
Figure 8: **Courbe contraintes-déformation pour le cas d'étude (E est en MPa).**

Pressure distribution (MPa)

Corresponding structural stress (MPa)

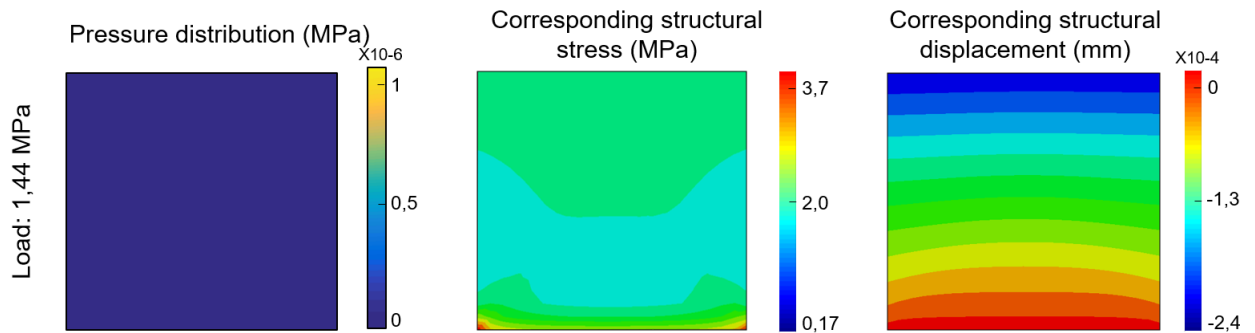Corresponding structural displacement (mm)

Load: 0,36 MPa
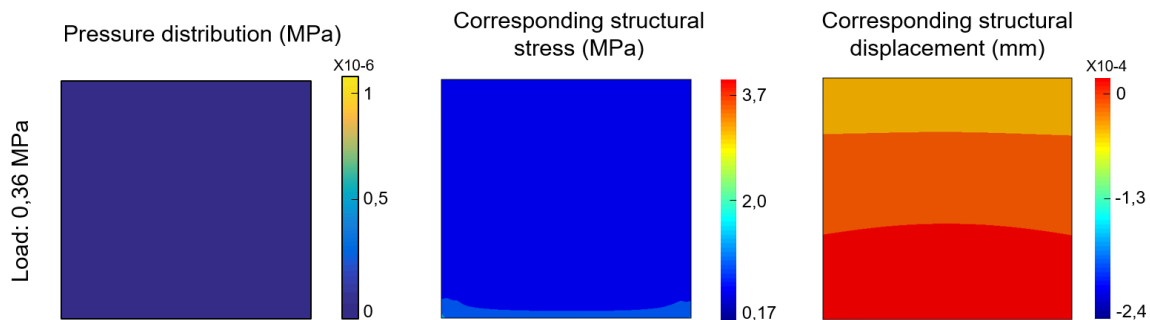
Figure 9: **Répartition de la pression (en MPa), de la contrainte de la structure correspondante (en MPa) et du déplacement de la structure (en mm), sous une pression de 0.36 MPa.**

notion de qualité osseuse est essentielle dans la détermination des propriétés mécaniques de l'os et sont l'objet de nombreuses recherches avec les techniques d'imagerie médicale.

Alors que le projet de thèse s'ouvre sur la perspective de l'introduction du remodelage osseux au modèle développé et validé, les perspectives pour répondre à la problématique énoncée plus tôt peuvent s'envisager sous de nombreuses formes. Il faudrait entre autres être en mesure d'estimer avec précision les sollicitations mécaniques induites par le clin-

Pressure distribution (MPa)

Corresponding structural stress (MPa)

Corresponding structural displacement (mm)

Load: 1,44 MPa

Figure 10: **Répartition de la pression (en MPa), de la contrainte de la structure correspondante (en MPa) et du déplacement de la structure (en mm), sous une pression de 1.44 MPa.**
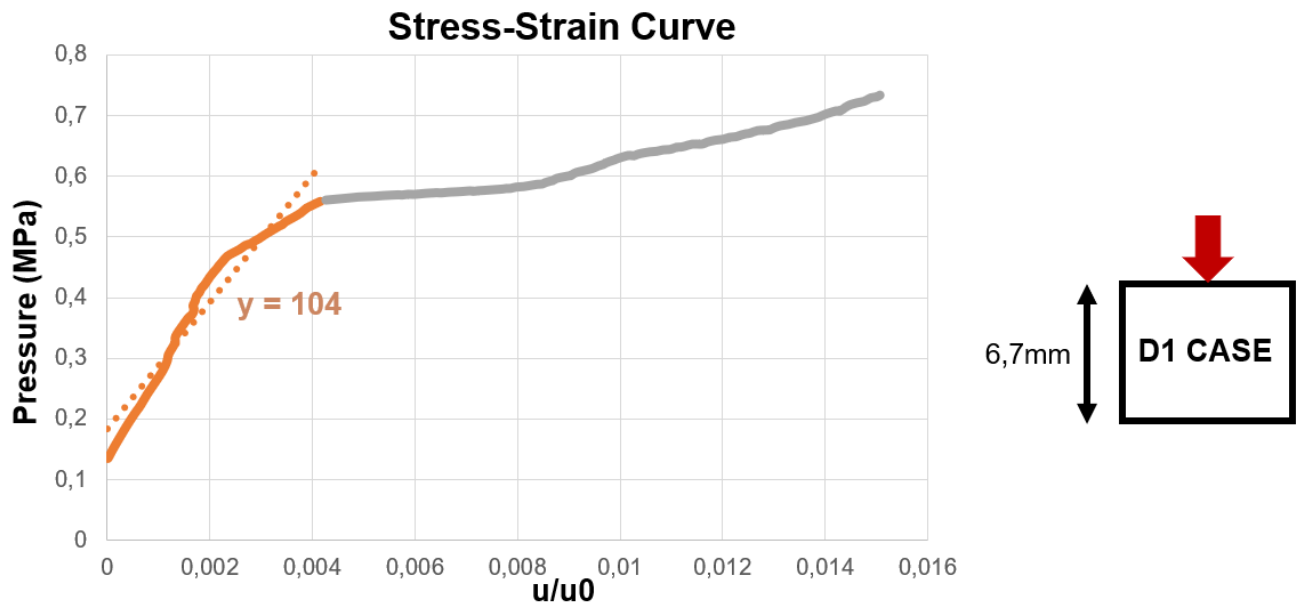
Figure 11: **Courbe de contraintes-déformation pour le cas D1.**

icien lors de l'implantation ou d'évaluer les paramètres d'implantation (orientation, profondeur de la prothèse) sur la reconstruction osseuse. L'objectif final est de fournir un outil numérique dont le principe est simple : pour chaque patient qui a un squelette unique et une identité osseuse spécifique, il est possible de déterminer la prothèse la plus adaptée et le scénario d'implantation optimale en analyse pré-opératoire par le clinicien. Cela limiterait les risques de descellement et augmenterait
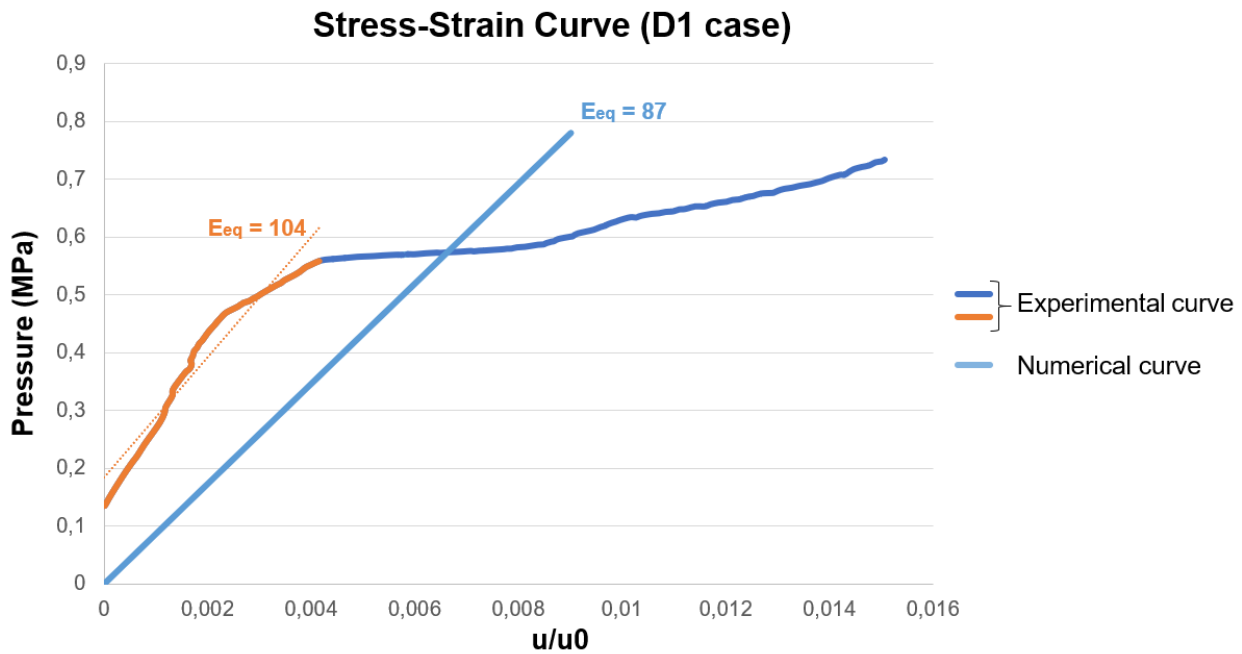
Figure 12: ***Courbe de contraintes-déformation pour le cas D1.***

considérablement les chances que le patient retrouve une certaine qualité de vie, en oubliant sa prothèse dans sa vie de tous les jours.

Contents

List of Figures

3

Nomenclature

α Biot effective stress coefficient tensor

δ Kronecker symbol

ϵ Scale ratio between the microscopic and the macroscopic scale

μ Fluid viscosity

μ_{eff} Effective viscosity parameter

∇ Gradient operator

∇_x Gradient operator for the macroscopic (also referred as global) scale

∇_y Gradient operator for the microscopic (also referred as local) scale

ν Poisson's coefficient

$\Omega_{f/s}$ Solid and fluid designation respectively

ϕ Porosity of the poroelastic material

$\rho_{f/s}$ Density of the fluid or the solid respectively

$\sigma_{f/s}$ Stress tensor in the fluid and in the solid respectively

$\vec{\eta}$ Microscopic solid displacement vector within the elementary cell (due to a unit value of the macroscopic strain tensor)

$\vec{\xi}$ Microscopic solid displacement vector within the elementary cell (due to a unit value of the fluid pressure

$\vec{u}_s$ Displacement in the solid part

$\vec{v}_f$ Fluid velocity

b Biot coefficient

C Elastic stiffness tensor

C_f Forchheimer coefficient

C_{eff} Effective elastic stiffness tensor

$D(\vec{v}_f)$ Strain tensor in the fluid part

E Young's Modulus

$E(\vec{u}_s)$ Strain tensor in the solid part

k Permeability coefficient

K_b Bulk modulus of the drained skeleton

K_f Bulk modulus of the fluid part

K_s Bulk modulus of the solid part

p_f Fluid pressure

Q Biot modulus

q Derivative of the expression for the fluid accumulation

General Introduction

Total Hip Arthroplasty consists in the replacement of the whole hip joint by a medical device. As this surgery is one of the most performed, with 120 000 implantations in France in 2015, and the number of implants is increasing with global life expectancy and improvement in devices, it appears that this orthopedic field centralizes several stakes.

The most obvious one is the care given to the patient that needs such a procedure. For this purpose, his physician has to be able to offer him the best care, consisting in an efficient surgical procedure to implant an appropriate device. The aim is to avoid any possible complications, such as implant loosening and the associated pain.

Therefore, the success of the surgery is attributed to the cooperation of two main actors: the surgeon, who is in charge of patient care from its first consultation to its post-operative follow-up, and the prosthesis manufacturer, who is expected to provide biocompatible devices able to meet the structural needs of the human body.

It is now well known that bone is a very complex material, with a large number of features that gives it exceptional mechanical characteristics. This makes its study as interesting as it is demanding, particularly when it is combined with another material, after the implantation of a prosthesis. This is a main problematic, which the physician and the prosthesis manufacturer need to work hand in hand, to provide each specific expertise which has to be complementary to ensure the best outcome for the patient.

Research in biomechanical engineering can develop the gathering of the knowledge of both parts involved, then synthesize them and to work on the development of numerical tools needed by each actor in the process. This is specifically the ambition of the project in which the work presented in this thesis is developed.

Specifically, the focus is addressed to the interaction between the bone and the prosthesis. Indeed, for instance, the development of additive manufacturing is revolutionizing the way in which prostheses are thought, designed and produced. Within this technic, a new generation of devices can be considered, designed for each patient and its specificities regarding to its bone structure and quality. This involves a thorough knowledge of bone tissue and its ability to remodel itself, specifically around a prosthesis. Indeed, bone is a living material that is able to adapt its structure according to the mechanical environment in which it is placed.

The work presented in this document aims to initiate and lay the foundation of a numerical approach of bone material modelling, to go toward a better understanding of the bone behavior after the mechanical and biological trauma caused by the implantation of a hip prosthesis.

The present document is organized within four chapters. In the first chapter, the biomedical context is settled. More precise information on the hip and the total replacement of the joint (called Total Hip Arthroplasty), needed in the treatment of some pathologies, is provided. All the elements involved in this procedure are described: the anatomical implication and bone specificities from both the biological and mechanical point of view; the prosthesis and its characteristics; and finally the procedure, its stakes and challenges and the possible negative outcomes that can be taken as improvement pathways. Once the framework is settled, a state-of-the-art is developed to define the positioning of this thesis, regarding to the literature and the specificities of the final aim of the research project. The complexity of the bone mechanical behavior is difficult to catch and to grasp in a numerical framework; therefore, a careful attention is put on the assumptions that are critical for the issue considered here. It appears that the porous aspect of bone and the fluid flow inside the pores play a determinant role in bone reconstruction and remodeling, especially the flow occurring at the cell scale. This led to the

formulation of the problem in the form of the development and the computation of a multiscale poroelastic model of bone material, through a homogenization technique.

These elements allowed to develop an algorithm to implement in the commercial softwares Abaqus and Matlab. The details of the different steps and how this algorithm has been built are presented in the third Chapter. All the blocks of the proposed algorithm are directly put in practice through a step-by-step presentation and a modelling of a simple case, corresponding to the numerical computation of a bone sample submitted to a compressive load.

In the end, once the numerical approach and algorithm presented, a validation of the model is proposed in two steps, which are presented in the fourth Chapter. The first consists on the computation of multiple cases, varying the inputs of the model and studying the consistency of the corresponding results. This step allowed for determining the accuracy and limitations of the developed algorithm, before proceeding to a confrontation with experimental results obtained on bone sample compressive tests.

Finally, as the whole algorithm has been developed and applied, on the bases of precise assumptions, several conclusions can be reached regarding the possible improvement of the presented work and, above all, the scope of the given outcomes.

Biomedical Context

This chapter aims to set the biomechanical framework of the thesis. It presents the societal issue in which the research project is settled and brings some background on the elements involved in the hip replacement as a surgical procedure, consisting in the implantation of a medical device in the body. Especially, understanding the biological events occurring at the interface during and after the implantation will allow for a correct formulation of the problem and for specifying the thesis positioning.

While the biomedical literature is condensed in this chapter, in order to positioning the work, the specific numerical and biomechanical literature contributions have been reported into each specific session, where the methodology and modelling choices have been settled down.

1.1 The Hip

1.1.1 The Hip Anatomy

After the knee, the hip is the second largest weight-bearing joint of the body, both in static (e.g. standing) and in dynamic (e.g. walking or running) loading conditions.

It links the pelvis and the thigh and involves the iliac bone and the femur, allowing the motion of the whole lower limb. It plays a significant role in the global posture and the human body posture.

The Joint.

From a mechanical point of view, it is a ball and socket joint. The rounded head of the femur (the thighbone) forms the ball, called femoral head, which articulates with the acetabulum (socket) (See Figure 1.1), giving a large range of mobility to the joint among three degrees of freedom (as seen on Figure 1.2):

- Flexion/Extension (or Anteversion/Retroversion)
- Abduction/Adduction
- Internal (or Medial)/External (or Lateral) rotation
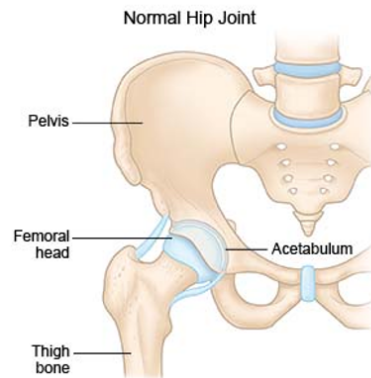
*Figure 1.1: **Anatomy of a hip [1].***

The bone surfaces of the two parts in contact are covered by a cartilage layer that contributes to accommodate the relative movement. The joint has a capsule structure made out of ligamentous tissue. Inside the capsule, the surfaces of the hip joint are covered by a thin tissue called the synovial membrane. This membrane nourishes and lubricates the joint with synovial fluid.
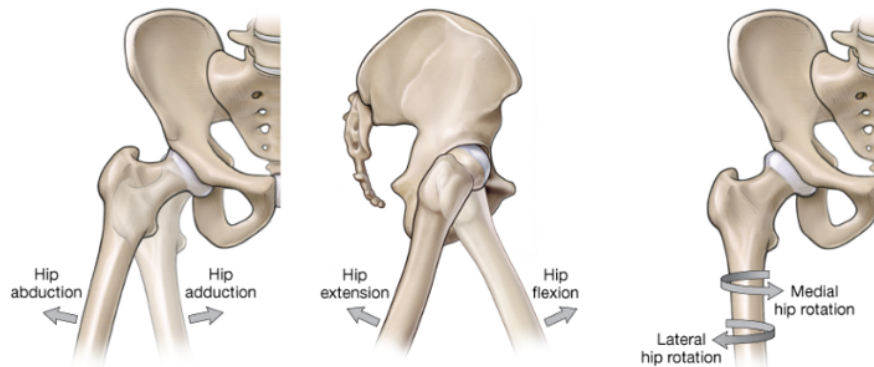
Figure 1.2: ***The degrees of freedom allowed by the hip joint [2].***

1.1.2 Morphological specificities

As everything in the human body, each individual presents its own unique specificities. Some aspects of the bones involved in the joint, as well as the global posture and kinematics of the body, can lead to slight or much larger deformities in the joint.

Unfortunately, those morphological specificities may affect the whole joint. From a certain level of severity, if not treated soon enough, the loading and functioning of the joint can induce damages, such as pain and loss of function. The deformities are attributed to patient specificities in bone geometry that cause compensatory loading in other parts, not shaped for this purpose, in order to keep a normal function.

In the hip joint, two main parameters can unbalance the whole joint: the angle between the femoral neck and shaft of the femur (called Femoral Neck Angle), or the inclination of the axis of the femoral shaft with respect to the femoral neck axis.

In the first case, the femurs are usually divided in three categories (see Figure 1.3):

- The standard femurs, with angles included between 120° and 135°.
- The "coxa valga" or "valgus" femurs, with angles superior to 135°.
- The "coxa vara" or "varus" femurs, with angles inferior to 120°.

In the second case, the angle refers as the torsion of the femur with respect to the body axis (see Figure 1.4). Three categories are also defined:
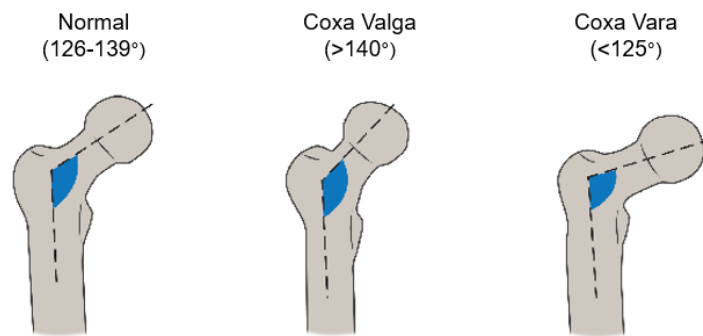
Figure 1.3: ***From left to right: an example of a standard femur, a coxa valga femur and a coxa vara femur [3].***

- Normal version is a forward (towards the front of the body), angle of 12-15 degrees.
- If the femoral neck is rotated too far forward it is an anteversion.
- If the femoral neck is rotated backward (toward the back of the body), it is a retroversion.
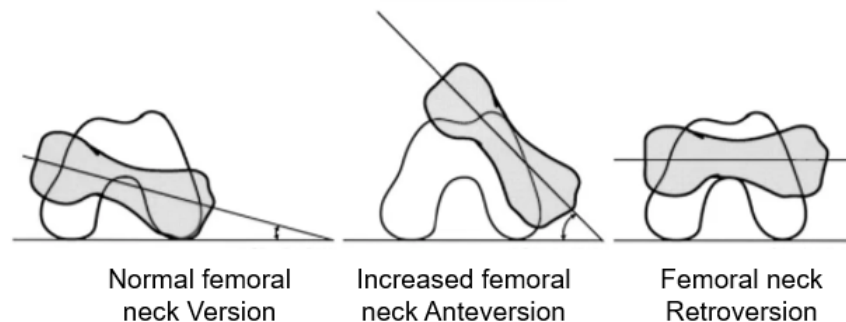
Figure 1.4: ***From left to right: an example of a standard version, an increased anteversion and a retroversion [4].***

In both cases, if not appropriately treated, the considered angles can create an imbalance in the hip joint and the articulation of the different structures. Therefore, irretrievable damages can occur on the surfaces in contact, especially on the cartilaginous layer, leading to arthritis [7].

1.1.3 Hip Pathologies

The sources of hip pain are numerous, and some of them imply the im- plantation of a medical device. The main ones are described in the following.

1.1.3.1 Arthritis

Arthritis is the main cause of hip pain and source of THA (Total Hip Arthroplasty). It consists in a cartilage deterioration until the cartilaginous layer disappears, leading to painful bone friction. Moreover, as the cartilage is a non-innervated tissue, arthritis is an asymptomatic disease, and no other option can be intended when hip pain appears. From then, as this process is irreversible, hip replacement is often the best option for the patient to regain quality of life.

This arthritis can have several forms:

- Osteoarthritis, which is age-related, occurring mainly in 50-year-old people and older, who may have a family history with arthritis or presenting a deformity as presented below. It represents over 70% of the hip replacements [8].
- Rheumatoid arthritis, an auto-immune disease in which the synovial mem- brane becomes inflamed and thickened.
- Post-traumatic arthritis that can follow a serious hip injury or fracture.

1.1.3.2 Hip avascular necrosis

Also called osteonecrosis or bone infarction, it consists in bone tissue cell death. This is due to a vascular occlusion or coagulation that inhibits blood sup- ply. It can be caused by old-age, alcoholism or trauma among many others possible causes. As bone tissue becomes necrotic, hip replacement is usually used in this case.

1.1.3.3 Osteoporosis

Osteoporosis is not specifically attributed to the hip, as it is a bone pathology that occur in every bone in the body. It is an excessive bone

resorption, which induces an increased bone weakness. The risk of broken bone is thus largely increased and it is the most common reason for a broken bone among the elderly, especially in the women population. As the hip accumulates a large number of load cycles, it is a common zone of rupture. In the context of a hip replacement, osteoporotic bone would require a specific treatment as it might not be strong enough to receive an external medical device.

For this specific cases and a large number of others, such as bone fracture or bone tumors, a hip replacement is required. This involves a surgical procedure that is called the Total Hip Arthroplasty.

1.1.4   The Total Hip Arthroplasty

1.1.4.1   Stakes

Total Hip Arthroplasty consists in the total replacement of the hip joint by an artificial device. This surgery is one of the most performed in the orthopedic field: in 2015, 120 000 implantations have been reported in France, with a 10% increase on the last 4 years [9]. This number is expected to continue its growth, as the global life expectancy is increasing and, as previously presented, numerous sources of hip pain are age-related.

Moreover, with the constant improvements in technical capabilities and surgical technics, the implanted population is also expanding, as younger and more active patients are now implanted [10], as well as older patients (more than 80 years-old), even when presenting other comorbidities. Therefore, the Total Hip Arthroplasty represents a major societal stake.

Furthermore, as the price of the procedure can reach 4500 euros, the economic impact is also substantial.

1.1.4.2   Challenges

Considering these numbers, this field is full of challenges from all the parts involved.

The biomedical industry, which is manufacturing the devices, leans on the recent technical progress and material research to provide competitive products: prosthesis coating is becoming a standard as it supposes to provide a better bone reaction, while additive manufacturing is revolutionizing the global prosthesis design and production.

In the hospital, in order to reduce patient hospital stay, Total Hip Arthroplasty are realized through ambulatory care. Combined to improvements in imaging technics, the pre-operation phase becomes much more thorough and precise. It allows the surgeon to have precious information of the patient bone geometry and bone quality, to anticipate what will happen in the operating room.

For the patient, a Total Hip Arthroplasty represents the chance to widely increase its quality of life: in the long term, the aim for him is to live as if he has two healthy hips. To reach this goal, the healing and post-operative care need to be optimized; at this aim, an efficient pre-operative planification is needed. The ideal for him would be to have a prosthesis especially designed for his needs and specifications to avoid complications.

All those elements lead to the introduction of patient-specific devices that an- swers all the actor expectancies. It would allow the prosthesis manufacturer to provide efficient tools, the physician to propose a secure and easier procedure and the patient decreases significantly the odds of bad outcomes. To go towards this concept, one needs to determine the key factors of the bone/prosthesis interaction, for the definition of the specifications of such devices. A correct modelling of the bone response to the introduction of the medical device is one of the actual challenges to reach such results.

1.2 Bone Material: generalities

In order to have a better understanding of the bone-prothesis system, first, let's focus on the bone material, that presents many complex aspects.

1.2.1 Bone functions

Bone is the structural element of the skeleton. It represents in average 15% of the total skeleton mass and plays an important role in the global functioning of the human body [11].

1.2.1.1 Mechanical functions

The most obvious ones are the mechanical functions, as it gives the structural resistance.
Bones are protecting important and delicate organs, as the skull is protecting the brain and the rib cage is protecting the heart and the lungs, thanks to its mechanical properties.

They are shaping the whole human body and are allowing to move in the 3D space via a system of skeletal muscles, tendons, ligaments and joints.

1.2.1.2 Synthetic function

Bone tissue has a synthetic function as it is the house of bone marrow. Bone marrow contains hematopoietic stem cells. Those cells are able to produce red blood cells, platelets and white blood cells, that then enter the circulation [12].

1.2.1.3 Metabolic functions

On top of that, bone plays the role of storage or several indispensable elements for the human body.

- Mineral storage as it is an important source of minerals such as calcium and phosphorus. Indeed, it contains 99% of the calcium present in the body and 90% of the phosphate [13, 14].

- Fat storage inside the yellow bone marrow.

Finally, bone balances essential quantities. It absorbs and release if needed alkaline salts to regulate pH, and balance calcium level forming and resorbing bone tissue.

All these essential functions are made possible through the specific and complex structure of bone, build on several levels.

1.2.2 Bone structure at different levels

The bone organization can be described within the study of four main scales: macroscopic (cm scale), mesoscopic (mm scale), microscopic (μm scale) and nanoscopic (nm scale). Each scale is the theater of multiple events, both biological and mechanical, whilst presenting specific structures.

1.2.2.1 Macroscopic scale

The human skeleton is made out of an average of 206 bones, connected to each other with tendons, muscles or cartilage. Depending on their position and main function, bone shapes can be considered as optimal structures and are very diversified.

Structural description.
Bones are usually classified in three categories [15]:

- Long bones, located in the limbs and thus having a particular kinematic. They consist of a shaft (diaphysis) with an expansion at each end (metaph- ysis). The diaphysis is a hollow tube, inside of which the medullary cavity contains the bone marrow.
- Short bones, presenting numerous articular faces.
- Flat bones, that have a dimension very smaller than others and mainly protective (for instance skull bones).
- Irregular bones for the bones left out of the previous categories.

Mechanical description.

From a mechanical point of view, bones need to have a sufficient mechanical resistance to be able to withstand everyday loading. It also has to keep enough elasticity not to break easily. This mainly depends on the primary function of the considered bone.

This mechanical feature is made possible thanks to a complex structure at smaller scale as it will be further described [16].

1.2.2.2   Mesoscopic scale

At this scale, we can distinguish two types of bone: cortical and trabecular bone, responsible for the peculiar mechanical behavior of bone.

Structural description.

- Cortical bone
  Also called compact bone, cortical bone can be found in the midshaft of long bones. The structural units of the cortical bone are the osteons, or haversian system. These are cylindrical structures (few millimeters long, around 0.2mm in diameter), aligned longitudinally along the main stress applied on the bone. They consist in a superposition of concentric layers, called lamellae. Their particular shape allows the bone's blood supplying through the central harversian canal.
  Cortical bone has a structural function: it is responsible for the strength of the whole. It also protects the inside components of bone: bone marrow and trabecular bone [17].

- Trabecular bone
  Also called cancellous bone, it differs from cortical bone especially in its low density and therefore stiffness. Cancellous bone is typically found at the end of long bones, proximal to joints and within the interior of the vertebrae. It has the particularity to contain red bone marrow, where hematopoiesis, the production of blood cells, occurs. As a structural point of view, it appears that cancellous bone is made

out of rods and plates, called trabeculae, forming a porous structure (80% of porosity [17, 18].

Mechanical description.

Those two bone types have large differences regarding the mechanical capacities.

Cortical bone, due to its structural and protective functions, contributes to the whole bone competence and fragility [19]. Even if technically anisotropic, cortical bone is often considered transversely isotropic. This is due to the fact that it is mainly stronger and stiffer, when loaded longitudinally along the diaphyseal axis compared to "transverse" direction [20].

Regarding the trabecular bone, it is less stiff thanks to its structural properties. It can absorb substantial energy on mechanical failure and gives to the bone its elasticity [20]. Anisotropic, it can be considered transversally isotropic because of the trabeculae alignment along the main mechanical solicitation axis, according to Wolff's law [19].

1.2.2.3 Microscopic scale

Knowing the structural units of cortical and trabecular bone, i.e. osteons and trabeculae, let's focus on their composition.

Structural description.

- Osteons

  Osteons are made out of concentric lamellae arranged around the central canal. Those lamellae are cylinder-shaped layers of calcified matrices. The central canal extends lengthwise through the center of each osteon and allows blood circulation, place for the innervation of bone tissue. We can also notice the lacunae, which are small spaces in bone matrix containing bone cells, tissue fluid and canaliculi. Canaliculi are ultra-small canals connecting the lacunae. Together, they constitute the lacuno-canalicular system, which plays an important role in mechanotransduction, as it will be further described.

- Trabeculae

  A trabecula is constituted of parallel lamellae oriented parallel to trabecular surfaces. Those lamellae have the same composition than osteons' lamellae and present similar lacunae and canaliculi.

Mechanical description.

At this scale, the mechanical description is directly related to the mineral content of bone tissue. Yet, the microscopic level is also the result of bone cells actions, since they are acting at the same scale. This involves major differences in trabecular and cortical bone, due to the different contents of bone cells. Furthermore, it implies the coexistence of different bone tissue of different age, highlighting heterogeneous bone behavior.

Within the previously described structures, the bone cells are embedded, orchestrating the bone global behavior. The presence of those bone cells implies that this scale is the theater of important cellular events.

Bone remodeling.

One of the most important bone characteristics is its ability to adapt its structure according to the mechanical environment. That's why, for instance, tennis players may have a difference in their bone density between their two arms, or why astronauts need to keep a physical activity during space mission, to balance the microgravity environment.

Four main types of bone cells have been identified [21]:

- Osteoblasts

  They are dedicated to bone formation. They are differentiated product of mesenchymal stem cells and synthesize components of bone matrix, called osteoid, that will then mineralize.

- Osteoclasts

  They are able to destroy bone matrix when needed, that is when it presents alterations or cracks. They eliminate altered tissue by destroying collagen fibrils composing bone matrix.

- Osteocytes

  They are the most numerous cells in bone. They are in fact old os-

teoblasts trapped in bone matrix. They are often qualified as the "conductors" of bone remodeling because they have been identified as mechanosensors: they are able to perceive mechanical stimuli and transduce the information to osteo- clasts and osteoblasts to initiate bone remodeling. This phenomenon is therefore crucial, but still need investigation to be fully understood.

- Bone lining cells
  Located at the bone surface, they might be involved in the perception of mechanical solicitation.

The bone remodeling process occurs naturally in the body. However, around the 30s, bone tends to resorb itself more than it is created. This unbalance may become critical and induce osteoarthritis, especially for women after menopause. Indeed, bone cells activity may be related to hormone balance.

The precise bone remodeling process and bone cells activation is widely discussed in the literature, as many theories are developed on bone cells activation [22, 23, 24].

Mechanotransduction.

As the cells are mechanically activated, a difficulty is to understand how they are coordinated by mechanobiological factors [21]. At this scale, mechanical solicitations are perceived as bone matrix deformation. This involves insterstitial fluid movements inside the lacuno-canalicular system, where osteocytes are located.

Several hypothesis have been proposed to determine how those cells are perceiving mechanical signals, but the more convincing one is that they are particularly sensitive to interstitial fluid flows. Even if osteocytes are mechanically activated, they coordinate the action of other bone cells, through complex molecular processes that are yet under investigation and the subject of many researches [23]. These considerations highlight the need of a modelling approach able to account for the complexity of the bone structure, including interstitial fluid flows.

1.2.2.4 Nanoscopic scale

Structural description.
We find at this scale the elementary structural components of bone tissue.

- Collagen
  It is the main component of the organic bone matrix, called osteoid. Collagen is a protein than can be found in numerous biological tissues, such as skin or connective tissue of every organs. They come either from osteoblasts synthesis or from blood.
- Hydroxyapatite (HA)
  HA crystals correspond to 50% of bone content. The chemical of HA is $Ca_5(PO_4)_3(OH)$, which indicates that bone mineral components are mainly calcium phosphate and calcium carbonate. The formation of HA crystals is the result of the mineralization process [16].

Mechanical description.
It has been established that collagen is responsible for bone elasticity and HA for bone stiffness. Therefore, the description of the evolution of mineralization is a required information to determine bone quality. The mineralization process has been identified as a highly non-linear process. This is the complex interplay of bone remodeling, resulting in the production of soft bone material, and mineralization, that determines bone quality and performance throughout life. With its structural variations, this explains the heterogeneity of bone tissue [21, 23].

Mineralization.
As we have seen previously, bone is able to adapt its structure through bone remodeling. But it is also able to adapt its intrinsic properties, changing collagen or HA proportions. This is called mineralization.

The mineralization process takes action in two parts. The first phase is a rapid mineralization that occurs during only a few months and where the mineralization rate goes from 0 to 20%. Then, during the second phase, mineralization slows down and stabilize over the years, reaching a maximum at almost 25% of mineralization of bone tissue. Finally, when bone is too calcified, it becomes too brittle and can either be the cause

of a major fracture, or microfractures indicating the beginning of a new remodeling cycle [16].
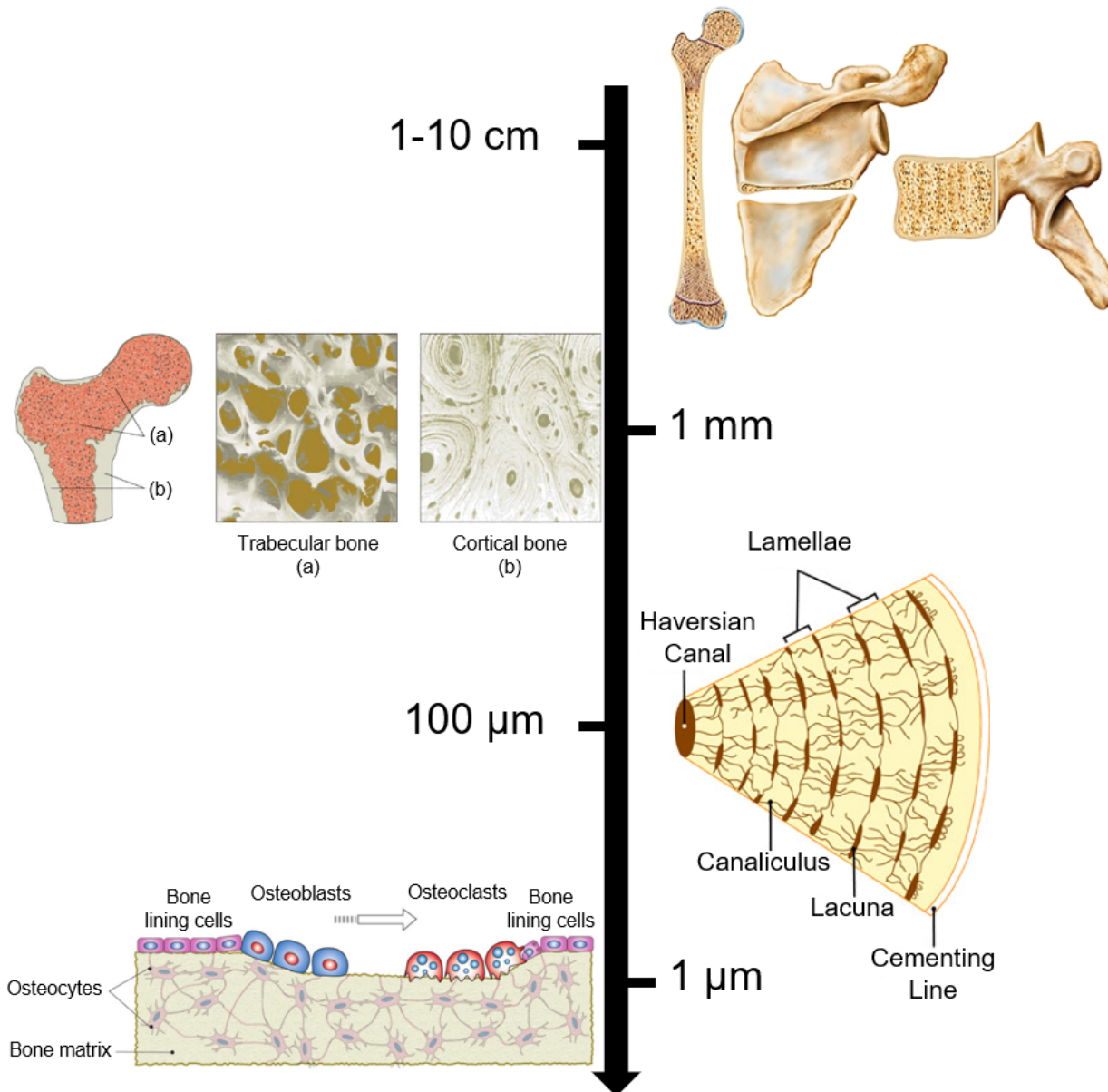
Figure 1.5: ***Bone accross the scales [5].***

In conclusion, bone presents a hierarchical and complex structure as showed on Figure 1.5. When a surgery, and more specifically a joint replacement is required, the device implanted need to fulfill several requirements in order to fit at best with these specificities.

1.3 The Device: the Hip Prosthesis

The total hip prosthesis is mainly composed of three elements: the femoral stem, the ball and a cup. These three elements move in a way reproducing the natural hip joint.

Indeed, while the femoral stem is fixed in the intramedullary canal of the femur and the cup in the acetabular of the pelvis, the ball, replacing the femoral head, allows the rotation of the hip.
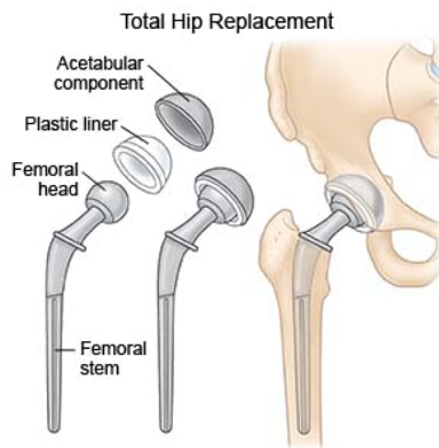
Figure 1.6: **The components of a hip prosthesis [1].**

As the aim is to provide the most appropriate device, it is interesting to investigate the ways of improving the prosthesis. The parameters that can be improved are the geometry, its material and possible coatings of the device and its fixation.

1.3.1 Geometry

First, let's focus on the global shape of the prosthesis.

1.3.1.1 Acetabular cup

As it can be seen on Figure 1.6, the acetabular is placed in the hip socket.

We find two main shape of acetabular cup:

- Modular cups, that consists in two pieces, a shell and a liner as presented on Figure 1.6.
- One-piece acetabular cups, that are monobloc. They consist in shells with the articular surface machined on the inside surface of the cup.

1.3.1.2 Femoral stem

We consider two main categories of femoral stems: the straight stems and the anatomic stems (Figure 1.7).

The straight stem.
It corresponds to the oldest design. As there is no antero- posterior curvature, it gives to the surgeon the choice in the stem positioning, according to the patient bone quality or specific geometry. Its proximal part is flared and its sections are rectangular-shaped. It ensures a good stability as soon as its implantation is performed. Especially, the shape of its sections allows a good stability in rotation. However, it requires an important bone adaptation.

The anatomic stem.
More recently, a new stem design appeared: the anatomic stem. Its goal is to provide a better integration in the femur natural shape, as it presents non-zero anteversion and helitorsion angles. Like the straight stem, its proximal parts are flared and its rectangular-shaped section ensures a good stability just after the surgery and for rotating movements.

Anatomic or straight, prosthesis manufacturers provide wide ranges of devices, so that the surgeon can choose the one that fits at best patient specific requirements. They can vary in leg length, offset and version.

1.3.2 Material

The first criteria defined in the choice of the material when producing a hip prosthesis, as any other medical device implanted in the body, is the biocompatibility.

Figure 1.7: **Two devices provided by Stryker: on the right a straight stem Secure-Fit Advanced and on the left an anatomic stem Anato.**

1.3.2.1 Acetabular component

The shell of the acetabular is a two blocks component in metal. On the outside, a porous coating may be used to get friction with the bone and facilitate the fixation. On the inside is designed a locking mechanism to fix the liner. The liner is in polyethylene or ceramic to allow articulation with low friction.

The monobloc acetabular components can be in UHMWPE (Ultra-High-Molecular-Weight-Polyethylene) or in metal. The choice in material will condition the used fixation.

1.3.2.2 Femoral components

The femoral stem is usually made of stainless steel, cobalt-based alloy or tita- nium based-alloy.

The femoral head can be either made of metal or ceramic. Metal heads (usually chrome-cobalt) have the advantage to provide hardness but need polish to reduce wear. In the other hand, ceramic head are smoother, but, due to ceramic brittleness, they may have more chance to break after the implantation.

1.3.3 The Fixation

Cemented fixation.

The principle of a cemented fixation is to fill the gap between the bone and the implant to stabilize the bone-implant system. However, cement is a durable and hard substance whereas bone is an organic material. The mismatch in the elastic modulus can lead to loosening. Still, the cemented bone is generally very durable and reliable with a considerable and successful history of usage.

It is mainly used in the case of elderly patients presenting poor bone quality.

The cement used is usually polymethylmethacrylate, that is a self-curing acrylic polymer [8].

Cementless fixation.

Recently, the development of new kind of materials and designs allows attachment to the bone without cement. For example, porous surfaces or coatings may enhance bone growth around the prosthesis, leading to a stable implantation. Because that depends on new bone growth for stability, cementless implants require a longer healing time and are not recommended for patients with osteoporosis. However, we can qualify the bone remodeling around the implant as more "natural" and, therefore, better long-term reliability.

Hybrid fixation.

The different components of the prosthesis are fixed with a combination of both of the previously presented methods.

Screws.

The acetabular components can be screwed in the pelvis to ensure the fixation.

Coatings and surface treatments.

Each component may present surface technologies to enhance bone fixation and limit surface damages such as wear and corrosion [25].

Surface treatments may include ion implantation and methods to control surface topography, as grit, sand blasting or plasma treatments.

A large variety of coatings have shown interesting results. We can find hydroxyapatite, titanium oxide and nitride, zirconium oxide, pyrolytic carbon or diamondlike carbon [26].

All the parameters of the prothesis described below are chosen in order to provide the best bone-prothesis interaction for the patient. A thorough study of the events and mechanims involved and its anticipation through a numerical tool as developed here is particularly relevant.

1.4   Bone-Prosthesis Interaction

The first contact between the bone and the prosthesis occurs during the surgical procedure.

1.4.1   The Surgery

Before any surgical intervention, the surgeon proceeds to a thorough planification of the surgery, in order to choose the most appropriate device according to the patient specific requirements in bone geometry and quality.

In the operating room, the first step consists in the removal of the femoral head. The incision is particularly small in order to limit the bleeding and post-surgery healing and follow-up, but it leaves him with reduced space to perform the surgical procedure. Then, the surgeon rasps with a specific tool the interior of the femoral bone (in the medullary cavity) to prepare the implantation of the femoral stem. On the upper part of the stem, a metal or ceramic ball is placed in order to replace the femoral head.

The damaged cartilage surface of the acetabulum is then removed and replaced with a metal socket, that may be fixed with cement or screws

when needed. A plastic, ceramic or metal spacer is inserted between the new ball and the socket to allow for a smooth gliding surface.

1.4.2 Bone healing phase: the primary stabilization

The initial response of the body to a foreign material is a succession of biological events [27]:

- Protein adsorption at the prosthesis surface.
- Hematoma formation and platelet activation, release of cellular signaling molecules.
- Blood coagulation.
- Inflammation, increased blood flow and vascular permeability.
- Proliferation of stem cells and differentiation based upon mechanical and biological signals.
- New vessel formation to prepare ossification.

Those actions end in the formation of a fibrin clot, stable enough for the deposit of growth factors and for allowing osteoconduction.

Osteoconduction can be defined as the migration and differentiation of osteogenic cells into osteoblasts and is needed for contact osteogenesis to occur at the implant surface. We called contact osteogenesis the formation of new bone on the implant surface, in distinction with distance osteogenesis, when bone grows from the old bone surface toward the implant. Those events are very similar to the ones occurring during fracture healing [28]. This allows the primary stabilization of the prosthesis, the first step before the formation of solid bone around the implant [29].

1.4.3 Bone remodeling phase: secondary stabilization

After the primary stabilization, contact and distance osteogenesis result in immature woven bone that will provides secondary stabilization within the host bone. The main sake of this secondary stabilization is to ensure bone remodeling around the implant to solidly anchor the prosthesis to the limb.

Bone remodeling will first happen within the host bone, which has been stressed during the surgery and then within the woven bone formed

in the peri-implant gap. We can also notice that at the time of implantation, damage has been made beyond the site of implantation (1 to 2mm). Therefore, bone remodeling can occur in a large zone around the prosthesis.

In the end, the woven bone resulting from the primary stabilization will be re- placed by mature lamellar bone, which is mechanically stronger, corresponding to the desired result. The prosthesis can be considered as fully integrated to the femur.

1.4.4 Possible complications

During the previously described procedure, several aspects can represent major difficulties for the surgeon.

Firstly, in his pre-operative planification, the surgeon chooses among the available range what he considers the most appropriate model and size of the device, according to the patient specific anatomy.
He also uses imaging techniques in order to have an idea of bone quality: obviously, osteoporotic patients will require an appropriate surgical technique, to avoid any more damage on the bones.

During the procedure, the surgeon needs to work inside the smallest possible space, with angular tools, in order to proceed to a surgery as minimally invasive as possible. Having thoroughly prepared the surgery and spent time on the planification with efficient tools allow the physician to reduce the time in the operating room. In this framework, numerical modelling of bone would be a major advancement in surgical procedures.

Obviously, numerous complications need to be anticipated to avoid major post- operative issues. As in any surgery, blood clots are able to travel in problematic areas or infection can occur during the classical healing process. On a longer term, serious complications need to be looked after.

1.4.4.1 Dislocation

Dislocation occurs when the artificial head goes out from the hip socket. It represents the second cause of prosthesis revision and up to

70% of average additional cost against the primary THA, as it may require a revisional surgery. Right after the primary THA, between 2% and 4% of the patients are facing a dislocation and, after a first episode, the risk of relapse is increasing exponentially. Many factors are susceptible to increase the risks of dislocation. It may come from the specificities of the patient, the implant, the surgical procedure, or during the post-operative follow-up [30].

Thus, only a more precise and thorough pre-operative study may prevent such complication.

1.4.4.2 Aseptic loosening

Implant loosening can occur if bone has trouble to reconstruct itself around the prosthesis. It is nowadays the main cause of revision of arthroplasties. Several hypothesis are made on the origin of this phenomenon as it is identified as multifactorial [31, 32]. It can come from:

- Unsuccessful initial fixation, due to infection or insufficient primary stability.
- Poor bone reconstruction around the device. During the secondary stability, occurring after the implantation and achieved through bone remodeling, the new loading conditions applied to the host bone can lead to bone loss in the zones that are not solicited enough. This is called stress shielding and is hardly predictable during the upstream surgery planification.
- Osteolysis (i.e. bone destruction) due to wear debris. The contact in the artificial joint can induce particle creation that can damage bone tissue and/or bone tissue creation; or from material deterioration such as corrosion.

1.4.4.3 Squeaking

Especially with ceramic-on-ceramic hip protheses, an audible squeaking may appear until several years after the surgery. Even if it is painless, the disturbance of this noise is a real matter of concern for the patients. It has recently been highlighted that squeaking is also a multifactorial phenomenon. Indeed, squeaking can be attributed to [33]:

- The design of the device [34].
- The material itself, the friction between the femoral head and cup, and when disruption of fluid-film lubrication can occur.
- The initial positioning and/or the stability allowed by bone reconstruction during the secondary stability.
- Patient specificities in bone quality, age and its impact on bone remodeling.

These unfortunate events may lead to revision surgeries. Revision hip replacement is a longer and more complex procedure, that requires extensive planning from the surgeon and the use of specific implants and ancillary. This type of surgery can imply either the revision of some of the components, or the total removal of the prosthesis. On top of mobilizing hospital resources, the procedure is particularly heavy for the patient.

In order to avoid or prevent these complications, it is needed to develop tools for understanding and controlling the mechanical and biological events involved during and after the surgery, resulting in the successful implant integration in the host bones.

1.5   Thesis positioning

Accounting for the biomedical and biomechanical considerations reported above, the success of a Total Hip Arthroplasty may be directly correlated to the quality and strength of the bone reconstruction around the device, especially around the femoral component. This location is in fact prone to multiple possible complications, from infection to dislocation.

As aseptic loosening is nowadays the main cause of hip replacement failure, it is important to be able to provide an accurate prevention of this complication. This involves a better understanding of the bone-implant

interaction, with a focus on the secondary stability. Understanding this phase will help the determination of the critical parameters involved during the process. At this aim, numerical modeling can be considered as a powerful tool for simulating the mechanical response of the bone under the applied loads when introducing the medical device. This thesis presents the development of a reliable numerical model of the bone, that could bring a step forward in the availability of a virtual laboratory for analysis and simulation of the bone remodelling.

The final aim of this work is to provide a tool that will allow multiple advances:

- Provide a better understanding of the bone-prosthesis interaction on the long term.
- Create a planification tool for the surgeon to implant the most appropriate device for each patient, taking into account its specificities, such as its own and unique bone geometry and bone quality.
- Giving to the prosthesis manufacturers a guidance in their implant design, in order to product devices that will include at best in the biologic and anatomic reality.

The proposed numerical tool, as powerful as it can be, requires a compromise between its biological and anatomical accuracy and an ease and speed of execution. The work presented here is based on this compromise.

To fulfill the prediction issues, without struggling with the difficulties of bone material experiments and being totally non-invasive for the patient, the development of a numerical model seems particularly accurate. The main features of the proposed model are a direct consequence of the actual biomechanical knowledge on bone remodeling.

On one hand, bone reconstruction around the device is the result of bone re- modeling. As it has been previously explained, bone remodeling occurs through successive bone cell actions and at different scales. On the other hand, the intended application is to give information at the prosthesis scale (Figure 1.8). The separation of the scales of interest requires the development of a tool that can take into account and couple the important criteria. Accounting for the main scales of interest is then one of the

main characteristics of the methodology presented in this work, in order to develop a reliable numerical model.
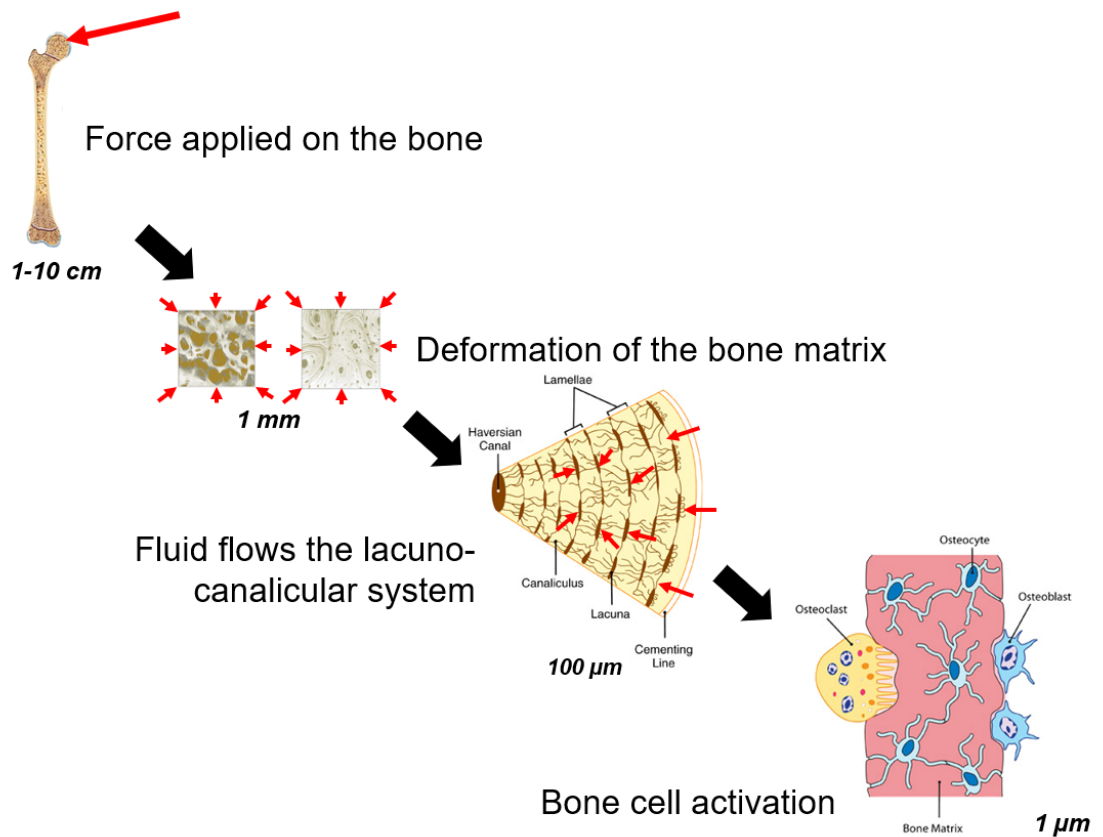
Figure 1.8: **Bone remodeling across the scales, from the load applied on the femur to the deformation induced on the bone matrix to the corresponding fluid flows to bone cell activation [5].**

Furthermore, many researches addressed bone remodeling, in order to understand the mechanisms allowing its functioning. A special focus is put on osteocytes and their ability to perceive mechanical stimuli. Their location in the lacuno-canicular system, immerged in bone fluid, and their shape are giving clues on their specific sensitivity to bone fluid flows. Through mechanostranduction, they transform this mechanical stimulus in chemical information [23]. Therefore, in order to keep as faithful as possible to biological reality, the numerical model needs to include a fluid component.

In addition, osteocytes are located in the lacunae of the bone, which are pores at the microscale. Indeed, the porosity of the bone, at every scale, impacts its mechanical behavior. In that respect, from a mechanical point of view, the most appropriate material definition, to be included in the numerical model, is poroelasticity. It allows to account for the fluid component and its interaction with the solid matrix of the bone.

The sum of all these elements defines the framework of the work presented here. Aiming to the elaboration of the previously described tool, the work of this thesis consists in the development of a poroelastic model of the bone, through a multiscale formulation.

State-of-the-Art and Numerical Approach

Following the biomedical context which have been set, the focus of the mechanical view of this issue is detailed in this chapter, while developing the proposed numerical approach. A review of bone mechanical characterization and its numerical modeling is presented in order to support the hypotheses and choices made in the presented work, regarding poroelasticity and multiscale formulation. This leads to the numerical development of a model, which mathematical methodology and algorithm implementation will be detailed further.

2.1   Bone Mechanics and Numerical Modeling

As seen in the previous chapter, bone has a very complex structure, spreading on several scales and containing several components. Thus, the mechanical description and characterization of bone is a challenge, so as providing an accurate numerical modeling.

2.1.1 Bone Mechanical Characterization

Bone mechanical characterization is difficult because of its herarchical and composite structure. Indeed, numerous are the parameters that have been identified as determinant in the mechanical response of bones.

At the tissue-level, five methods are mainly used [35]:

- Tensile or three-(four-) point bending tests
- Buckling studies
- Acoustic methods
- Back-calculation from finite element simulation
- Micro- or nano- indentation

Most of the measures below the microscale have been done by nanoindentation [36, 37, 38, 39, 40]. This technique was developed since the mid-1970s and is commonly used to test the mechanical properties of materials. It consists in a hard tip, which size depends on the size of the sample and the desired accuracy, that is pressed on the studied material. Applying a known load, the area of the residual indentation is then measured. The slope of the curve obtained, together with the indentation area, are used to characterize the hardness and stiffness of the sample.

The overall mechanical properties are a function of the different structural elements which constitute the bone.

2.1.1.1 Structural elements playing a role in bone mechanics

Mineral.
As presented in the previous chapter, bone is a composite material. At the nanoscale, mineral components can be found in the shape of apatite crystal. Their location at this very small scale and their very small size make their mechanical contribution very difficult to assess.

In [39], the elastic modulus of the crystals along the basal plane has been estimated to be $E_b = 135 \pm 1.3$ GPa , while along the transversal plane $E_t = 125.9 \pm 1.6$ GPa. In [40] the measurements results were respectively $E_b = 150.38$ GPa and $E_t = 143.56$ GPa. These studies also

mention that the crystal itself shows anisotropic properties, and its orientation could have an influence on the anisotropic properties at the higher level. It is important to note that these values describe the isolated apatite crystal. The properties of the global mineral phase are much harder to measure and the corresponding stiffness is reducing to 40.9 GPa, obtained by diffraction method [41].

Collagen.

The apatite crystals are embedded in an organic phase made of collagen. This organic part is the responsible for fracture resistance, as it gives elasticity to the bone.

According to the considered level, collagen is organized along different patterns. The one that is the easiest to measure is the collagen fibril. Obviously, the percentage of mineralized material impacts the global mechanical behavior of the fibril. By nanoindentation, an average elastic modulus can be measured and it varies between 1 and 1.5 GPa for unmineralized collagen fibril.

By diffraction, an average elastic modulus $E = 18.3$ GPa is measured in [41] for collagen fibril *in situ*, highlighting the role of mineral in collagen mechanical behavior.

Lamella.

The bone structural organization at each level is responsible for the bone global mechanical behavior.
Collagen fibrils are organized by lamellae, in which their orientation is difficult to assess. It has been established that they do not respond with the same stiffness when solicited axially or transversally. Lamella organization differs in cortical or trabecular bone: they gather either on osteon or in trabecula.

In osteon, structural element of cortical bone, the elastic modulus is estimated at 17.7 ± 4.0 GPa [42], but as shown in [43], the state of mineralization of the studied sample of lamella have a large impact on its stiffness, until more than 10 GPa between samples defined as highly mineralized (21.30 ± 3.0 GPa) and as low mineralized (12.95 ± 2.66 GPa).

Mineralization and bone quality are the main sources of bone heterogeneities, as the nanostructure itself largely differs among lamellar types, anatomical sites and individuals [37].
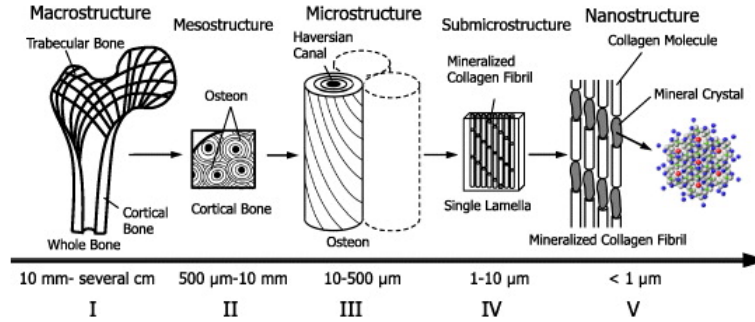
Figure 2.1: ***Bone at the different scales, down to the mineral part [6].***

Global Mechanical Behavior.

At bone tissue scale, elastic modulus varies mainly with the considered type of bone, because cortical and trabecular bone differ in shape, structure and mineralization even if they are made out of the same components. Whereas cancellous bone is extremely anisotropic and heterogeneous, cortical bone shows a more linear behavior.

Nanoindentation measures have been done, and bone elastic modulus at this scale can vary between 5 and 25 GPa [37, 44, 38, 42, 45].

At this scale, compression and traction tests can also be performed in order to extract the stress-strain curves of the material, and from these curves the apparent Young Modulus or the maximal stress can be calculated [46], even to appreciate anisotropy properties of the bone material [47]. Micro-CT analysis can also be performed allowing bone quality characterization [48].

The large range of value obtained can be explained by the non-linear stress-strain behavior of the collagen fibrils contained in bone internal structure as highlighted in [49]. The presence of fluid in bone also impact its mechanical behavior but is very difficult to characterize experimentally. However, through water imbibition of bone samples [50] or internal medullary pressure measurements as in [50] among others. In all the

performed mechanical tests, it is important to note the importance of the freshness of the tested tissue sample and the conditions of testing, which can have a significant impact on bone mechanical behavior (the hydratation of the sample [51], the environment temperature during the test [52] or the experimental set-up itself due to edge-effects).

All these considerations allow us to increase our knowledge of bone material, from an experimental point of view, to have as well material inputs for the numerical models.
In addition, these data give the opportunity to validate the numerical models from a mechanical point of view.

2.1.2 Bone in Numerical Models

Numerical models aim to reproduce bone behavior to provide information on bone mechanical behavior. They are considered as well a step toward bone reaction prediction, as a tool for orthopedic surgeon.
As bone presents a very complex structure, several approaches have been proposed into the literature.

2.1.2.1 Elastic models

Isotropic models.
Elastic isotropic models are the simplest models developed as the number of required mechanical properties is limited to the elastic modulus and the Poisson coefficient. It implies that bone has identical values of mechanical properties along every direction, with a linear stress-strain response, which can be a rough estimation regarding bone biological and anatomical reality.

Indeed, as presented above, at the macroscale, average quantities can be determined and these models can result still relevant in bone mechanical studies.

However, they do not consider the events occurring deeper in the material and give only a macroscopic description. In our case, it represents a critical limitation.

Orthotropic models.

As bone anisotropy is well-known, isotropic models may seem over simplified, while providing computing efficiency.

To get closer to actual bone mechanical behavior and structural adaptation capacity, orthotropic modeling can be considered. Orthotropic materials are defined by the existence of three mutually-orthogonal axis of symmetry.

Several studies have put forward the transversely isotropic aspect of bone, especially cortical bone that shows preferred directions in its internal structure, and transversally isotropic material are special orthotropic materials that have only one axis of symmetry [53, 54].

But even orthotropic material, by introducing mean elastic coefficients, may be limited to reproduce the complexity of bone behavior, especially at the smaller scales.

2.1.2.2 Viscoelastic models

A viscoelastic material exhibits both creep and relaxation.
During nanoindentation measurements of bones, time dependency has been noticed, indicating that the stress does not only depend on the strain, but also on the time history of the strain. Therefore, viscoelastic models are interesting for modeling bone under dynamic loading for example. Several hypotheses can be made on the origin of this particular behavior [55].

- It has been shown that this viscoelastic behavior can be due to the interaction between mineral and organic contents [56].
- Porosity is also considered as an actor in bone viscoelastic behavior, as the relaxation time parameter is positively correlated to water content in torsion. Also, hydrated bone shows more damping when submitted to a range of different frequencies [57, 58].

Therefore, considering bone porosity may be an important criterion.

2.1.2.3 Poroelastic models

To consider bone porosities in bone mechanical behavior and assess the impact of internal fluid flows, poroelastic modelling could be an appropriate approach.

The porosities contain fluid, which composition is difficult to be precisely determined, but is usually assimilated to saline water at 37°C. Three main levels of porosities appear in bone [59]:

- **The vascular porosity.**
  They are the largest and they consist in the center of osteonal structures. The bone fluid in this porosity stays largely inferior to the pressure due to blood circulation.

- **The lacunar-canalicular porosity.**
  This is the porosity where osteocytes are immerged. Thus and because of the roles of osteocytes in mechanotransduction, this is the most important porosity for the consideration of mechanical and mechanosensory effects in bone. It is also associated with the slower relaxation of the excess pore pressure due to mechanical loading. This is also a place where we can find molecular network and nutriments for the osteocytes [60]. This is therefore a main feature to account for in this work.

- **The collagen-apatite porosity.**
  It consists in the spaces between the collagen and crystals of apatite. Due to its very small size, bone water at this scale is considered in the collagen apatite structure. Fluid flows at this scale are therefore neglected.

Then, poroelastic modelling of bone is an interesting solution to provide bio-reliable numerical models of bone. A wide range of models and approaches can be found, as a function of the considered scale and the elements accounted for in such models. They differ in the assumptions made to treat the poroelastic aspect, and the choice in the mathematical description for such structures.

They almost all rely on the Cowin [59] work on poroelasticity, which formulated the poroelasticity theory to bone in a detailed way and dedicated several studies and reviews on this topic.

Other works dealt with the determination of bone poroelastic parameters, such as [61, 62, 63], to gain in biological accuracy or to provide information on fluid pressure inside the bone [64], very difficult to assess *in vivo* or *in vitro*. Others are using the porous aspect of bone and the determinant role of the lacunar-canalicular porosity to provide a multiscale and multi-physic model of bone, aiming to the inclusion of every aspects in bone response and bone remodeling [65, 66]. Two of the main porosity levels may be considered as well. The choices in modeling are dictated by the final aim of the developed model, and considering the wide range of possibilities, the list of the different work cited here is obviously non-exhaustive.

All these elements are supporting the choice of providing, in the framework of this thesis, a poroelastic model of bone.

2.2 Poroelasticity and Porous Material modeling

Poroelasticity refers to a theoretical model of the mechanical behavior of a porous structure filled with fluid

2.2.1 Historical background

Poroelasticity has been first conceptualized and formulated by Biot in the 40's and its work on soil consolidation, starting from the observation that a soil under load has the ability to settle gradually, especially sands saturated with water [67, 68].

This first theory has then been extended to the most general case of anisotropy. It describes the stress and strain distributions in a porous

solid, composed of a purely elastic skeleton containing a compressible viscous fluid.

Since then, the theory has been proven particularly accurate and has been the subject of many developments, as presented in [69]. Mostly, this theory was applied in soil mechanics and other fields of geotechnical problems, such as rock mechanics.

2.2.2 The numerical approaches

The theory of poroelasticity involves some basic equations than can be developed into different approaches, as presented in [59]. They are all built around the notion of averaging.

2.2.2.1 Effective medium theory

The effective medium theory, also called effective medium approximations is often used for describing the macroscopic properties of composite material. The aim is to calculate macroscopic properties from the average of the constituents' properties that make up the considered material, defining a Representative Volume Element (RVE).

Then, as the values of the properties are impossible to compute at the constituent level, the global property is obtained [70].

2.2.2.2 Mixture theory

A mixture is defined as a material with at least two components that can be either solid or fluid. Each fixed spatial frame in the solid-liquid mixture is occupied simultaneously by a material point of each constituent, and from this point the flux of the species is considered [71].

Thus, mixture theories are based on diffusion models. It presents the main advantage to handle the description of many solid and fluid constituents and the possibility of having chemical reactions between these constituents [72] and this is why they are particularly relevant for studying multiphase material.

It mainly differs from the Effective Medium Theory presented above in the averaging method used. As the description involves the flow of

different constituents, the averaging process is density-weighted on the basis of the density of each species, while in the Effective Medium Theory, the average is done over a finite area or a finite volume of the porous material.

2.2.2.3 Multiscale Approach

More recently, multiscale approaches have been used to model and describe porous material behavior. They have the advantage of providing a thorough description of the events and components involved in the global behavior, which lacks the Effective Medium Theory.

Several works can be found in the literature modeling bone as a poroelastic material with a multiscale formulation, but the different models are not developed for the same purpose. Some works [73, 74] bring a better understanding of osteocytes activation, while in [62] the model is dedicated to predict the qualitative changes in anisotropy due to variations in the structure at the mesoscale. In [75, 65, 66, 76] this formulation of modeling is used to produce a complete and rigorous model of bone targeting a solid bio-reliability, considering several porosities and not only the hydraulic component of osteocytes activation. The multiple porosity aspects and anisotropic properties of bone can be introduced as well, e.g. in [77, 78, 79], to thoroughly enlarge the scope of application.

But, as the challenge here is to keep a delicate equilibrium between accuracy and efficiency, mixture theory is not the most appropriate either. It is important to note that some models have been developed in which mixture law are applied in RVE, as it can be seen in [72] for modeling growth tissue, but the kinematics of the constituent remains challenging.

This explains the focus put here on the choice of a multiscale approach to model bone as a poroelastic material.

2.2.3 Definitions

Going further in the mathematical and mechanical description requires the proper definition of the concepts and parameters directly linked to poroelasticity.

2.2.3.1 Porous medium

A porous medium is a material that is defined by a skeletal portion, often called 'matrix'. This part can be either solid or softer, as a foam type of material. It contains pores that are voids part. Those pores are typically filled with a fluid, that can either saturate the matrix or not.

The characterization of the fluid part, such as its viscosity, if it is Newtonian or not, and also its interaction with the matrix are determinant for the mechanical definition of the porous media.

This kind of material involves several specific characteristics and parameters presented in the following.

2.2.3.2 Porosity

Intrinsic and crucial characteristic of porous materials, porosity is denoted by ϕ and defined by the ratio between the total pore (void) volume V_p and the total volume V occupied by the material.

$$\phi = \frac{V_p}{V} \tag{2.1}$$

2.2.3.3 Permeability

It can be defined as the property of the material to allow the fluid to flow through it. Therefore, it depends on the geometry and structure of the solid matrix, meaning the configuration of the pore and if there are considered as closed (isolated) or open (communicating). Its inverse represents the resistance induced by the friction forces between the solid and the fluid.
It is expressed in m^2 and its order of magnitude is given by one pore section.

2.2.3.4 Reynolds number

Flow regime in porous media can be characterized by a dimensionless number, the Reynolds number, denoted Re and involving fluid parameters such as its density ρ (kg/m^3), its viscosity μ ($Pa.s$) and its Darcy's

velocity v_f (m/s) (see Section 2.4.1 for details), but also the characteristic length of the porous media l (m).

$$R_e = \frac{\rho v_f l}{\mu} \tag{2.2}$$

These main features give the basic concepts for the study of a poroelastic material. Once defined, a focus can be put on the further description of the method chosen for this work.

2.3 Multiscale modeling

Bone being a hierarchical structure and showing ability to modify its structure on several levels, added to the interest of considering its poroelastic aspect, the choice of developing a multiscale model seems obvious.

2.3.1 Concept

The aim of multiscale modeling is to obtain material properties or system behavior at one level using information coming from the other levels. Each level addresses a phenomenon over a precise window of length and time.

It allows the description of "microscopic" events, such a composite material degradation for instance, and its consequence at a larger scale. It can provide more precision on the mechanisms that dictate the macroscopic behavior of the considered material.

Thus, as macroscale models may not be accurate enough and microscale models not efficient (computationally) enough, combining these two viewpoints offers an interesting compromise between accuracy and efficiency. The idea is to decompose the levels that are interesting and coordinate them, downscaling or upscaling the levels.

Downscaling determines the boundary conditions of low levels based on a global study whereas upscaling allows the determination of the global behavior based on the resolution of the microscopic problem.

Thus, two key points condition the validity of this method:

- Relevant scale separation in both the behavior and the modeling.
- Coupling the events occurring at the different chosen scales with the right relations.

The development of a multiscale model requires the use of a mathematical tool, called multiscale analysis. This analysis consists in the mathematical relations that link the different considered levels. They are involved in the resolution of the mechanical problem, through a specific formulation applied on the equations involved.

2.3.2 Overview of multiscale analysis

In the literature, it can be found many attempts which have been made to formulate a macroscale model from complicated microscale models through mathematical development. Among these techniques, two main classes appear and are detailed below:

- Local analysis to analyze localized singularities.
- Averaging methods that allow the description of macroscale models by averaging over small scales.

2.3.2.1 Matched asymptotic expansion

This is a method to extract the local structure of singularities or sharp transition layers in solutions of differential equations, by dividing the domain of interest in an inner and outer region. The inner and outer solutions are obtained by solving order differential equations and matching these approximate solutions over the intermediate region, when the inner and outer regions overlap.

From its construction, the matched asymptotic method is particularly relevant when solving singularly perturbed differential equations.

2.3.2.2   Averaging methods

This method is for the analysis of ordinary differential equations with multiple time scales. The idea is to obtain effective equations for the slow variables, over long time scales, by averaging over the oscillation of the fast variables [80].

In multiscale modeling, averaging methods are used when multiple time scales are considered.

2.3.2.3   Homogenization methods

They were first developed for analyzing the effective behavior of partial equations with multiscale coefficients, representing material properties of the heterogeneous macroscale model [81, 82].

2.3.3   Focus on the Homogenization Technique

The final aim of this work is to model the mechanical response of the bone to quantify bone reconstruction around a medical device, providing a parametric tool for the planification of the surgeon and for helping in designing efficient prostheses. Then, among the mathematical formulations described previously, the homogenization technique seems to be the most relevant to reach the goal of this study.

Knowing the biology and structure of bone, its porous aspect has to be a major feature in the development of such numerical tool, especially the fluid flows. Yet, to provide a reliable poroelastic model, a consideration of the microscale events is required. Here, the focus needs to be put on the structural consequences of fluid flows in order to give information on the structural evolution of bone tissue and to obtain relevant information without going too far into details; in this context, the results of fluid flows in the solid matrix are more important than their detailed description. This is why, among the practicable solutions stated previously, a homogenization technique is the most appropriate choice.

2.3.3.1 Principle and interest

The aim of the Homogenization Technique is to obtain a simple and homogeneous approximation of a medium composed by a heterogeneous microstructure. At fine-scale, the details of the heterogeneities are visible: the fibers in a composite material, the microcracks in damaged materials or in our case pores in a porous material. These heterogeneities are included in a Representative Volume Element (RVE), which is a small volume which size and shape is determined in order to provide all geometrical information and peculiarities necessary for obtaining an appropriate homogenized behavior.

Through the homogenization process, at a larger scale, these details are no longer noticeable. The main stake of homogenization technique is to give the possibility to consider the interactions between the scales; consequently, the solicitations at the large-scale impact the structure at the smaller scale (See Figure 2.2).
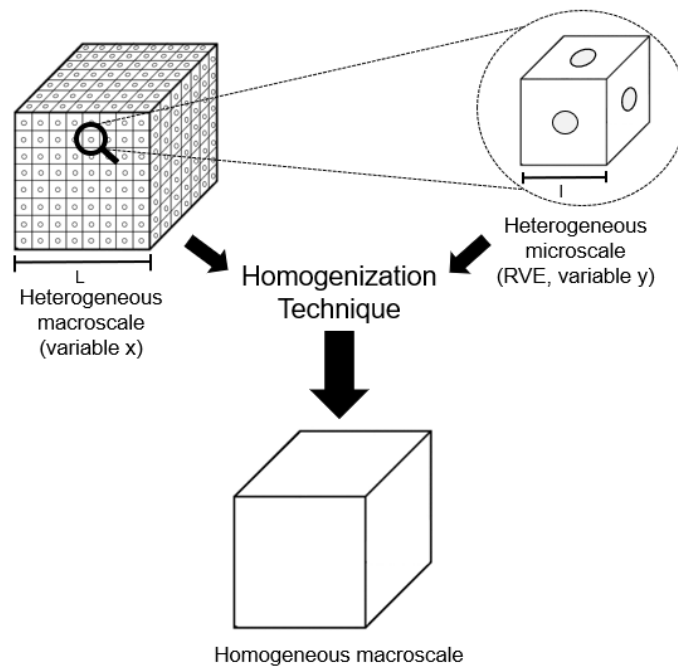

Figure 2.2: **Representation of the homogenization technique as an approach for multiscale modeling.**

According to the considered geometry, its size, the dimensions, the

periodicity or non-periodicity of the microstructure, several homogeniza-tion techniques can be used; one of the most thorough approach is the asymptotic homogenization, introduced in [81, 83].

From a mathematical point of view, the asymptotic homogenization allows the resolution of partial differential equations through an asymp-totic expansion, thus considering two variables, one at the macroscale and one at the microscale [84].

The corresponding scope of application is very large [85], including composite material modeling, but also investigation of porous materials, following both linear and non-linear poroelasticity laws [86].

2.3.3.2 The assumptions

The homogenization technique relies on two main assumptions that are required for the proper definition of the multiscale model.

Scale separation.
Basically, almost all homogenization methods are based on a scale separa-tion. Relatively to the macroscopic length scale, the more the microscopic one is small, the more the heterogeneities that it represents are small. Thus, the corresponding average macroscopic properties are accurately calculated.

This is as well one the main limitation of the homogenization meth-ods, i.e. if the scale separation is not respected, all the mathematical background does not hold anymore and it is inapplicable.

However, some solutions are under investigation to overcome this is-sue and more expandable homogenized model are proposed [87].

Periodicity of the microstructure.
The ideal homogenization of a material would require the perfect defi-nition of both the macroscopic and microscopic geometries, in order to provide an accurate global property definition from the local property definition.

Therefore, a perfect periodicity of the material helps in a rigorous and complete definition of the material. As it is very rare to be in such framework, two cases can be considered:

- Non-periodic material and statistic modeling.
  Several studies have been conducted to generalize homogenization methods to non-periodic materials. It can be done through the introduction of prerequisites at the macroscale, for example an elastic macroscopic behavior such as in [88], or the statistic determination of the RVE.
- However, some materials can be considered periodic. This allows the perfect definition of the material, facilitates the determination of the boundary conditions at both scales and the averaging step [84].

Once the assumptions are properly settled, the mathematical formulation can be settled.

2.3.3.3 Theoretical Background

The period previously mentioned constitutes the Representative Volume Element (RVE). The definition of the RVE needs to match the geometrical recurrences and particularities of the actual heterogeneities; it also has to fulfill the requirements of the mathematical accuracy of the homogenization technique. The scale separation assumption involves a parameter called the scale ratio,ϵ. It defines the quantity between:

- The microscopic RVE scale of characteristic length l, represented and described by the variable y.
- The macroscopic scale of characteristic length L, represented and described by the variable x.

ϵ needs to be as small as possible to validate the scale separation assumption:

$$\epsilon = \frac{l}{L} << 1 \qquad (2.3)$$

Thus, a physical quantity ϕ can be formulated properly across the scales and built within asymptotic expansions in the power of ϵ (the exponent

referring to the order number).

$$\phi = \phi^0(x, y) + \epsilon \phi^1(x, y) + \epsilon^2 \phi^2(x, y) + \dots \qquad (2.4)$$

Finally, as ϵ is defined as in the Equation 2.3, the gradient operator becomes:

$$\nabla = \nabla_x + \frac{1}{\epsilon} \nabla_y \qquad (2.5)$$

where the subscript x refers to the macroscale and y to the microscale.

The use of the Equations 2.3, 2.4 and 2.5 in the variable definition of the considered problem will allow for the settlement of the homogenized equations.

2.4 Fluid description in a porous material

A multiscale model allows the description of a poroelastic material. However, considering the pores of a saturated material, a description of the fluid flows within the material is required to be complete and to consider the fluid component in the material global behavior.

Fluid flows in porous materials are the subject on many studies. In Biot's theory, Darcy's law is used to describe the fluid behavior in the solid matrix.

Several mathematical models have been developed in the last decades in order to have an accurate description of fluid flows in porous media. Since Darcy's law, in the mid-19th century, many researchers have been working to find the more precise way to describe the behavior of fluid through porous materials. This description is decisive to provide rigorous mechanical analysis of porous materials imbibed with fluids.

2.4.1 Darcy's experimental study

The most basic way to express fluid flows in a porous material is to use the Darcy's law, established in 1856. From experiments on fluid flows

of sand beds [89], Darcy showed that the total discharge is proportional to the total pressure drop, divided by the fluid viscosity. It basically says that the pressure gradient ∇p in one direction is directly proportional to the mean velocity of the fluid v_f in the porous media:

$$\nabla p = -\frac{\mu}{k} v_f \tag{2.6}$$

k and   being respectively the permeability of the porous media and the viscosity of the considered fluid.

However, to extend Darcy's law applicability to more complicated configurations of fluids flows that the ones originally considered by Darcy, several corrections have been investigated [90].

2.4.2 Additional terms

In order to extend the domain of validity of Darcy's law and to fit at best with as many porous media and fluid associations, many attempts have been made to correct and adjust this formulation.

For a proper and precise definition of the fluid flows in a porous structure and to extend the domain of validity of Darcy's law, this expression can be corrected by two terms, taking into account specific physical aspects: the Forchheimer correction term and the Brinkman correction term [91, 92].

2.4.2.1 Forchheimer correction's term

The Forchheimer term has been added to introduce the nonlinear aspect, which can be significant as the fluid velocity increases. It requires a parameter called the Forchheimer coefficient C_f, believed to be fixed for a given class of porous media and dimensions [91].

In this case, Equation 2.6 is modified as follows:

$$\nabla p = -\frac{\mu}{k} v_f - \frac{\rho C_f}{\sqrt{k} v_f{}^2} \tag{2.7}$$

ρ being the density of the considered fluid.

As the Forchheimer's equation is constituted of the Darcy term and another term, one can note that the ratio of both these terms lead to a

term representing the Reynolds number. The only difference is that it considers the permeability of the material:

$$R_{ef} = \frac{\rho\sqrt{k}}{\mu}v_f \tag{2.8}$$

Therefore, comparing this number to one, we can estimate the importance of the inertial effects in the considered flow.

2.4.2.2 Brinkman's correction term

In order to provide information on the interaction between the fluid and the walls of the pores, a diffusion term may be added to the mathematical description, as developed by Brinkman in 1947 [92].

The Brinkman term corresponds to a diffusion term that is added to Darcy's law to consider the interface phenomena between the fluid and the wall of the pores. It is an empirical term that involves an effective viscosity parameter μ_{eff}, and it is formulated as follows:

$$\nabla_p = -\frac{\mu k}{v_f} - \mu_{eff}\Delta v_f{}^2 \tag{2.9}$$

Because it involves the second derivative of the velocity, the relevancy of the Darcy-Brinkman model is determined by the velocity variations within the fluid flow.

The effective viscosity μ_{eff} is a parameter widely discussed in the literature and determine the applicability domain of the Darcy-Brinkman's equation.

2.4.2.3 The effective viscosity parameter

Since 1947, many researches were led on the effective viscosity, finding no clear consensus about its determination. However, it appeared that several aspects can be involved in the determination of the effective viscosity:

- The considered type of fluid
- The velocity of the fluid
- The porosity of the material

- Its permeability
- The bounding walls

Overall, it has been admitted that the effective viscosity is more a material parameter depending on the structure of the pores than simply a fluid parameter. It is often presented as a function of porosity of the porous medium.

Different kinds of porous structures have been studied in the past: a swarm of particles fixed in space, a bundle of rods, two plates packed with regular arrays of cylinders or channel-type porous medium.

Einstein expression for dilute solutions.
Brinkman initially used Einstein's formula for the viscosity of suspensions, which relates pure fluid viscosity and effective viscosity. It follows the formulation:

$$\mu_{eff} = \mu(1 - 2.5(1 - \phi)) \tag{2.10}$$

Many objections have been formulated regarding this expression of the effective viscosity; for instance, its validity is limited to particularly high porosities (almost 1) [93] and only for the case of suspended particles [94].

Breugem's estimate.
In order to overcome these limitations and to estimate μ_{eff} in the case of channel-type pores, Breugem formulated the following expression of μ_{eff} (for porosities higher than 3/7) [95].

$$\mu_{eff} = \frac{\mu}{2}(\phi - \frac{3}{7}) \tag{2.11}$$

This formulation comes from matching the macroscopic Brinkman solution to the volume average of the Stokes solution for microscopic flows.

Study of the ratio between dynamic and effective viscosity.
Usually, the accuracy of using Brinkman's formulation for fluid flows in a porous media is determined by the study of the ratio between dynamic and effective viscosity.

It has been found that this ratio can go from slightly less than unity to as high as 10. Still mainly depending on the geometry of the pores, the

magnitude of the viscosity ratio needs to be close to 1 in order to satisfy the non-slip boundary conditions at the bounding walls [96].

Even if the exact value of effective viscosity is still wildly discussed, one consensus is reached regarding the porosity: the effective viscosity parameter is relevant in the cases of high porosity and so is the use of Brinkman's formulation for fluid flow description [93, 97, 95, 96, 98]. One can note that all of these investigations are conducted with the hypothesis that the porous materials are constituted of a spatially uniform porosity [95].

Porous media can become heterogeneous, in terms of porosity, near macroscopic boundaries or when submitted to certain amount of loading. Indeed, these conditions involve changes in the geometry of the pores, but also a change in the permeability of the material [98].

2.4.3 In the case of bone

The aim of choosing a poroelastic model to model bone is mostly to consider the fluid part in its mechanical behavior, as it plays an important role in osteocyte activation. Therefore, the choice of the mathematical law dictating bone fluid flow requires a particular focus in order to choose the most appropriate one.

As it has been presented in the previous chapter, fluid flow in a porous material is usually following Darcy's law. This law can be refined with the introduction of two optional parameters depending on specific conditions.

2.4.3.1 Critical case definition

To evaluate the relevance of other terms of the chosen fluid flow law, in the framework of our study, a focus is put on the critical loading conditions of the hip. From these critical loading conditions, it will be possible to design a corresponding critical case. The study of this worst-case scenario will allow for the validation of the most appropriate mathematical law of the fluid description.

Especially, as presented in the previous Chapter, the Forchheimer's term is relevant to consider inertial effects in fluid flows. This is why the focus is put on the most demanding loading case.

Loadings of the hip.

Due to its position in the human body, the hip is the location of numerous loading cases that generate severe loading concentrations. Among them running, climbing stairs, stumbling or standing up are some of the most critical examples. To quantify these loadings, two approaches can be considered:

- A computational approach, which has the benefit to be non-invasive and easily repeatable, but might be imprecise [99].
- An *in vivo* measurement approach that requires a large set up of instrumented devices and post-treatment softwares, but provides real time information and values, as detailed in [100] and [101].

Both these methods agree on the fact that stress in the hip is subjected to large variations, with the presence of high peaks, whose values are largely discussed in the literature. In [100]the study of the variations of the hip loading is done in the perspective of providing standardized data for implant design purposes. The aim of these studies is to measure the contact forces in the joint with instrumented hip implants in subjects during frequent and demanding physical activities, as climbing stairs of standing up. The measured values are expected to increase during sport activities or unpredictable loading, for instance stumbling. In this last case, a peak that reach 11000 N is measured in [101], whereas in everyday life it usually does not exceed 4000 N.

In [102] the pressure in the hip is measured through a transducer in which it is found that the more the pressure is measured a long time after the surgery, the more its value is important, as the musculature and healing around the hip is achieved. The data also reveals very high local and non-uniform pressures, up to 18000 MPa during the rising up of a chair.

This last measure as been found on a two subjects study, and a value as large as 18000 MPa as not been found again since. However, as it is

the most important one and regarding the purpose of the critical case definition, this one has been selected for the proposed analysis.

Geometry and boundary conditions of the critical case.
Considering the data compiled above, the aim here is to put in place a critical test case to study how the fluid into the bone flows under extreme conditions. As for the configuration of the hip and the circumstances of these extreme load case, the solicitation can be approximated by a compression load. Consequently, the simulation of the bone loading has been reduced to a simple bone cube under compression, which is supposed to give the maximal value of the pressure in the bone under these conditions.

2.4.3.2 Elimination of the Forchheimer's term

From the previously determined critical case, it is possible to conclude on the relevancy of the Forchheimer term in the case of the present work.

To do so, it is required to calculate the Reynolds number corresponding to this configuration, as the Forchheimer's term represents the inertial effects in the fluid flow. According to the expression of the Reynolds number given in the previous chapter, it is calculated from the maximal value found for the velocity magnitude, corresponding to the critical case.

Indeed, in a cube under a compressive load of 18000MPa, and with pore in shape of canals of 10 μm of diameter as it is supposed here, the Darcy's pressure is computed in order to have its order of magnitude in this case. Through the algorithm developed further, it is possible to compute the corresponding velocity of the fluid, and thus the Reynolds number corresponding to this flow. With bone fluid properties and with the value of the maximal magnitude of the fluid velocity (found at $2,48.10^{-10}$ mm/s), the Reynolds number is equal to $3,94.10^{-9}$, which is largely inferior to 1. This allows for asserting that inertial effects are negligible in the femur, in a specific mechanically demanding situation. The use of the Forchheimer term in the computation of the pressure is therefore not necessary.

2.4.3.3 Elimination of the Brinkman's term

As it has been developed above, the introduction of the Brinkman's term in the fluid flow description is a widely discussed subject. As this term allows for imposing the continuity of the velocities and tangential forces at the interface between the solid and the fluid part, the inclusion of the wall interaction between the pores and the fluid is thus possible.

However, the relevancy of considering this term in the framework of the study presented here can be questioned. As it has been previously mentioned, a consensus is reached concerning the minimal porosity from which the conservation of the Brinkman's term is relevant. In the case of the porosity of the lacunar-canalicular system considered here is estimated to 5%. Therefore, following this consideration, the value is too low to be considered in the Brinkman formulation.

But this may be valid only when only the hydraulic component of bone fluid is considered. Indeed, as its composition is complex, as is bone material and therefore the solid matrix, this can involve another level of discussion on this topic.

A feature of bone fluid that needs to be accounted for is that it is electrically charged. This term can therefore be kept to consider the electro-osmotic and osmotic contributions in nanoscopic fluid flows, and the presence of the peri-cellular matrix. In this case, a specific permeability at this very local scale is introduced, in which the interaction between the well of the pores and the fluid can no longer be neglected [65, 66].

From these considerations, the use of the Brinkman's correction term appears to be particularly relevant when the scope of interest is very local and when the aim is to provide a very precise description of the events occurring at a scale lower than the microscale. In the case of the study presented here, one of the main stakes is to provide a relevant compromise between the macroscopic model and an accurate description of the microscopic events. For this reason, the use of this term does not appear consistent and therefore is not considered in the formulation of the fluid flow mathematical law.

In the end, considering the assumptions of the developed model and

the perspectives that are foreseen for its application, the mathematical law describing the fluid flow can be established. Thus, the fluid pressure and the fluid velocity in the cortical bone are calculated with Darcy's law added to the fluid accumulation term, as at will be developed and detailed in the following Chapter. This fluid accumulation term will allow for the accounting of the solid matrix deformation in the pressure computation, providing the fluid-structure interaction dimension to the numerical model.

2.5 Conclusion

This chapter presents the numerical framework developed within this thesis. Considering the final aim of the project, which is to build a predictive tool of bone remodeling, and its applications, the equilibrium between accuracy and efficiency is crucial to achieve. This dictated our choices in modeling, directing our work toward a poroelastic model in order to consider the fluid flows in the bone, which are very important for bone remodeling. The choice of a multiscale formulation allows then for considering the different scales involved in the process.

This lead to the development of a multiscale poroelastic model, set up with a homogenization technique with a proper definition of the Representative Volume Element, and the corresponding algorithm developed in order to easily compute bone numerical simulation, as it will be developed in the following Chapter.

Numerical Development and Application

The framework of the numerical development has been settled in the previous Chapter, in order to have all the elements in hand to develop a multiscale poroelastic model of bone.

First, the mathematical development of the concerned equations is performed within the homogenization technique, and an algorithm is developed step-by-step to ensure the numerical consistency of the procedure. Allowing the numerical simulation of poroelastic material within a multiscale formulation, it is then possible to apply it to bone numerical modeling. Each presented step needs to be achieved to complete the overall material modeling.

Once the material properties have been determined, one needs to compute the effective properties to solve the RVE problem. The chosen RVE needs to fulfill geometrical requirements of the heterogeneous microstructure and be submitted to the boundary conditions derived from the homogenization technique. Then, the pressure is computed, as required by the expression of the stress in the poroelastic material, to finally have all the required elements for the computation of the multiscale poroelastic problem.

3.1 Multiscale poroelastic modeling of bone

The literature review previously presented in this Chapter set the framework for the model developed here.

In the case of bone modeling, in which is the topic of the work presented here, the modeled bone microstructure corresponds to the lacunar-canalicular system. As in any biological structure, a perfect periodicity cannot be achieved regarding the continuous remodeling of bone tissue. However, in the context of cortical bone in the femur, where the structure is notably organized along the principal mechanical loading, the regularity of the canaliculi and the lacunae is considered to be a valid assumption [94, 103].

3.1.1 Representative Volume Element definition

In order to settle the framework of the homogenization technique in the context of poroelastic modeling, an appropriate RVE needs to be carefully chosen.

The RVE must represent the microstructure of the poroelastic material under consideration. Keeping in mind the final aim of the developed model, and considering the structure of the bone matrix, the pore shape is composed of communicating canals. The size is determined from the biological dimension of the lacunar-canalicular system that has to be modeled, corresponding to a porosity of about 5% [59] (See Figure 3.1).

3.1.1.1 The solid part

The solid portion of this RVE (referred to by the symbol Ω_s) is considered to be elastic. The viscoelastic component of the bone mechanical behavior is attributed in this model to the fluid part.

Furthermore, being the model developed mainly with the aim of predicting bone remodeling and the structural changes in bone, the solid part is considered isotropic and evolving according to the small deformation assumption.
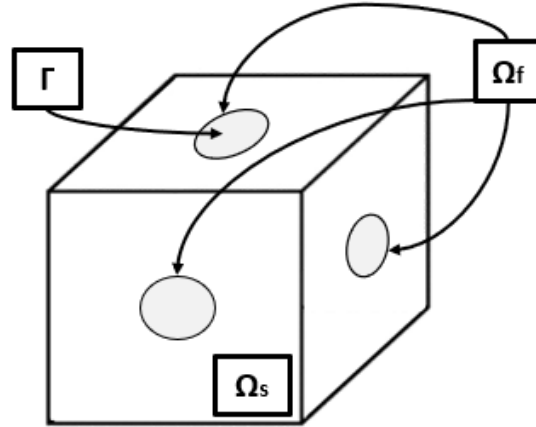
Figure 3.1: **Representation of the chosen RVE for the modeling of bone.**

Regarding its geometry, at this scale, the porosity of the bone is estimated at 5% and the diameter of the canals considered is on the order of 0.3 μm [59]. Thus, the poroelastic RVE is a drilled cube of 100 μm length with 10 μm canals, as shown in Figure 3.1.

3.1.1.2 The fluid part

The bone fluid is assumed to saturate the pores and is referred to by the symbol Ω_f . However, its exact composition and viscosity are assimilated to the one of interstitial fluid, as it is difficult to analyze it.

Interstitial fluid is defined as the fluid "interposed between the plasma and the cells [...], with an ionic composition similar to that of plasma" [104], even it is an assumption widely discussed [60]. As it is mainly composed of water, it is considered incompressible and Newtonian. Its viscosity is estimated to the one of saline water at 37°C [59].

3.1.2 Mathematical Development

Once the RVE is defined, the general equations can be given and developed with the homogenization technique.

3.1.2.1 General Equations

At the macroscale, the poroelastic material is considered homogeneous, isotropic and saturated by a fluid as defined in the RVE.

In the solid portion.
In Ω_s, without external forces and under the assumption of small deformations, the equation of motion is written:

$$\nabla \cdot \sigma_s = \vec{0} \tag{3.1}$$

where σ_s is the stress tensor in the solid matrix.

As the solid matrix is considered elastic, one can write $\sigma_s = C : E(\vec{u_s})$, where C is the corresponding elastic tensor, $E(\vec{u_s})$ the strain tensor and $\vec{u_s}$ the displacement vector in the solid portion.

In the fluid portion.
In Ω_f, without external forces, the equations of motion are written:

$$\nabla \cdot \sigma_f = \vec{0} \tag{3.2}$$

where σ_f is the stress tensor in the fluid and is defined as

$$\sigma_f = -p_f \delta + 2\mu D(\vec{v}_f) \tag{3.3}$$

with p_f the pressure of the fluid and μ, δ being the identity tensor, $D(\vec{v}_f)$ the strain rate tensor in the fluid and $\vec{v}_f$ the velocity vector in the fluid.

This latter is defined by the following equation of motion:

$$\nabla \cdot \vec{v}_f = q \tag{3.4}$$

q is the derivative of the expression for the fluid accumulation in the RVE, defined by:

$$q = \frac{1}{Q}\dot{p}_f + bTr(E(\dot{\vec{u}_s})) \tag{3.5}$$

Equation (3.5) involves Q, the Biot modulus that considers the compressibility, and b, the Biot coefficient expressed with the bulk modulus of the drained solid matrix and the solid matrix itself:

$$Q = (\frac{b - \Phi}{K_b} + \frac{\Phi}{K_f})^{-1} \tag{3.6}$$

$$b = 1 - \frac{K_b}{K_s} \tag{3.7}$$

where K_s, K_b and K_f are, respectively, the bulk modulus of the solid part, of the drained skeleton and of the fluid phase.

At the interface.

Between the two parts, at the interface called Γ, continuity conditions are applied:

$$\vec{v}_f = \frac{\partial \vec{u}_s}{\partial t} \tag{3.8}$$

$$\sigma_f \vec{n} = \sigma_s \vec{n} \tag{3.9}$$

where $\vec{n}$ is the normal vector to the interface.

3.1.2.2 Application of the homogenization technique

Within the poroelastic material, the three unknown variables of the considered system, as presented in the previous section (3.1.2.1) are the displacement in the solid part $\vec{u}_s$, the velocity of the fluid $\vec{v}_f$, and the pressure of the fluid p_f.

According to the homogenization technique previously described, these three variables are written in the form of an asymptotic expansion (2.4):

$$\vec{u}_s(x,y,t) = \vec{u}_s^{\,0}(x,y,t) + \epsilon \vec{u}_s^{\,1}(x,y,t) + o(\epsilon^2)) \tag{3.10}$$

$$\vec{v}_f(x,y,t) = \vec{v}_f^{\,0}(x,y,t) + \epsilon \vec{v}_f^{\,1}(x,y,t) + o(\epsilon^2)) \tag{3.11}$$

$$p_f(x,y,t) = p_f^0(x,y,t) + \epsilon p_f^1(x,y,t) + o(\epsilon^2)) \tag{3.12}$$

It is reminded that the exponents are referring to the orders 0, 1 and 2.

Introducing the Equation (3.10), (3.11) and (3.12) in the conservation laws (3.1), (3.2) and (3.4) and using the gradient operator as defined in the previous Chapter (2.3.3.3) in the presentation of the homogenization technique, we obtain (as a reminder, the subscript x refers to the macroscale and the subscript y to the microscale): In Ω_s

$$\epsilon^{-2}\nabla_y \cdot \sigma_s^{-1} + \epsilon^{-1}(\nabla_x \cdot \sigma_s^{-1} + \nabla_y \cdot \sigma_s^{0}) + \epsilon^0(\nabla_x \cdot \sigma_s^{0} + \nabla_y \cdot \sigma_s^{1}) + \epsilon \nabla_x \cdot \sigma_s^{1} = \vec{0} \tag{3.13}$$

In Ω_f

$$\epsilon^{-1}\nabla_y \cdot \vec{v}_f{}^0 + \epsilon^0(\nabla_x \cdot \vec{v}_f{}^0 + \nabla_y \cdot \vec{v}_f{}^1) + \epsilon^1\nabla_x \cdot \vec{v}_f{}^1 = q \tag{3.14}$$

$$\epsilon^{-1}\nabla_y \cdot \sigma_f{}^0 + \epsilon^0(\nabla_x \cdot \sigma_f{}^0 + \nabla_y \cdot \sigma_f{}^1) + \epsilon^1(\nabla_x \cdot \sigma_f{}^1 + \nabla_y \cdot \sigma_f{}^2) +$$
$$\epsilon^2(\nabla_x \cdot \sigma_f{}^2 + \nabla_y \cdot \sigma_f{}^3) + \epsilon^3\nabla_x \cdot \sigma_s{}^3 = \vec{0} \tag{3.15}$$

On Γ

$$(\epsilon^{-1}\sigma_s{}^{-1} + \epsilon^0\sigma_s{}^0) + \epsilon\sigma_s{}^1)\vec{n} = \epsilon^0\sigma_f{}^0 + \epsilon^1\sigma_f{}^1 + \epsilon^2\sigma_f{}^2 + \epsilon^3\sigma_s{}^3\vec{n} \tag{3.16}$$

$$\epsilon^0\vec{v}_f{}^0 + \epsilon^1\vec{v}_f{}^1 = \epsilon^0\frac{\partial \vec{u}_s{}^0}{\partial t} + \epsilon^1\frac{\partial \vec{u}_s{}^1}{\partial t} \tag{3.17}$$

The tensors are defined as in the following.

In Ω_s:

$$\sigma_s{}^{-1} = C : E_y(\vec{u}_s{}^0) \tag{3.18}$$

$$\sigma_s{}^0 = C : (E_x(\vec{u}_s{}^0 + E_y(\vec{u}_s{}^1)) \tag{3.19}$$

$$\sigma_s{}^1 = C : E_x(\vec{u}_s{}^1) \tag{3.20}$$

In Ω_f:

$$\sigma_f{}^0 = -p_f^0\delta \tag{3.21}$$

$$\sigma_f{}^1 = -p_f^1\delta + 2\mu D_y(\vec{v}_f{}^0) \tag{3.22}$$

$$\sigma_f{}^2 = 2\mu(D_x(\vec{v}_f{}^0) + D_y(\vec{v}_f{}^1)) \tag{3.23}$$

$$\sigma_f{}^3 = 2\mu D_y(\vec{v}_f{}^1) \tag{3.24}$$

The idea is now to proceed by identification, i.e. analyzing the previous equations according to the powers of ϵ. This gives:

For the Equation (3.15) at the order ϵ^{-1}:
We have $\sigma_f^0 = v$ and $\nabla_y \cdot \sigma_f{}^0 = 0$ that gives

$$\nabla_y p_f^0 = 0 \tag{3.25}$$

That implies that the pressure p_f^0 does not depend on y.

For the Equation (3.13) at the order ϵ^{-2} and the Equation (3.16) at the order ϵ^{-1} :
We have $\sigma_s^{-1} = C : E_y(\vec{u_s}^0)$ to replace in $\nabla_y \cdot \sigma_s^{-1} = 0$ and $\sigma_s^{-1}\vec{n} = \vec{0}$ that implies that $\vec{u_s}^0$ admit one and only solution, independent from y.

3.1.2.3 Equations at the local scale

At the local scale, the microscopic displacements in the RVE are obtained from Equation (3.13) at the order ϵ^{-1}:

$$\nabla_x \cdot \sigma_s^{-1} + \nabla_y \cdot \sigma_s^{0} = 0 \tag{3.26}$$

and

$$\sigma_s^{0}\vec{n} = \sigma_f^{0}\vec{n} \tag{3.27}$$

becoming

$$\nabla_x \cdot (C : E_y(\vec{u_s}^0)) + \nabla_y \cdot (C(: E_x(\vec{u_s}^0) + E_y(\vec{u_s}^1))) = 0 \tag{3.28}$$

and

$$C : (E_x(\vec{u_s}^0 + E_y(\vec{u_s}^1)))\vec{n} = -p_f^0\delta\vec{n} \tag{3.29}$$

but as we just established that $\vec{u_s}^0$ is independent from y, leaving only:

$$\nabla_y \cdot (C : (E_x(\vec{u_s}^0) + E_y(\vec{u_s}^1))) = 0 \tag{3.30}$$

and

$$C : (E_x(\vec{u_s})^0 + E_y(\vec{u_s})^1)\vec{n} = -p_f^0\delta\vec{n} \tag{3.31}$$

Solving the system composed of the Equations (3.30) and (3.31) for $\vec{u_s^1}$ and knowing that it admits only one solution, we deduce that $\vec{u_s^1}$ consists of the superposition of two particular solutions ($\vec{\xi}^{kl}$ and $\vec{\eta}$) of this system, solved within two particular sets of boundary conditions (4.1) and (4.2).

$$p_f^0 = 0; E_x(\vec{u_s}^0) = \frac{1}{2}(\delta_{jl} \cdot \delta_{km} + \delta_{jm} \cdot \delta_{kl}) \tag{3.32}$$

with k and h fixed.

$$p_f^0 = 1; E_x(\vec{u_s}^0) = 0 \tag{3.33}$$

3.1.2.4 Equations at the global scale

Equilibrium equation [105]

The aim is now to write the equation at the macroscopic scale. It is obtained from the Equations (3.13) and (3.15) at the order ϵ^0 and the Equation at the interface (3.16) at the order ϵ^1.

This gives in Ω_s:

$$\nabla_x \cdot \sigma_s{}^0 + \nabla_y \cdot \sigma_s{}^1 = \vec{0} \tag{3.34}$$

In Ω_f:

$$\nabla_x \cdot \sigma_f{}^0 + \nabla_y \cdot \sigma_f{}^1 = \vec{0} \tag{3.35}$$

And on Γ:

$$\sigma_s{}^1 \vec{n} = \sigma_f{}^1 \vec{n} \tag{3.36}$$

These three last equations enable the writing of the final equilibrium equation.

The total stress is the sum of the stress in the solid and in the fluid part.

$$\sigma_{total} = \sigma_s{}^0 + \sigma_f{}^0 \tag{3.37}$$

Transposing this expression in the equilibrium equations (3.34) and (3.35), integrating on the cell and taking into account the boundary condition (3.36):

$$\sigma_{total} = \sigma_s{}^0 + \sigma_f{}^0 \tag{3.38}$$

The averaging symbol $< \cdot >$ on the elementary cell indicates $< \cdot > = \dfrac{1}{\Omega} \int \cdot d\Omega$ where Ω is the cell volume.

$$\nabla_x \cdot < \sigma_{total}^0 > = \vec{0} \tag{3.39}$$

That finally gives:

$$< \sigma_{total}^0 > = C_{eff} : E_x(\vec{u}_s{}^0) - \alpha p_f^0 \tag{3.40}$$

where C_{eff} and α are respectively the effective elastic property tensor and the effective Biot tensor, defined as follows:

$$C_{ijkl}^{eff} = < C_{ijkl} + C_{ijmn} : E_y(\vec{\xi}^{kl}) > \tag{3.41}$$

$$\alpha_{ij} = \Phi \delta_{ij} + < C_{ijmn} : E_y(\vec{\eta}) > \tag{3.42}$$

Fluid flow equation

The equation of the fluid flows is obtained from the Equation 3.14 at the order ϵ^{-1} and the Equations (3.15) and (3.17) at the order ϵ^0.

In Ω_f:

$$-\nabla_x p_f^0 - \nabla_y p_f^1 + 2\mu \nabla_y (D_y(\vec{v_f^0})) = 0 \tag{3.43}$$

and

$$\nabla_y \vec{v_f^0} = 0 \tag{3.44}$$

and on Γ:

$$\vec{v_f^0} = \frac{\partial \vec{u_s^0}}{\partial t} \tag{3.45}$$

To solve this system of equations, we introduce a change of variable, defining $\vec{w_f^0} = \vec{v_f^0} - \frac{\partial \vec{u_s^0}}{\partial t}$, transforming this system in the following equations.

In Ω_f:

$$-\nabla_x p_f^0 - \nabla_y p_f^1 + \mu \nabla_y (D_y(\vec{w_f^0})) = 0 \tag{3.46}$$

and

$$\nabla_y \vec{w_f^0} = 0 \tag{3.47}$$

and on Γ:

$$\vec{w_f^0} = 0 \tag{3.48}$$

This system admits a unique solution as explained in [105], which involves a parameter k, defined as the intrinsic permeability of the porous material. In the end, we obtain, in Ω_f:

$$\vec{w_f^0} = -\frac{k}{\mu} \nabla_x p_f^0 \tag{3.49}$$

which corresponds to the Darcy's law and demonstrating, by the homogenization technique, the experimental results presented in the 2.4.1.

3.1.3 Corresponding algorithm

In order to transpose these equations to a numerical code, a solution algorithm is developed. It is articulated through the commercial softwares Abaqus and MATLAB (Figure 3.2).
The main components of the solution alghorithm are described below:

1. **INPUTS**

   The geometry, the mesh, the material properties and the boundary conditions, both in the structure and in the fluid, are defined and given as inputs to the code.

2. **RESOLUTION OF THE RVE PROBLEM**

   To determine the effective properties required for the computation of the stresses in the poroelastic material, and after the determination of the RVE geometry, the resolution of the microscale problem is performed. It involves the boundary conditions defined in 3.1.2.3 (Equations (4.1) and (4.2)) and the mathematical development of the homogenization technique. The boundary conditions are introduced in ABAQUS and the RVE problem is solved by the Finite Elements Method. The results and corresponding effective properties are then calculated in MATLAB.

3. **COMPUTATION OF THE PRESSURE**

   During this step, the pressure of the fluid in the porous material is computed. This is done by the finite difference method on MATLAB. The pressure computation account for the fluid accumulation into the pores. The convergence is considered reached when the pressure variation between two iteration at each node.
   Once it is reached, pressure is computed without external force (loading or structural strain) to let fluid stabilization occurring.

4. **COMPUTATION OF THE STRESS**

   All the elements are now gathered to compute the stress in the poroelastic material, according to the Equation (3.40). The introduction of the effective properties and the pressure component is done by the writing of a UMAT subroutine in Fortran within the Abaqus code.

5. **OUTPUTS**

As the fluid accumulation in the porous material and its impact on the strain is considered, the convergence in the pressure is checked before finishing the computation. In the end, the stress and strain distributions can be extracted, as well as the displacements under the considered set of macroscopic boundary conditions. This allows, for instance, the computation of the apparent Young Modulus, giving information on the equivalent stiffness of the poroelastic material. The pressure distribution can be as well extracted, in order to study the pressure distribution evolution inside the porous material.
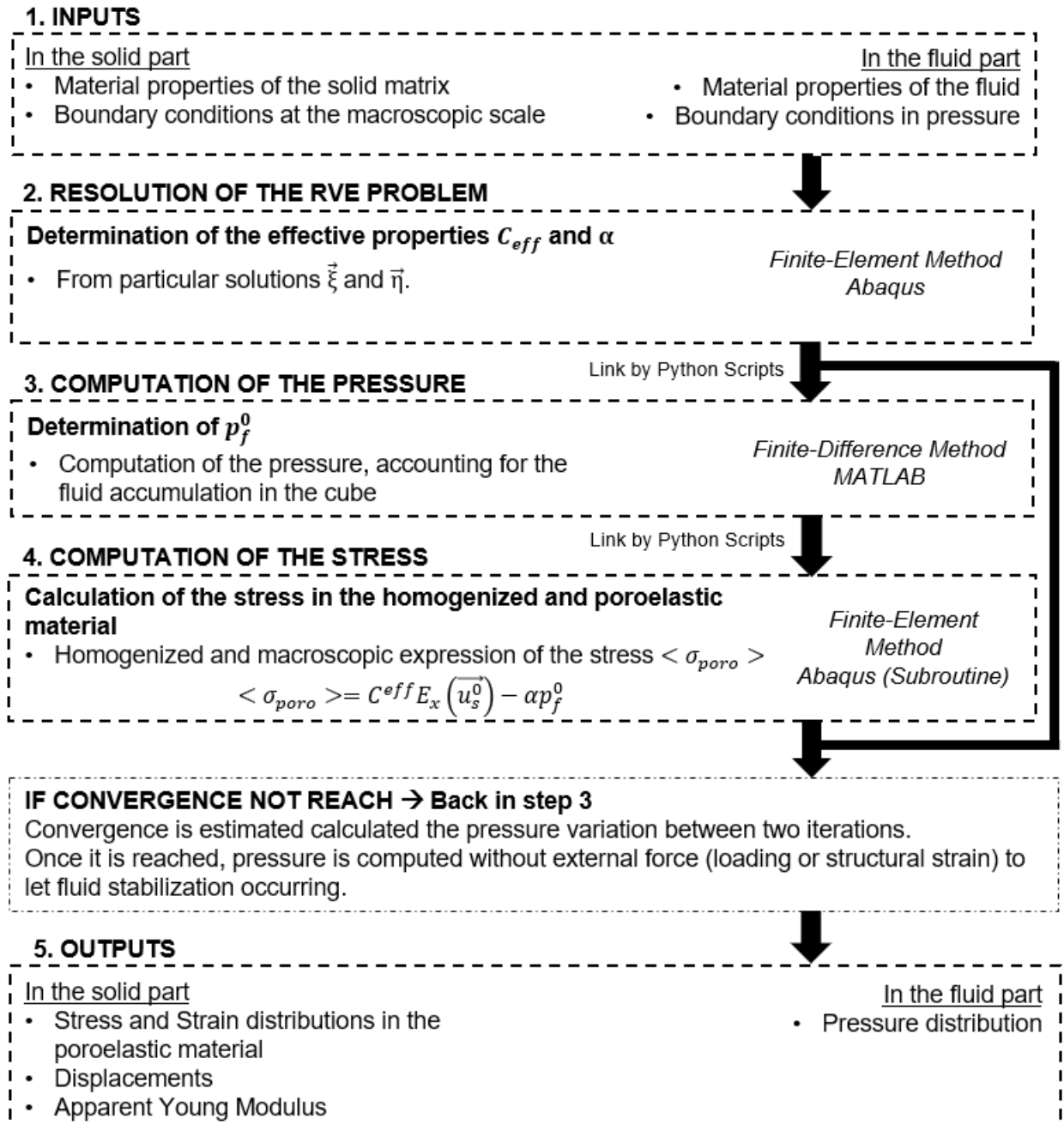
1. INPUTS

In the solid part
- Material properties of the solid matrix
- Boundary conditions at the macroscopic scale

In the fluid part
- Material properties of the fluid
- Boundary conditions in pressure

2. RESOLUTION OF THE RVE PROBLEM

Determination of the effective properties C_{eff} and α

- From particular solutions $\vec{\xi}$ and $\vec{\eta}$.

Finite-Element Method
Abaqus

Link by Python Scripts

3. COMPUTATION OF THE PRESSURE

Determination of p_f^0

- Computation of the pressure, accounting for the fluid accumulation in the cube

Finite-Difference Method
MATLAB

Link by Python Scripts

4. COMPUTATION OF THE STRESS

Calculation of the stress in the homogenized and poroelastic material
- Homogenized and macroscopic expression of the stress $< \sigma_{poro} >$

$$< \sigma_{poro} > = C^{eff} E_x \left(\vec{u_s^0} \right) - \alpha p_f^0$$

Finite-Element Method
Abaqus (Subroutine)

IF CONVERGENCE NOT REACH → Back in step 3
Convergence is estimated calculated the pressure variation between two iterations.
Once it is reached, pressure is computed without external force (loading or structural strain) to let fluid stabilization occurring.

5. OUTPUTS

In the solid part
- Stress and Strain distributions in the poroelastic material
- Displacements
- Apparent Young Modulus

In the fluid part
- Pressure distribution

Figure 3.2: **Flowchart of the algorithm developed for the numerical multiscale study of a poroelastic material.**

3.2 Inputs (Algorithm Step 1)

Before proceeding to any computation, a careful attention to the material inputs needs to be provided. In our framework, the modeled material is cortical bone and its lacunar-canalicular system. This corresponds to a solid matrix composed of bone material, filled with bone fluid. During the computation, the material is submitted to a set of loads and boundary conditions that require an accurate definition.
The material properties are summarised in Table 3.1.

3.2.0.1 For the solid part

As it has been exposed in the previous Chapter, the mechanical properties of the solid bone matrix are difficult to assess, due to the complexity of bone structure and the difficulty to conduct experimental tests in reproducible conditions.

The value of 14000 MPa for the elastic modulus is chosen, as it has been found through nano-indentation tests performed in our laboratory and as it matches the range of value found for such bone in literature presented above [38, 45].

3.2.0.2 For the fluid part

Bone fluid and its properties are difficult to indentify as it has been previoulsy mentionned. However, as its composition seems to correspond to saline water, the chosen properties for the fluid part are corresponding to saline water, at 37°C.

3.2.0.3 Geometry, mesh and boundary conditions

The developed model is extended across two scales. Its geometry is defined to represent the microstructure of the material and its mesh is determined for its correct computation. With the homogenization technique, the boundary conditions at the microscale are defined within the mathematical development and are therefore implemented during the computation of the RVE problem (i.e. the following step).

Solid part: elastic cortical bone	
E (Young Modulus)	14000 MPa
ρ (Density)	1.6 g/cm^3
ν (Poisson's coefficient)	0.3
k (Material permeability)	1.5e^{-14} mm^2
Fluid part: interstitial fluid	
μ (Dynamic viscosity)	6.5 (mPa.s)

Table 3.1: Cortical bone material properties used as input in the poroelastic model [59].

At the macroscale, the geometry corresponds to the macroscopic size and shape of the bone sample that the model aims to reproduce. The mesh is defined by the size of the RVE to have a perfect match between the two scales. In this first case, the geometry is a 2x2x2 mm^3 length cube composed of 8000 elements. These elements correspond to RVEs and their properties are defined to match their features.

At the macroscale, two sets of boundary conditions need to be settled: in one hand from a structural point of view, in another hand from a fluid point of view. The aim of the definition of these boundary conditions is to model an easily reproducible experimental test, in order to outcome with an equivalent stiffness of the sample and anticipating a further experimental validation.

Structural boundary conditions.
On the solid matrix, the lateral walls of the cube are kept free. The bottom of the cube is considered clamped and all the degrees of freedom are blocked. On the top face, a pressure is applied and an arbitrary linear increase of the pressure is imposed.

The imposed pressure varies from 0.36 to 1.44 MPa, and before each increase of the imposed pressure, a plateau with no pressure variation is left to let the fluid pressure stabilized itself.

Fluid boundary conditions.
From a fluid point of view, on the lateral walls, a reference pressure (set

to zero) is imposed. To match the structural boundary conditions, impermeable conditions are imposed both at the top and at the bottom face. Numerically, the impermeable conditions correspond to:

$$\frac{\partial p}{\partial x} = 0 \tag{3.50}$$

where x is the direction normal to the impermeable face.

3.3 Computation of Effective Properties (Algorithm Step 2)

The computation of the effective properties is done solving the RVE problem at the microscopic level, reminding that they are calculated from the displacements at the microscopic level. This step involves the use of the Abaqus software to define the geometry, the mesh and the boundary conditions, while Python scripts allow for computing the results.

3.3.1 Geometry and meshing

3.3.1.1 Definition of the geometry and meshing

As it has been settled in the previous chapters, the microscale aims to represent the lacunar-canalicular level in bone structure. This is the location of bone cells, especially osteocytes, which are sensitive to the flows of the fluid in which they are immerged.

The lacunar-canalicular system presents a very complex structure. It is articulated in lacunae, the places where the osteocytes are located, which are communicating through canals called canaliculi. Bone fluid flows in all the lacunar-canalicular system due to mechanical loading and solid matrix deformation, creating movements affecting the osteocytes.

The RVE, in the present model, aims to reproduce a simplified lacunar-canalicular system, representing it as porous canals communicating with

each other, forming a porous solid matrix. The dimensions of the pores are determined according to the biological reality of the lacunar-canalicular system. At this scale, the porosity of the bone is estimated at about 5% and the diameter of the considered canals is on the order of 0.3 μm. However, as the lacuna in which the osteocytes are immerged have a diameter of around 10 μm, the RVE defined here is reduced to a drilled cube of 100 μm length, with 10 μm canals, as previously shown, to fit the 5% porosity constraint. While this choice is not the most faithful representation of the biological reality of the lacunar-canalicular system, and may be improved in a further development, the aim here is to provide a preliminary validation of the proposed methodology.

The resolution of the microscopic RVE model is done within Abaqus. Therefore, the geometry is defined through the options given by this software, so as the meshing.

In order to fit at best with the circular parts of the RVE, tetrahedral elements are chosen and 8830 quadratic elements compose the whole mesh. A mesh convergence has been performed and evaluated on the final value of the effective properties obtained.

3.3.2 Boundary conditions implementation

Two kinds of boundary conditions need to be applied on the RVE to compute the effective properties: the ones that come from the homogenization technique and from the writing of the equilibrium equations at the microscopic level and the ones that come from the assumption of periodicity of the RVE in the methodology development.

3.3.2.1 From the homogenization technique

As it has previously been established, the development of the homogenization technique imposes two boundary conditions at the microscopic level, that consist solutions of the displacement vector at this level. These two sets of boundary conditions are reminded below:

$$p_f^0 = 0; E_x(\vec{u_s}^0) = \frac{1}{2}(\delta_{jl} \cdot \delta_{km} + \delta_{jm} \cdot \delta_{kl}) \tag{3.51}$$

with k and h fixed.

$$p_f^0 = 1; E_x(\vec{u_s}^0) = 0 \qquad (3.52)$$

They result in the separation of two RVE problems in order to solve the two configurations required to compute both of the effective properties: C_{eff} and α.

For the set (**??**), the boundary condition is imposed in the structural portion: a unitary strain field is imposed. It is done thanks to Abaqus subroutine SIGINI, allowing for the definition of the corresponding pre-defined stress fields.

For the second set (**??**), the boundary conditions are imposed where the fluid is interacting with the solid portion, which corresponds to the internal faces. A unitary pressure is imposed on these faces.
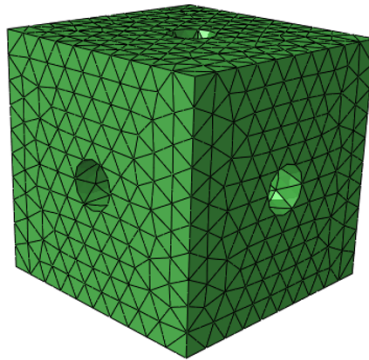
Figure 3.3: **Geometry and mesh definition of the RVE.**

3.3.2.2 Periodic boundary conditions

One of the assumptions for the application of the homogenization technique is the periodicity of the RVE. This periodicity is considered both from a geometrical point of view in the regular distribution of the porosities and involves boundary conditions on the RVE.

In practice, these boundary conditions are defined on each external face with respect to the opposite face. Through a Python script that defines the appropriate set of nodes, it is imposed that each node of external face will move with the exact opposite value as the node located across on the opposite face, see Figure 3.4.
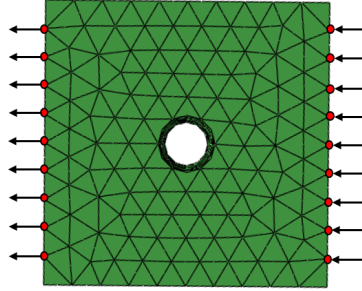
Figure 3.4: ***Representation of the periodic boundary conditions applied on the RVE.***

3.3.3 Results

The computation of the effective properties is done extracting the strain field from Abaqus with Matlab via Python script, following the expressions:

$$C_{ijkl}^{eff} =< C_{ijkl} + C_{ijmn} : E_y(\vec{\xi^{kl}}) > \tag{3.53}$$

$$\alpha_{ij} = \Phi\delta_{ij}+ < C_{ijmn} : E_y(\vec{\eta}) > \tag{3.54}$$
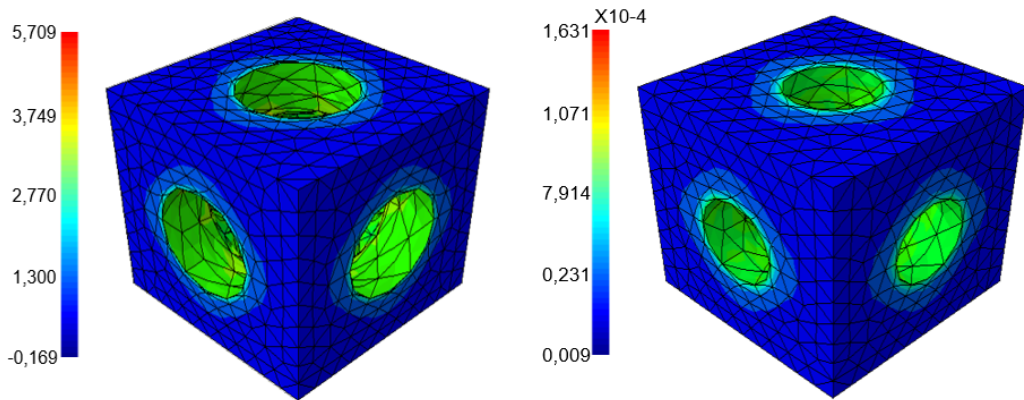
Figure 3.5: ***Strain distribution in the two considered cases (on the left for $\vec{\xi}$, on the right $\vec{\eta}$).***

3.4 Fluid flow description (Algorithm Step 3)

The pressure is a critical element in the mechanical behavior of a poroelastic media. In this work, its computation has been implemented on MATLAB by a Finite Difference Method.

3.4.1 Geometry and mesh

The geometry and the mesh for the computation of the pressure is defined by the ones chosen for the macroscale modeling.

To match the mesh chosen above (Section 3.2.0.3), 8000 nodes are created, corresponding to the 8000 elements of the model at the macroscale, as the aim is to compute the stress in all the RVEs.

3.4.2 The finite differences method

This method is easily applicable and has been proven to be accurate in multiple applications [106]. Here, for the computation of the pressure, it is reminded that the equation to be solved is (3.4: $\nabla \vec{v}_f = q$), in which the derived expressions are discretized with a centered difference scheme on all the three directions $\vec{x}, \vec{y}$ and $\vec{z}$:

$$\left(\frac{\partial^2 p}{\partial x^2}\right)_{i,j,k} = \frac{p_{i+1,j,k} + p_{i-1,j,k} + p_{i,j+1,k} + p_{i,j-1,k} + p_{i,j,k+1} + p_{i,j,k-1} - 6p_{i,j,k}}{\Delta x^2}$$

$$(3.55)$$

$$\left(\frac{\partial^2 p}{\partial y^2}\right)_{i,j,k} = \frac{p_{i+1,j,k} + p_{i-1,j,k} + p_{i,j+1,k} + p_{i,j-1,k} + p_{i,j,k+1} + p_{i,j,k-1} - 6p_{i,j,k}}{\Delta y^2}$$

$$(3.56)$$

$$\left(\frac{\partial^2 p}{\partial z^2}\right)_{i,j,k} = \frac{p_{i+1,j,k} + p_{i-1,j,k} + p_{i,j+1,k} + p_{i,j-1,k} + p_{i,j,k+1} + p_{i,j,k-1} - 6p_{i,j,k}}{\Delta z^2}$$

$$(3.57)$$

where p is the pressure, (i, j, k) the coordinates of the nodes and Δx, Δy and Δz the distance between two nodes.

The discretization method allows the computation of the Equation (3.4) within a MATLAB code.

3.5 Computation of the stress (Algorithm Step 4)

Once all the components involved in the computation of the stress in the poroelastic material are numerically determined, it becomes possible to compute the global macroscale poroelastic simulation. Indeed, the effective properties and the pressure at each node are computed, and the last step is the implementation of the stress gathering all these elements on Abaqus. The corresponding script is written in Python and involves the use of a UMAT subroutine coded in Fortran, which defines the new stress tensor.

3.6 Outputs (Algorithm Step 5)

Allowing the fluid to flow out from the cube as in this simulated case, gives the results showed on Figures 3.6 and 3.7, measured at the times marked with a red point on Figure 3.8.

As the fluid is free to flow out, the solid matrix tends to empty itself. In this case, the load is mainly supported by the structural matrix. This can be seen on the pressure distribution, where it can be noticed that the internal pressure is tending to reach 0 (the reference pressure value) at the end of the simulation. At the bottom of the cube, internal stresses
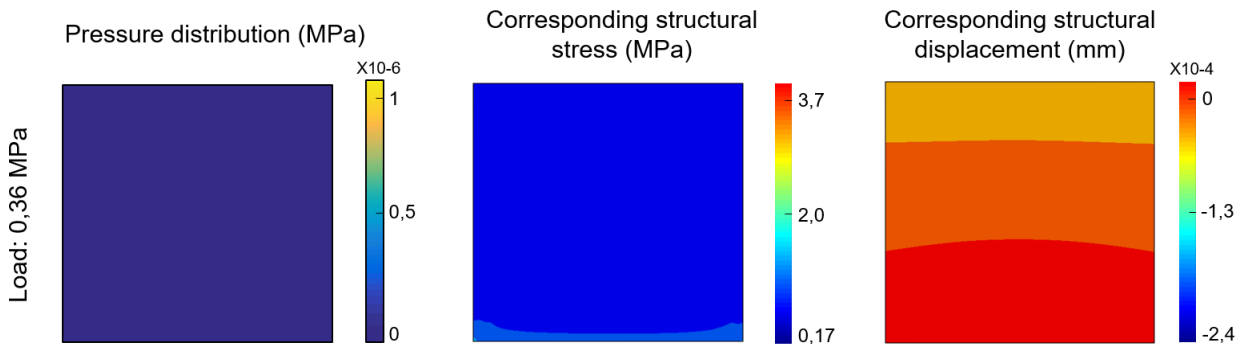
Figure 3.6: **Pressure distribution (in MPa), corresponding structural stress (in MPa) and corresponding structural displacement (mm) under a pressure of 0.36 MPa.**
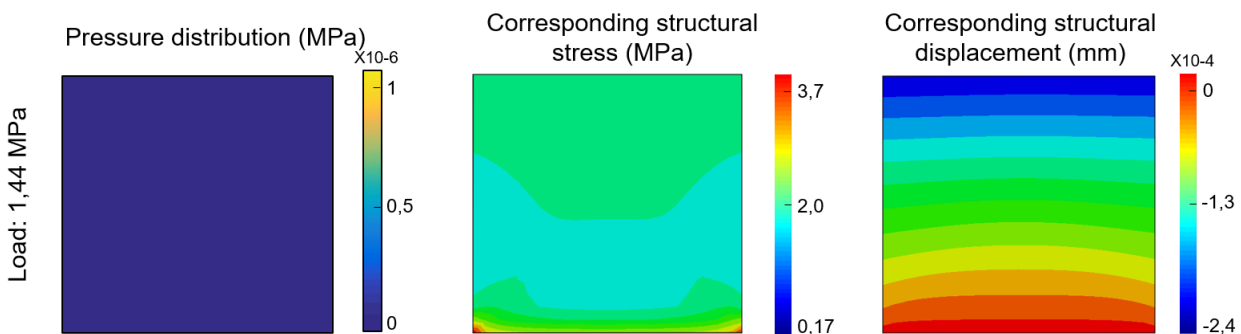
Figure 3.7: **Pressure distribution (in MPa), corresponding structural stress (in MPa) and corresponding structural displacement (mm) under a pressure of 1.44 MPa.**

gets higher due to fluid accumulation but mostly to the clamping of the face as it can also be seen on Figures 3.9 and 3.10.
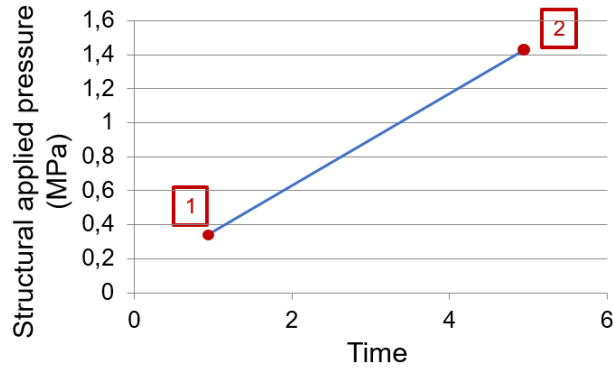
Figure 3.8: **The results are extracted at point 1 when mentioned that the loading pressure is 0.36 MPa and at point 2 when mentioned that the loading pressure is 1.44 MPa.**
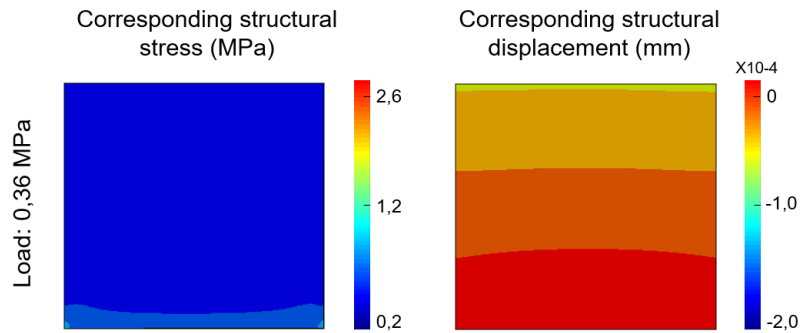
Figure 3.9: **Structural Von Mises stress (MPa) and structural displacement in an elastic and non-porous model with a Young Modulus of 14000 MPa, under a pressure of 0.36 MPa.**
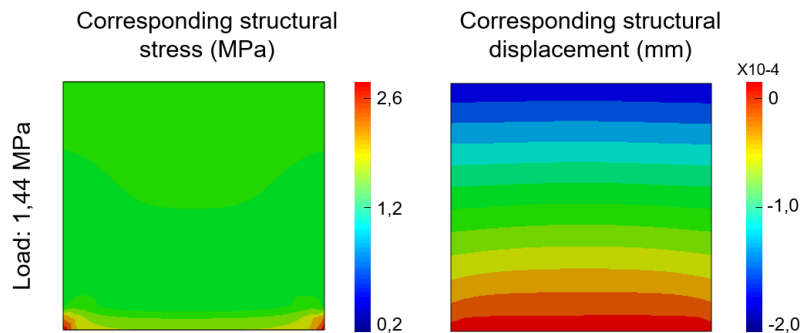
Figure 3.10: **Structural Von Mises stress (MPa) and structural displacement in an elastic and non-porous model with a Young Modulus of 14000 MPa, under a pressure of 1.44 MPa.**

This simulation allows to plot the stress-strain curve, giving information on the material macroscopic response and the value of the equivalent Young modulus of the porous material (Figure 3.11).

Stress-Strain Curve
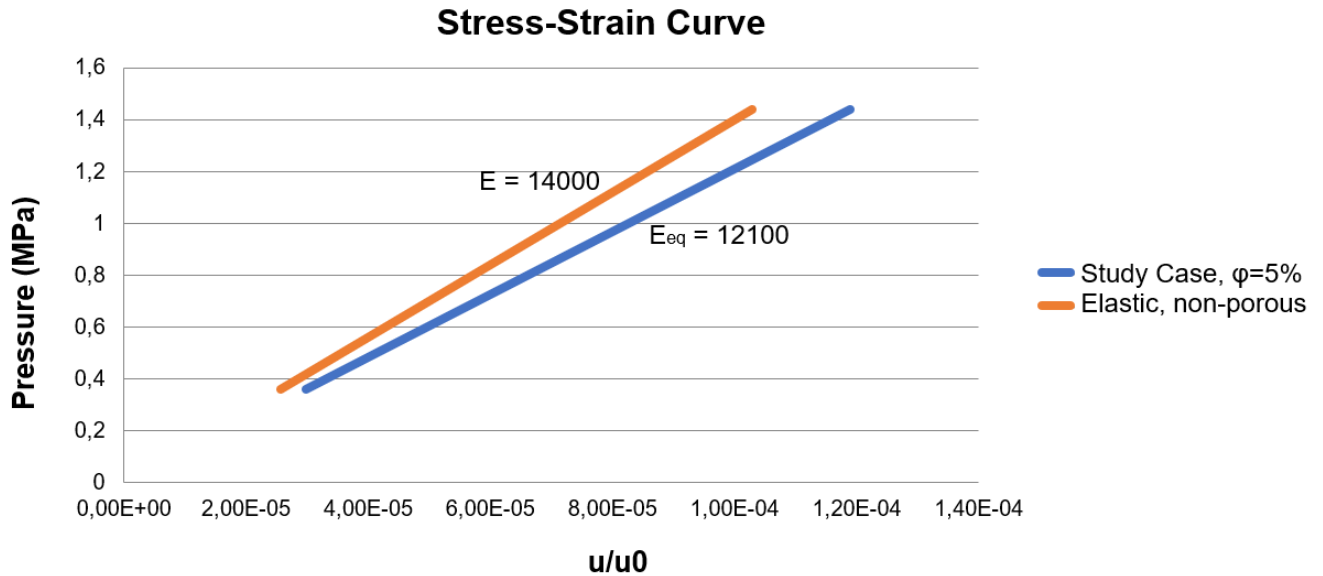
Figure 3.11: **Stress-strain curve for the study case (E is in MPa).**

As it is shown by the graph, the computed equivalent Young modulus is equal to 12100 MPa for a reference Young modulus of 14000 MPa (the one of the solid matrix). Thus, introducing communicating porosities and fluid flows in such material, induces a decrease of almost 14% of the equivalent stiffness.

3.7 Discussion and Conclusion

The developed algorithm, presented in the first part of this Chapter, has then been applied to a reference case.

The aim is to propose a first application of the developed approach by the modeling of a simple geometry of bone sample, under a simple

configuration. As a preliminary work, the definition of the mathematical law to represent the fluid flows in bone, according to the specificities imposed by the framework of the study, has been presented in the previous Chapter.

While the results of this first reference case, as it will be referred in the following, show the impact of fluid flows in the mechanical behavior of the simulated poroelastic sample, in the perspective of modeling bone in a biologically accurate configuration, several points still need to be discussed.

Concerning the boundary pressure conditions in-vivo, the pressure corresponds to the one exerted by the soft tissue around the bone and the pressure within the bone structure itself, especially during critical loading such as climbing stairs or rising from a chair. Physically, in the thigh, the in-vivo pressure boundary conditions are more constraining than keeping the walls free, without being completely impermeable [43, 107]. Thus, the biological mechanical bone behavior would be included between these two critical configurations. Therefore, a case with impermeable walls boundary conditions will be developed as well to verify the two extreme boundaries.

Moreover, the free wall boundary condition will be useful as representative for the experimental validation through compressive tests on bone specimens.

CHAPTER 4

Model validation

The algorithm for the computation of a multiscale poroelastic model of bone has been fully developed, and applied on a first study case, as presented in the previous Chapter. This frist study case will be used as a reference case, and to evaluate its accuracy, this Chapter presents a validation, divided in two steps: in the first part, a numerical validation is performed varying several targeted parameters, such as the boundary conditions, the porosity of the material or its material properties; in a second part, a comparison with experimental tests on femoral bone samples is presented.

4.1 Numerical Validation

The aim of this numerical work is to provide a preliminary validation of the developed approach, by varying some main parameters and checking if the results are the ones expected physically, before a confrontation with experimental tests. The following analyses have been set to verify the reliability of the simulation approach:

- Modification of the fluid boundary conditions.

- Modification of the material properties.

- Modification of porosity degree.

4.1.1 Modification of the fluid boundary conditions

On the structural side, the boundary conditions are kept the same as previously, i.e. with free lateral walls, clamped bottom and imposed pressure on the top face.

On the fluid side, the condition of impermeable wall is applied, in this case, on every face. This means that the fluid cannot flow out of the cube and is kept completely trapped in the volume.
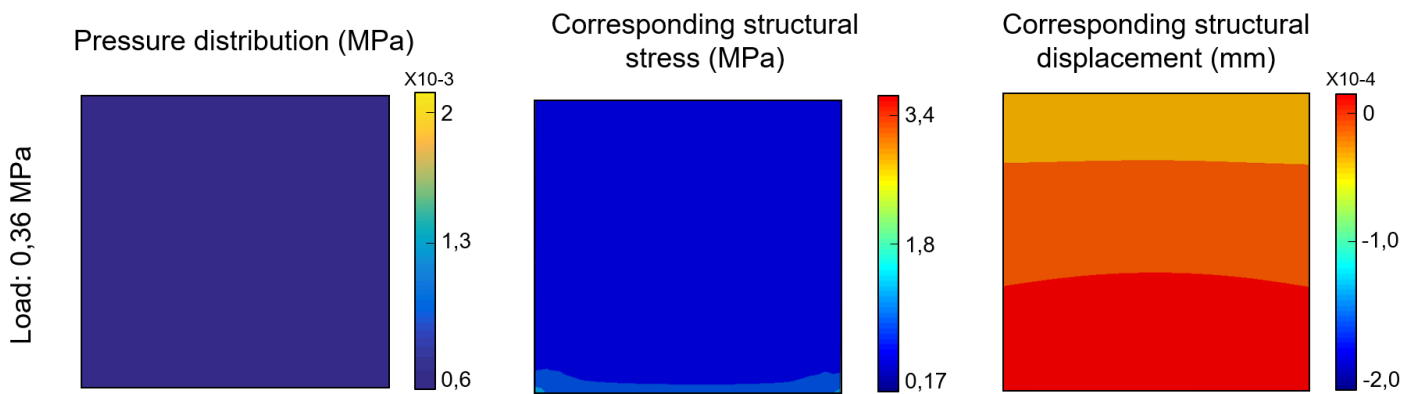

Figure 4.1: **Pressure distribution (in MPa), corresponding structural stress (in MPa) and corresponding structural displacement (mm) under a 0.36 MPa pressure, with impermeable boundary conditions on the fluid.**

Figures 4.1 and 4.2 present results obtained under this set of boundary conditions. The pressure distribution, the corresponding structural stress and displacement are plotted at the beginning and the end of the simulation, at the same times that presented on the reference case, reminded on Figure 4.3.

In this case, the pressure reaches a homogeneous distribution (Figures 4.1 and 4.2). As the pressure computation considers fluid flows and fluid accumulation in the body, an increase of the pressure can be noticed in the whole volume during the simulation, when comparing the results to those obtained at the beginning and at the end of the pressure ramp.
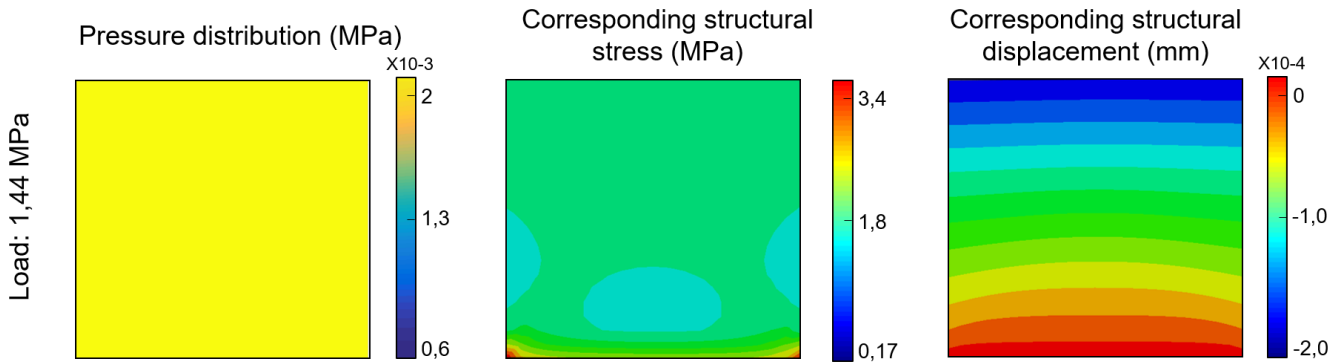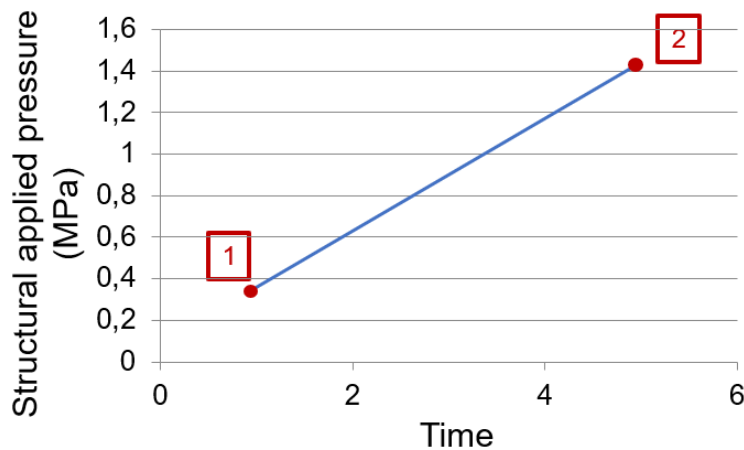
Load: 1,44 MPa

Pressure distribution (MPa)

X10-3

Corresponding structural stress (MPa)

Corresponding structural displacement (mm)

X10-4

Figure 4.2: ***Pressure distribution (in MPa), corresponding structural stress (in MPa) and corresponding structural displacement (mm) under a 1.44 MPa pressure, with impermeable boundary conditions on the fluid.***

Figure 4.3: ***The results are extracted at point 1 when mentioned that the loading pressure is 0.36 MPa and at point 2 when mentioned that the loading pressure is 1.44 MPa.***

The increase in the pressure field agrees with the entrapment of the fluid inside the body. Moreover, it agrees with the increase of the structural stress distribution, when comparing with the results from the reference case presented in the previous Chapter, because of the fluid entrapment.

Then, in this case, the stress-strain curve is plotted on Figure 4.4.

It can be observed that the impermeable equivalent Young modulus is of 13700 MPa. In fact, because the fluid is trapped in the solid ma-
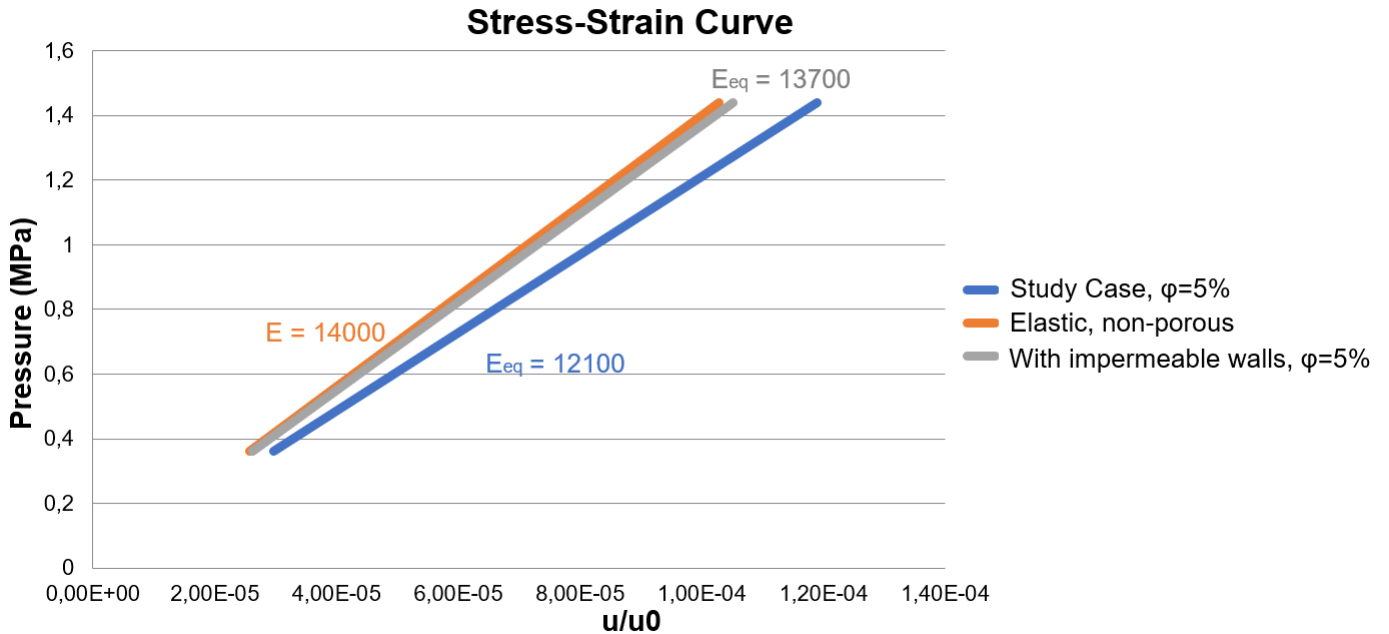
Figure 4.4: **Stress-strain curve for the case with impermeable boundary conditions on the fluid, compared to the reference case and the elastic case.**

trix, the material is almost as stiff as an elastic one, despite its porous aspect, which is in accordance with the results of the reference case of the previous Chapter and the elastic model.

4.1.2 Modification of the material properties

To rate the effect of a change in the material properties, several configurations are investigated. For this purpose, the value of the Young modulus of the solid matrix is modified.

Therefore, once the new values of the Young modulus of the solid matrix given (varying between 7000 and 28000 MPa), the corresponding RVE problems are solved to compute the values of the effective properties that are matching these new values. Then, the same mesh and same structural and fluid boundary conditions of the reference case (free walls in structure and in fluid, clamped and impermeable at the bottom face, load applied on the top face) are applied on the same 2mm length cube at the macroscale. Figure 4.5 presents the different stress-strain curves

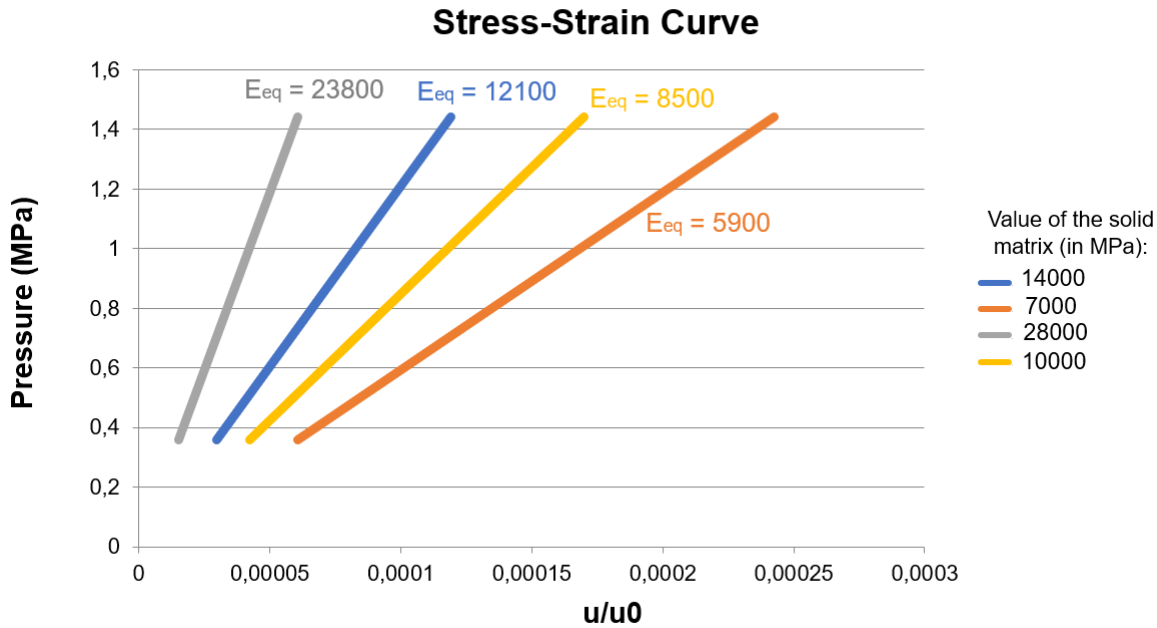obtained for increasing values of the matrix stiffness.

Figure 4.5: ***Stress-strain curves when the Young modulus of the solid matrix varies: 7000 MPa, 10000 MPa, 14000 MPa and 28000 MPa.***

The results obtained with different values of the equivalent computed Young modulus show an increase of the equivalent stiffness of the porous material with the increase of the stiffness of the solid matrix, which is consistent with the physical expectations. Moreover, plotting the variations of the equivalent Young modulus against the values of the Young modulus of the solid matrix (Figure 4.6) shows that according to our model, the equivalent stiffness of the poroelastic material follows a linear variation for a fixed porosity, giving a direct relation between these two parameters. The numerical results also indicate that in this case, with this RVE geometry and this porosity, the equivalent poroelastic stiffness is estimated to be 15% inferior with respect to the stiffness of the solid matrix.
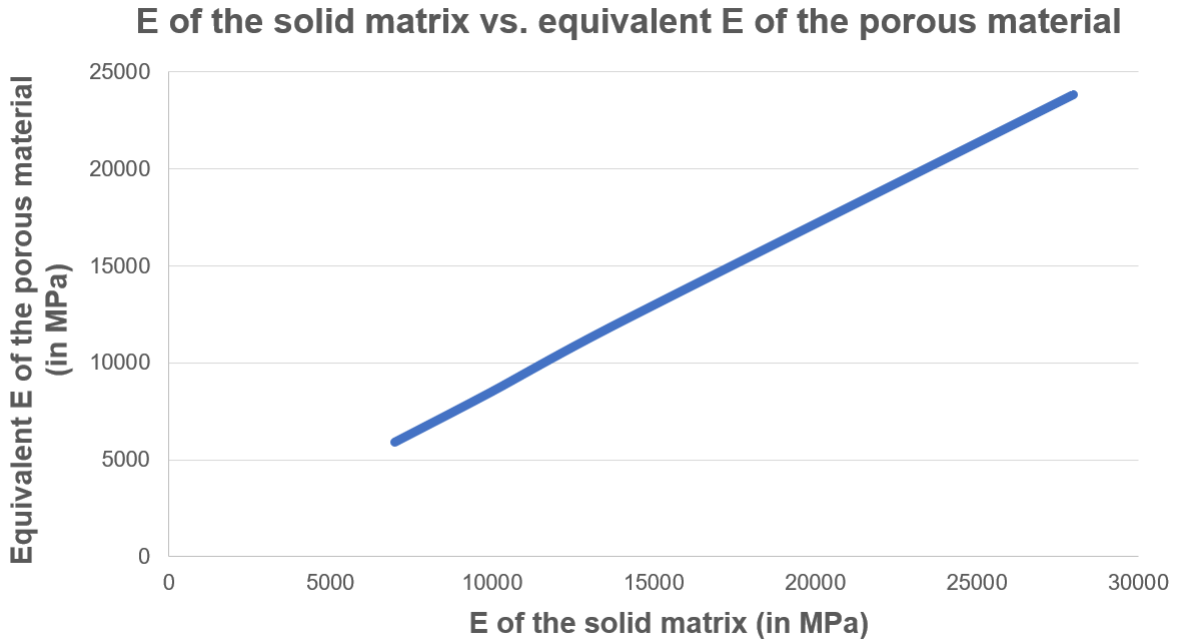
E of the solid matrix vs. equivalent E of the porous material

*Figure 4.6: **Variation of the equivalent Young modulus of the porous material as function of the value of the Young modulus of the solid matrix.***

4.1.3   Modification of the porosity degree

Finally, a parameter on which it is possible to play is the porosity of the material. In the case of cortical bone, the porosity of interest for this study has been estimated at 5%.

However, it is interesting to verify what is occurring when the value of the porosity increased. This section reports the results obtained when increasing the diameter of the canals of the RVE to 50 μm, while keeping the same shape of the communicating pores, which resulted with a 40% porosity (see Figure 4.7).

The boundary conditions applied on the RVE are the same as presented in the previous Chapter, as the same assumptions are kept on the modeled material (i.e. poroelastic material, with saturated and periodic pores). It consists in the periodicity on each external face and the two sets of boundary conditions reminded hereafter:

$$p_f^0 = 0; E_x(\vec{u_s}^0) = \frac{1}{2}(\delta_{jl} \cdot \delta_{km} + \delta_{jm} \cdot \delta_{kl}) \tag{4.1}$$
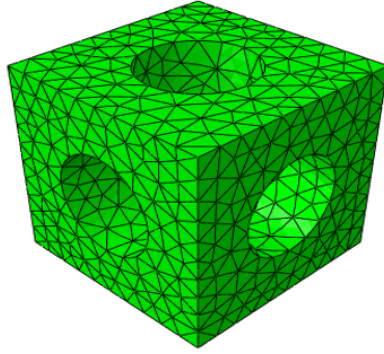
*Figure 4.7: **New geometry with increased porosity.***

with k and h fixed.

$$p_f^0 = 1; E_x(\vec{u_s}^0) = 0 \tag{4.2}$$

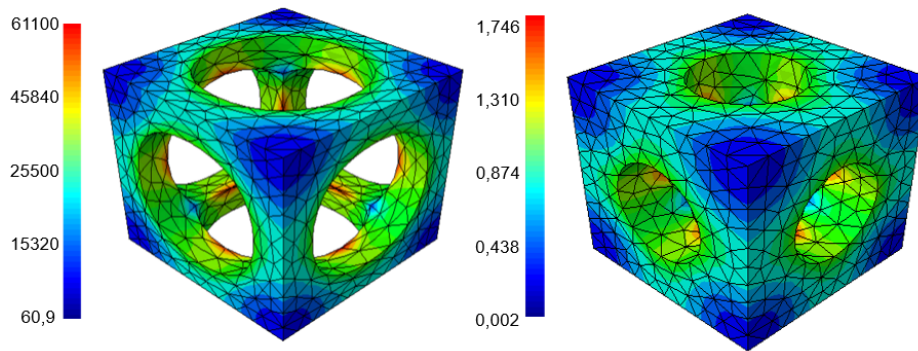The corresponding results are shown on Figure 4.8.

*Figure 4.8: **Strain distribution on the RVE for an 40% porosity material (on the left for $\vec{\xi}$, on the right $\vec{\eta}$).***

Here again, the boundary conditions at the macroscale are the same as in the previous case and in the reference case (i.e. structural imposed pressure on the top face, impermeable and clamped bottom face, walls kept free at the reference pressure).

Figure 4.9 shows the plot of the corresponding stress-strain curve and the computation of the equivalent Young modulus. Increasing the porosity of the material up to 40%, the final equivalent stiffness reduces to 6500MPa, i.e. more than 50% compared to the non-porous model. The results agree with the expected increasing contribution of the porosity, by resulting in higher compliance of the structural matrix.
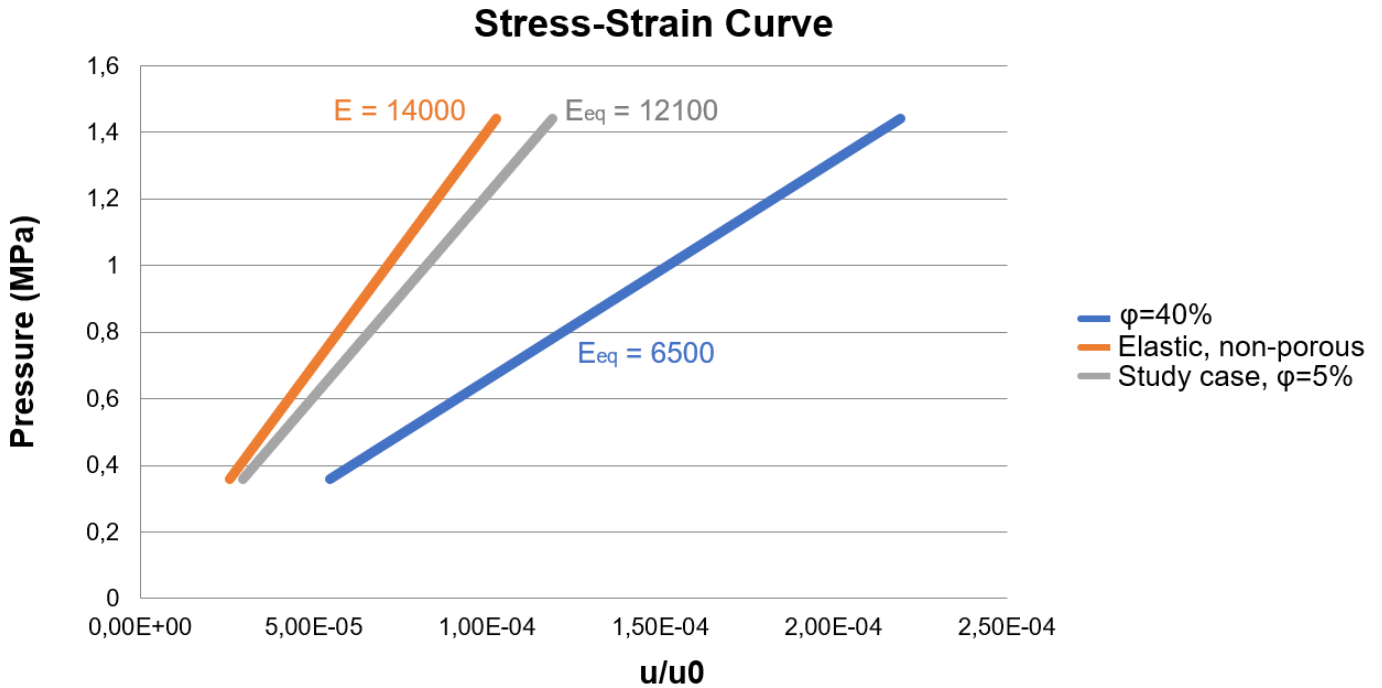
Figure 4.9: **Stress-strain curves of the 40% porous material and of the elastic non-porous and reference material to compare.**

4.1.4 Conclusion

The approach fully developed in the previous chapter has been applied to different configurations, on a reference case and when varying some main parameters such as the boundary conditions, the material properties and the porosity of the material.

The variation of these parameters allows us to draw some conclusions in order to perform a first numerical validation of the proposed approach and implemented algorithm.

One can notice that all the presented curves show linear behavior, which is consistent with the fact that our poroelastic formulation relies on linear poroelasticity. Changing the boundary conditions for the fluid, simulating a case where the fluid is completely trapped in the solid matrix, leads to consider an extreme configuration regarding the biological reality, as the real *in vivo* boundary conditions are difficult to assess. In this case, comparing the results with the reference case presented in the

previous Chapter, we are able to confirm that the structural stress distribution evolves accordingly with the fluid pressure evolution. Moreover, the evolution of the equivalent stiffness of the material is following the expected trends.

For a fixed porosity, a linear evolution is found with respect to the variation of the solid matrix properties. Nevertheless, for low values of Young modulus, it requires a specific attention to ensure that all the assumptions made during the elaboration of the model still hold, concerning how the fluid accumulation is treated.

Finally, varying the porosity showed a much important reduction of the equivalent stiffness of the porous material. However, as for an important reduction of the Young modulus of the solid matrix, the increase of the porosity would require a special study. As in the case of softer material, the pores can be expected to undergo strong strain field and this can impact the permeability of the whole material.

However, the obtained results are consistent with the expected physical responses on a poroelastic material. Furthermore, because we are aiming to focus on bone modeling and thus working with the porosity of the lacunar-canalicular system, which is very low, the numerical validation of the model can be taken for granted in this context. After the numerical validation, an experimental one is required to check the reliability with respect to the mechanical response of a real bone.

4.2 Experimental Validation

The experimental validation is presented in this section. We compare the results coming from the compression of human femur bone samples using the following device, performed in vitro, and the ones obtained numerically from our model , when introducing the appropriate geometrical and boundary conditions to reproduce the experimental set-up.

4.2.1 Set-up

The experimental data for the validation of the numerical model have been recovered by experimental compression tests performed on previous works of a research laboratory of La Sapienza [49, 48, 50]. A linearly increasing pressure is imposed on the top face and the displacement is measured. The bone samples are extracted from a human femur. The size of the sample is 6.7x8.1x7.8 mm^3. The sample is compressed in the three directions, by three successive tests called respectively D1, D2 and D3 in the following (see Figure 4.10)
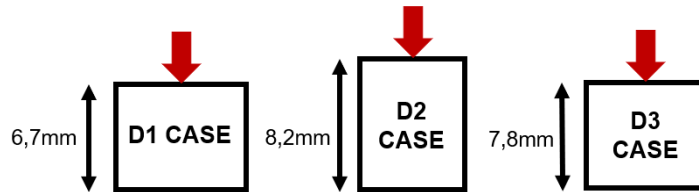

*Figure 4.10: **The three compression tests performed experimentally.***

4.2.2 Experimental results

The experimental tests allowed for the plot of the respective stress-strain curves, depicted in Figures 4.11, 4.12 and 4.13.

The dotted line reported in Figure is the linear approximation of the Stress-Strain branches. In the D1 and D2 cases, as the Stress-Strain curves are not linear and two zones can be identified. The three obtained curves are not presenting the same shape, which can be explained knowing that the same bone sample is kept for the three experimental tests along the three directions.

For the D1 case, the curve shows a slope that is steeper at the beginning and then get softer. For the D2 case, the opposite behavior is noticed, as the curve begins with a soft slope and that is increasing in the second part. These variations may be due to the difference in the structure and trabecular alignment of the bone sample with respect to the loading
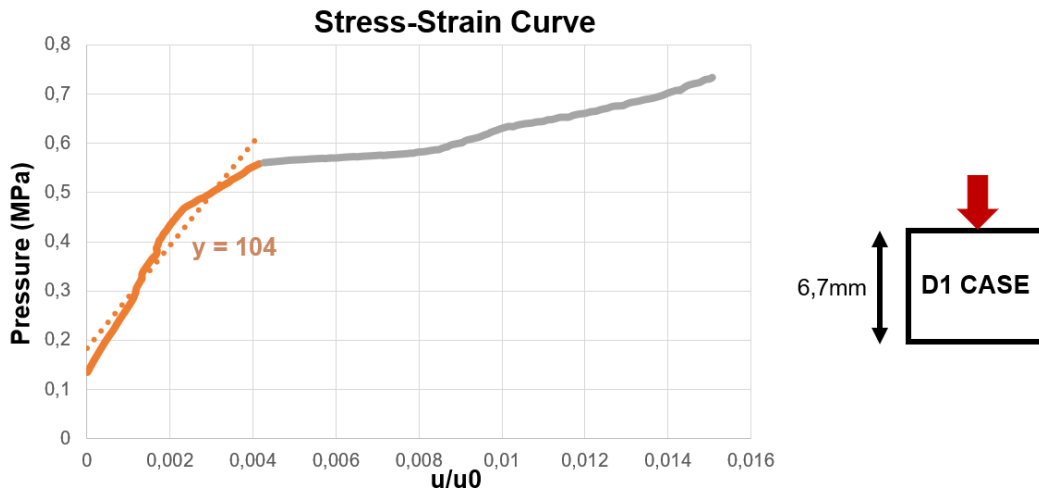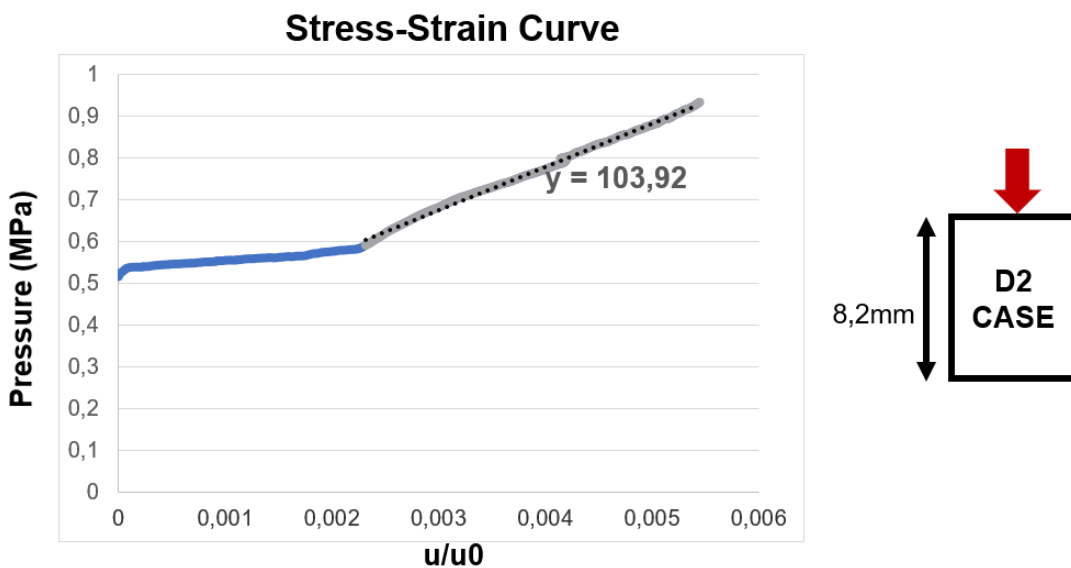
Figure 4.11: **Stress-Strain curve for the D1 case.**

Figure 4.12: **Stress-Strain curve for the D2 case.**

direction, as bone structure is not equally distributed and may show a preferred structural direction.

The slope of the lines gives us the equivalent stiffness within the corresponding compression range of the bone sample. Within the linear branches of the steeper parts of the curves, the equivalent stiffness mea-
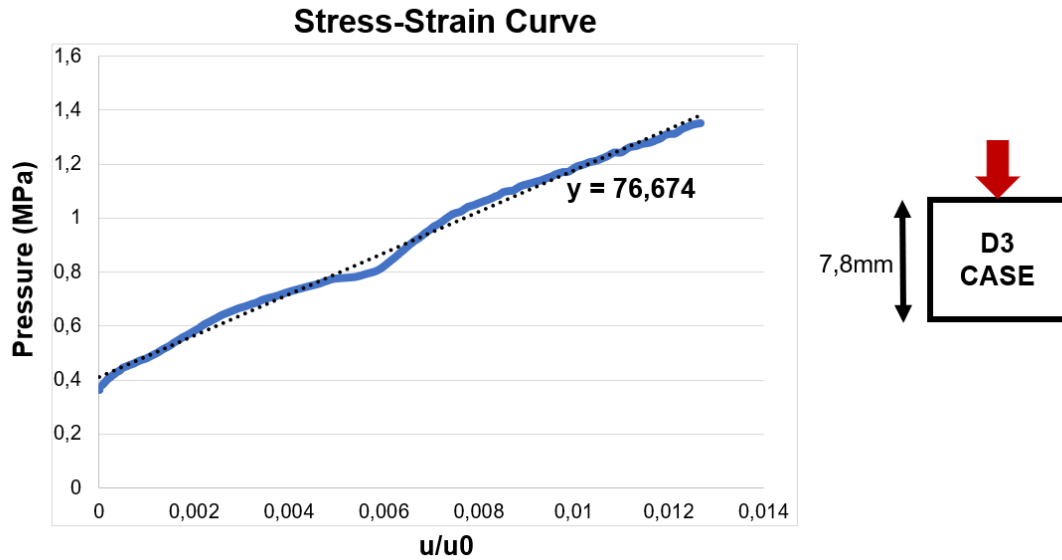
*Figure 4.13: **Stress-Strain curve for the D3 case.***

sured experimentally appears to reach 100 MPa in every cases. The lowest value (77 MPa) is found for the third case, when the bone microstructure could have been damaged through the two previous compressive tests.

4.2.3 Numerical compression tests

To compare experimental and numerical results, it is required to reproduce the testing conditions in the numerical model the most faithfully.

Geometry and mesh.

The macroscale geometry is defined to match the dimensions of the tested bone sample, which is almost cubic (6.8 x 7.2 x 8.1 mm^3). The microscale geometry, defined by the RVE, is the same as the one presented in the reference case, reproducing the lacunar-canalicular system. With this size of the RVE, the model is composed by 428532 elements at the macroscale.

Loading and Boundary conditions.

The loading is defined by a pressure, which is imposed on the top face and is increased linearly. To match the best with experimental conditions,

all the nodes of the upper surface are blocked in the surface plane (see Figure 4.14). The lateral walls are kept free, with the external pressure (atmosphere) set to zero. The bottom face is clamped from a structural point of view, and considered impermeable.
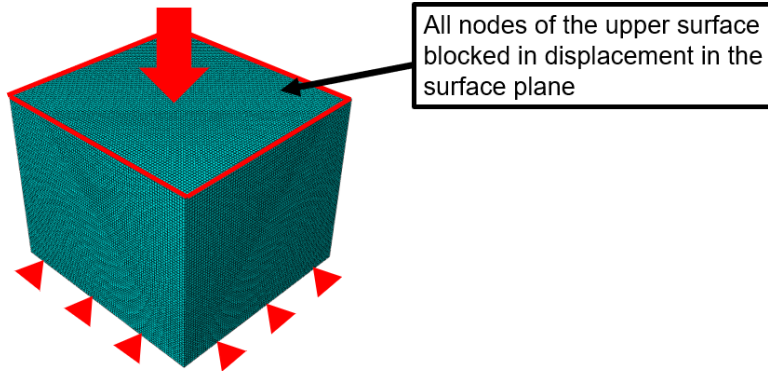

Figure 4.14: **Geometry, mesh and structural boundary conditions for the D1 case.**

Material properties.

The inputs for the material properties rise several questions. First, the bone samples have been extracted from the trabecular part of the bone and not the cortical one. Unfortunately, the Young modulus of the solid matrix of trabecular could be situated within a very wide range of values, as explained in Chapter 2.

For a first run, the value of 14000 MPa is kept, to verify the effect of the changes in the dimension of the sample. Nevertheless, this value might require to be reduced for this bone sample.

Regarding the fluid portion, the bone samples have not been tested right after the extraction of the femur of the body and have not been re-hydrated after. Therefore, even if a fluid has been released during the compressive test, its nature cannot be definitively assessed. For the same reason as for the solid part, the properties of the fluid are kept representing the properties of bone fluid (Dynamic viscosity = 6.5 mPa.s) for a first simulation. Nevertheless, it might be required to increase its viscosity to get closer to the bone marrow properties. Finally, the porosity and permeability are kept at 5% and $1.5e^{-14}$ mm² respectively, as we are

still considering the modeling of the lacunar-canalicular system at the microscale.

4.2.4 Numerical results

The numerical results are presented in the following. First, a case when modeling the cortical bone with a solid matrix of 14000 MPa is run in the three cases. Extracting the displacement and plotting the stress-strain curve, the computation of the equivalent stiffness gives a result of 12323 MPa, 12679 MPa and 12061 MPa for respectively the D1, D2 and D3 case, as it can be seen on Figure 4.15.
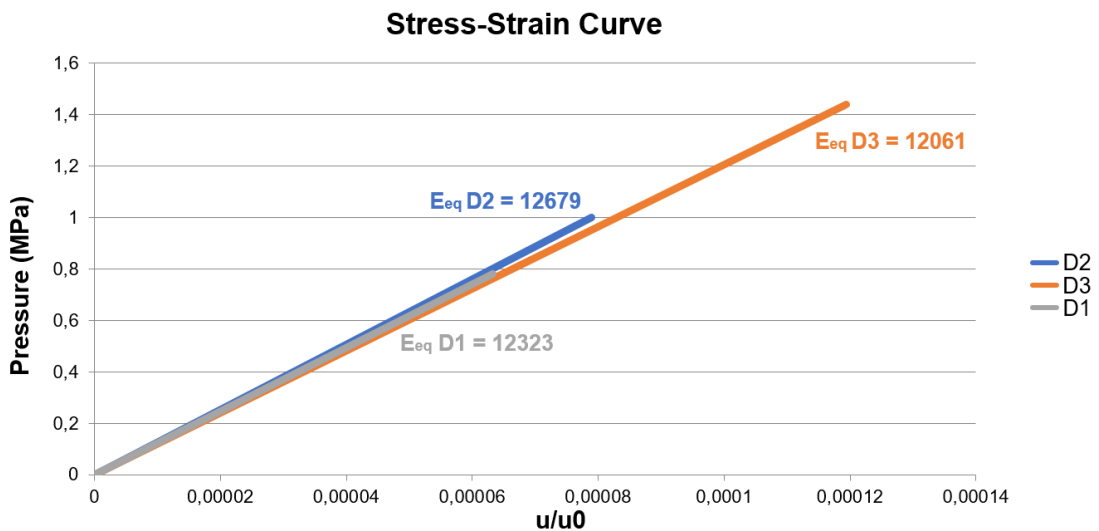
Figure 4.15: *Stress-Strain curve for the D1 case numerical simulation, with a solid matrix of 14000 MPa.*

This values are in accordance with the results presented in the previous Chapter, showing how a modification of the size and geometry of the modeled sample does not modify the mechanical property (equivalent stiffness) of the homogenized model of the bone.

Nevertheless, the values obtained are much larger than the one obtained through the experimental tests. Because this difference could be motivated by the lack of information on the actual state of the tested bone

sample, the value of the Young modulus of the solid matrix has been varied to obtain more conclusive results.

According to the curve plotted in the previous section, plotting the equivalent stiffness of the poroelastic material as a function of the stiffness of the solid matrix, the interpolation of the curve brings to a numerical model with an input of 100 MPa for the value of the solid matrix.

In accordance with the developed algorithm, all the steps showed in the previous Chapter are followed and the corresponding effective properties are computed. Running the simulations in all three cases, we end up with the results shown on Figures 4.16, 4.17 and 4.18.

*Figure 4.16: **Stress-Strain curve for the D1 case numerical simulation confronted with the experimental stress-strain curve, with a solid matrix of 100 MPa.***

As expected, the numerical curves are linear and the computed equivalent stiffness are respectively 87 MPa for the D1 case and 89 MPa for both D2 and D3 cases. This corresponds to a reduction of respectively 13% and 11% of the equivalent stiffness with respect to the solid matrix value. This matches the reduction of Young modulus reduction found in the previous section. Thus, for the first part of the experimental stress-strain curve for the D1 case, the second part for the D2 and D3, the numerical and experimental results are in accordance regarding this parameter. The non-linear
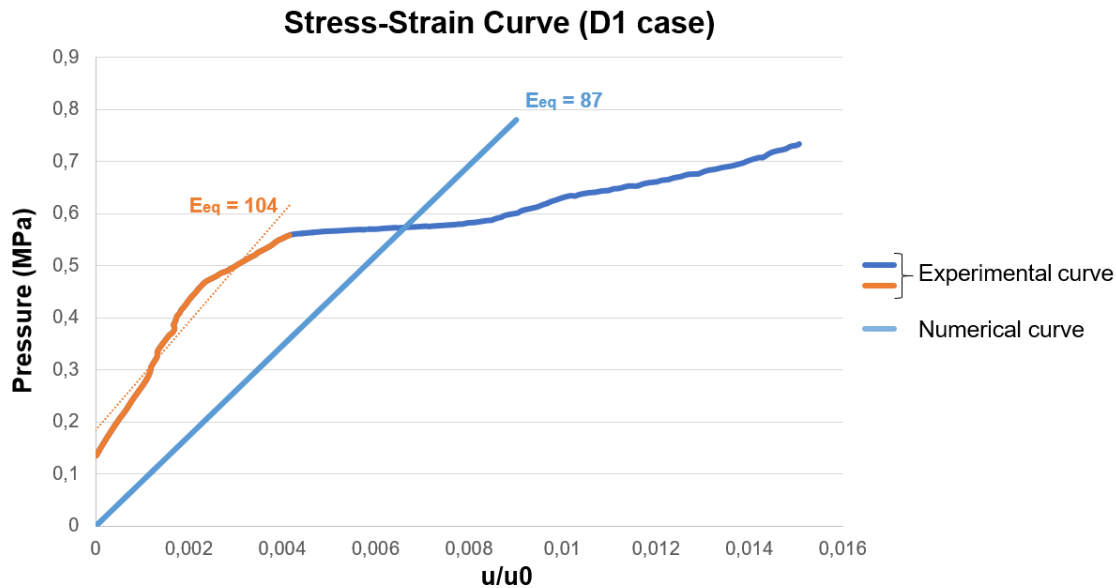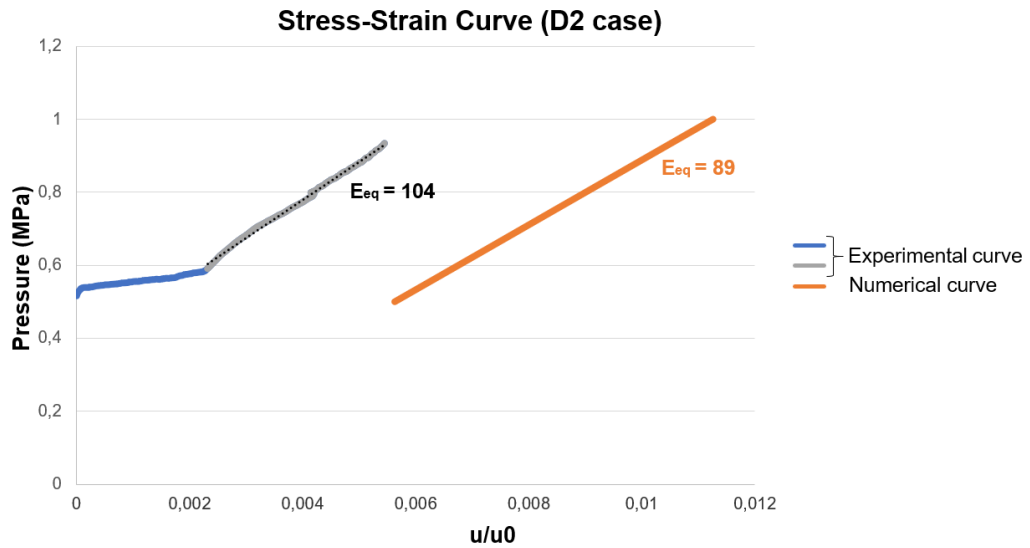
Figure 4.17: **Stress-Strain curve for the D2 case numerical simulation confronted with the experimental stress-strain curve, with a solid matrix of 100 MPa.**
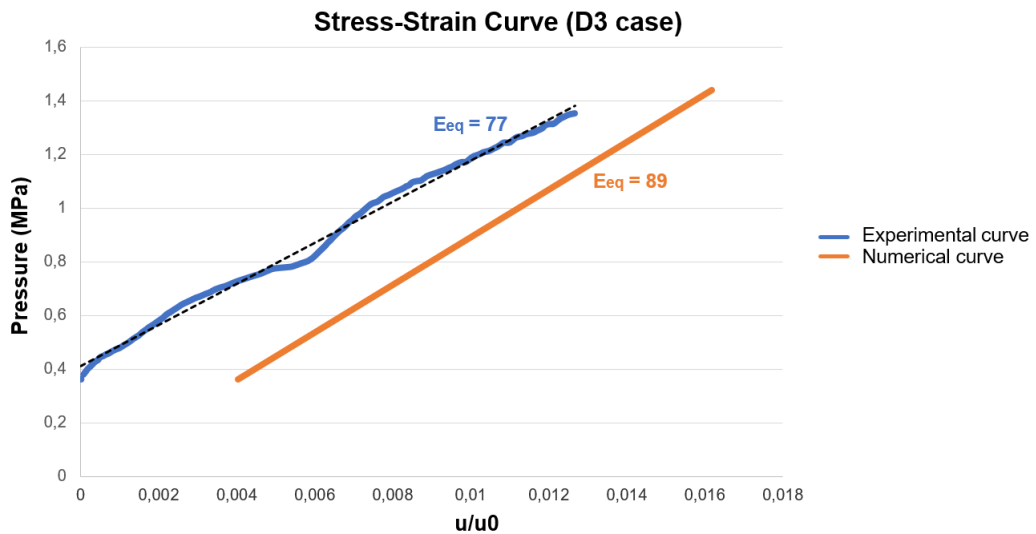
Figure 4.18: **Stress-Strain curve for the D3 case numerical simulation confronted with the experimental stress-strain curve, with a solid matrix of 100 MPa.**

part of the experimental curves can be attributed to the hierarchical structure of the bone, and the fact that during the compression, damage can occur at the lower scale, affecting the stiffness of the material, or by the fact that bone has not the same structural constitution in the three direc-

tions.

4.3 Discussion and conclusions

First, using the same value of the Young modulus of the matrix, as in the numerical validation, allowed us to ensure that our numerical model is still accurate when changing the macroscopic dimension and, therefore, confirmed its consistency. Moreover, the estimation of the reduction of the value of the equivalent stiffness, when introducing of a porosity of 5%, is confirmed when varying the dimensions.

Nevertheless, during the comparison of the experimental results done on a bone sample, the material properties, and more precisely the Young modulus of the solid matrix, have been reduced to 100 MPa, in order to match the experimental results.

This could be explained when considering the conditions in which bone samples have been extracted and preserved. Indeed, as previously mentioned, the bone samples have been extracted in the trabecular zone of a human femur. As the numerical model account for the porosity of the lacunar-canalicular system, it can be applicable for this type of bone. Nevertheless, in this case, the stiffness of the solid matrix needs to account for the structural conditions of the upper level of bone, i.e. the state and distribution of bone at the trabecula or osteon scale. Regarding the freshness of the bone, the preservation protocol and conditions imply necessarily an effect on water content of the bone, because it may involve freezing and therefore a state evolution of the fluid portion. However, it has been established that the values of the mechanical properties of bone still hold after storage periods up to one year [108, 109].

Another aspect of the state of the bone sample, which need consideration during the numerical transposition and possible adjustments of

the input values, is its hydration. In the experimental tests, the samples were not fully saturated as it is assumed in the numerical model, and the response of the bone to compression shows a viscous component, may be bone marrow remaining, located in the largest porosities of trabecular bone.

Not considering the other levels of porosity is one of the first assumption made in the development of the numerical model. Indeed, our main focus was to find an equilibrium between model accuracy and computational efficiency. Therefore, modeling all the porosities existing in bone has been excluded and the focus has been put on the porosity of the lacunar-canalicular system, as this is the location of mechanotransduction, the process that coordinates bone remodeling. This porosity level being essential for the structural evolution of the bone, the other level of porosities can be accounted by an appropriate quantification of the solid matrix stiffness, as it has been done here. Moreover, it has been suggested that the pressure in the vascular porosity is much lower than that in the lacuna-canalicular porosity and these two porosity levels are acting independently [59, 61].

From the fluid point of view, only bone fluid is considered, whereas other substances can be found in bone pores, such as blood or bone marrow. However, the same alternative solution can be proposed, integrating the interaction with bone solid matrix through an appropriate choice of values defining the solid matrix. Furthermore, as it has been mentioned in the State-of-the-Art that bone fluid is difficult to be carefully characterized and it is composed of many elements. This consideration results in a fluid that is electrically charged, and that can influence its behavior in the solid matrix. A way of considering this effect would be the introduction of the Brinkman term in the pressure computation, as it has been done with interesting results in [65]. In this project, we focused on the hydraulic component of the bone fluid behavior, in the perspective of mechanotransduction modeling, but revising mathematical description of the fluid flow is an improvement of the model that we need to keep in mind.

Another and promising way to improve the numerical model would

be to work with a RVE geometry, which would be more representative of the real geometry of the lacunar-canalicular system. Indeed, the one used in this model can seem too simple and only representing the canals, whereas in reality the osteocytes are immerges in lacuna. The diameter of the lacuna is larger than the diameter of the canaliculi which extend therefrom. This RVE configuration may be more realistic and may involve a different strain field, changing therefore the effective properties.

Finally, we came up with a multiscale poroelastic numerical model of bone, elaborated by the means of the homogenization technique. The development of the model lies on two bone features that are its porous aspect and its multiscale structure, allowing the formulation of appropriate assumptions for the development of the model. In the perspective of modeling bone reconstruction around an artificial device, we are looking into the mechanotransduction process and its triggering by fluid flows in bone pores. Modeling bone and having the information of bone fluid pressure in every pore during the computation is the first step toward this aim.

Confronted to a two-step validation, the developed model shows promising results in accordance with the expected results and the experimental data. It appears that the critical aspect, when computing our numerical model, is the determination of material properties input, for both the solid and fluid phases. Of course, this is one of the most challenging aspect of modeling biological tissues, and several ways can be considered to solve this issue. For instance, the use of imaging techniques, coupled with a segmentation software, can be an interesting way to evaluate, estimate and quantify bone quality and use it for our model input. It will allow the implementation of real bone geometry as macroscopic inputs in the numerical model, and also would correspond to the long-term ambition to fit the use of the developed model in a clinical procedure.

General conclusion and Perspectives

The work presented here falls within the research perspective of providing tools for a better understanding of the bone through its living characteristics. From a biological point of view, this is possible thanks to a better understanding and modelling of the mechanotransduction process, which is the action of mechanosensitive bone cells in the bone structure regulation. This process is regulated thanks to the sensitivity of these bone cells to the flows of the fluid in which they are immerged and their mechanical environment . This ability of bone is very important in everyday life to provide an efficient bone structure. Moreover, mechanotransduction is what allows bone to reconstruct after a fracture or, the case considered here, after the replacement of a joint by an artificial device.

As the replacement of the hip through a Total Hip Arthroplasty concerns more and more patients, in the last decade it became a major health and economical issue, bringing the study of bone and its reaction after the implantation of a device to the forefront of biomedical industries. The need of gathering together the academical knowledge of bone tissue and the efficiency to access this knowledge by the actors of the orthopedic field (both the clinicians and the prosthesis manufacturers) becomes urgent.

In this perspective, a model has been developed, based on the recent findings on the mechanical structure of bones and the corresponding as-

111

sumptions. As bone structural evolution is attributed to the mechanotransduction process, occurring at the cell scale due to fluid flows, we have chosen to base the development of our model of two main bone features: its porous aspect and its multiscale evolving structure. It led us to the development of a multiscale poroelastic material, which accounts for the main characteristics in bone reconstruction. This choice was reached in order to provide a necessary compromise between a computational efficiency, required by a practical application, and the accuracy of reproducing the main events involved in bone evolution.

The developed model has been transposed in a numerical algorithm. Assuming that cortical bone is the periodic structure at the macroscale, we based the mathematical development on the homogenization technique, that allows the consideration of bone as a homogenous material while considering its microscopical specificities.

This mathematical formulation constituted a base for the creation of a complete numerical algorithm, articulated with the softwares Matlab and Abaqus. This allowed the computation of a reference case, of which every step is detailed as an illustration of the developed methodology.

Then, this numerical model has been then extended in several other cases, in order to confront it to several configurations, varying different targeted parameters such as boundary conditions or material properties. The numerical model showed consistent results, in accordance with the proposed assumptions.

When reproducing experimental tests, convincing results have been obtained, even if the critical point for the simulations is the determination of the material properties input data. Nevertheless, solutions have been foreseen to overcome this aspect, including this work in the clinical project in which it is developed.

Indeed, the long-term aim of the project is to provide a tool to make the choice of the hip prosthesis the most relevant for the patient, giving to the clinician and to the prosthesis manufacturer indications on the patient bone ability to reconstruct itself around the device. Obviously, this model can be improved in terms of accuracy, even if this is not its main aim. The following step would be to introduce the living aspect of bone in the

model, to be able to simulate its reconstruction abilities when submitted to specific conditions, i.e. the ones involved in a hip surgery.

To do so, the idea would be to introduce a bone remodeling law into the model. Many laws have been formulated in the literature on this aspect, changing from one to another on the aspects they are accounting for. The simplest one is the phenomenological approach, that aims to describe the bone response as a function of the solicitation level. This approach is based on the "Mechanostat" concept, formulated by Frost in 1987 (Figure 1). It formulates the fact that the remodeling velocity is related to the strain energy density values, which activate or disactivate the creation of bone. The main advantage of this kind of models is that they remain easy to put in application, and leave latitude in the expression of the strain energy density.
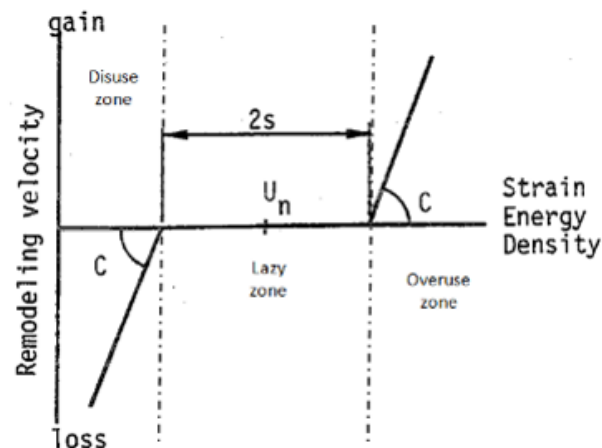
*Figure 4.19: **Representation of the "mechanostat" concept.***

Indeed, for our poroelastic model, this information is available and account for both the structural strain distribution and the fluid impact on this strain, which give to the remodeling model all its interest. According to the value of the strain energy density, bone density is either increasing or decreasing, quantifying bone reconstruction. If in the inputs, the loading conditions and material properties are faithful to a real femur during surgery, the information on the anticipation of bone reaction is a signifi-

cant improvement in the planification of the surgery, for the appropriate choice of the device or choice in the surgical approach.

This kind of information can also be the origin of a new generation a prosthesis, produced by additive manufacturing. The prosthesis could then be designed based on a mechanical property gradient, which is optimized regarding the bone quality and structure specificities of every patient, going towards a patient-specific kind of surgery that would be the best configuration for the patient. In the end, the perspectives given by further development of this model are endless. The exciting and constant technical progress in bone imaging technics and medical device manufacturing opens a whole new realm of possibilities. Therefore, the work presented here represents in fact the first brick towards a numerical tool, aimed to create an interface between all the actors involved in an orthopedic surgery, from the prosthesis manufacturer to the clinician, to increase the success rate of such surgeries and provide the best care for the patient.

Bibliography

[1]   Image credit: drugs.com.

[2]   Image credit: Dutton's orthopeadic examination, evaluation and intervention, 3rd edition.

[3]   Image credit: hss.edu.

[4]   Image credit: academic.oup.com.

[5]   Image credit: larousse.fr,   socratic.org,   ice.uthscsa.edu, wikipedia.com.

[6]   Shigeru Tadano and Bijay Giri. X-ray diffraction as a promising tool to characterize bone nanocomposites. *Science and Technology of Advanced Materials*, 12(6):064708, December 2011.

[7]   Total hip replacement-orthoinfo - aaos.

[8]   Jorge S. Siopack and Harry E. Jergesen. Total hip arthroplasty. *Western journal of medicine*, 162(3):243, 1995.

[9]   Sandrine Colas. *Etude des déterminants de la survie prothétique des prothèses de hanche en France, à partir des données du SNIIRAM.* PhD Thesis, Université Paris-Saclay, 2017.

[10]   Gavan P. Duffy, Daniel J. Berry, Charles Rowland, and Miguel E. Cabanela. Primary uncemented total hip arthroplasty in patients <40

years old: 10- to 14-year results using first-generation proximally porous-coated implants. *The Journal of Arthroplasty*, 16(8):140–144, December 2001.

[11] Kristin Walker. Bone.

[12] KS Fernández and PA de Alarcón. Development of the hematopoietic system and disorders of hematopoiesis that present during infancy and early childhood. *Pediatric clinics of North America*, 60(6):1273–89, 2013.

[13] Máire E. Doyle and Suzanne M. Jan de Beur. The skeleton: Endocrine regulator of phosphate homeostasis. *Current Osteoporosis Reports*, 134(6):134–141, 2008.

[14] D. Harold Copp and S. S. Shim. The homeostatic function of bone as a mineral reservoir. *Oral Surgery, Oral Medicine, Oral Pathology and Oral Radiology*, 16(6):738–744, 1963.

[15] Biomechanics: Mechanical Properties of Living Tissues - Y. C. Fung - Google Livres.

[16] Diplom Physikerin Carolin Lukas. *Modeling the influence of bone mineralization and remodeling on the structure of bone*. PhD thesis, Humboldt-Universität zu Berlin, 2012.

[17] Anatomy and Physiology - Kevin T. Patton - Google Livres.

[18] Ramin Oftadeh, Miguel Perez-Viloria, Juan C. Villa-Camacho, Ashkan Vaziri, and Ara Nazarian. Biomechanics and mechanobiology of trabecular bone: a review. *Journal of biomechanical engineering*, 137(1):010802, 2015.

[19] Peter Augat and Sandra Schorlemmer. The role of cortical bone and its microstructure in bone strength. *Age and Ageing*, 35(suppl_2):ii27–ii31, September 2006.

[20] Tony M. Keaveny, Elise F. Morgan, Oscar C. Yeh, and others. Bone mechanics. *Standard handbook of biomedical engineering and design*, 8:1–8, 2003.

[21] J. Klein-Nulend, R.G. Bacabac, and M.G. Mullender. Mechanobiology of bone tissue. *Pathologie Biologie*, 53(10):576–580, December 2005.

[22] L.M. McNamara, J.C. Van der Linden, H. Weinans, and P.J. Prendergast. Stress-concentrating effect of resorption lacunae in trabecular bone. *Journal of Biomechanics*, 39(4):734–741, January 2006.

[23] Jenneke Klein-Nulend, Astrid D. Bakker, Rommel G. Bacabac, Aviral Vatsa, and Sheldon Weinbaum. Mechanosensation and transduction in osteocytes. *Bone*, 54(2):182–190, June 2013.

[24] Lachlan J. Smith, Jeffrey P. Schirer, and Nicola L. Fazzalari. The role of mineral content in determining the micromechanical properties of discrete trabecular bone remodeling packets. *Journal of Biomechanics*, 43(16):3144–3149, December 2010.

[25] Ch A. Engh, J. D. Bobyn, and Andrew H. Glassman. Porous-coated hip replacement. The factors governing bone ingrowth, stress shielding, and clinical results. *The Journal of bone and joint surgery. British volume*, 69(1):45–55, 1987.

[26] Reijo Lappalainen and Seppo Santavirta. Potential of coatings in total hip replacement. *Clinical Orthopaedics and Related Research*, 430:72–79, 2007.

[27] Paul J. Harwood and David O. Ferguson. (ii) An update on fracture healing and non-union. *Orthopaedics and Trauma*, 29(4):228–242, 2015.

[28] John E. Davies. Understanding peri-implant endosseous healing. *Journal of dental education*, 67(8):932–949, 2003.

[29] Amreena Gill and PolsaniLaxman Rao. Primary stability: The password of implant integration. *Journal of Dental Implants*, 2(2):103, 2012.

[30] Domizio Suva, Anne Lübekke, François Pagano, Romain Dayer, and Pierre Hoffmeyer. Luxation d'une arthroplastie totale de la hanche

: étiologie et prise en charge. *Revue Médicale Suisse*, 5:2544–2550, 2009.

[31] Mikael Sundfeldt, Lars V Carlsson, Carina B Johansson, Peter Thomsen, and Christina Gretzer. Aseptic loosening, not only a question of wear: A review of different theories. *Acta Orthopaedica*, 77(2):177–197, January 2006.

[32] Yousef Abu-Amer, Isra Darwech, and John C. Clohisy. Aseptic loosening of total joint replacements: mechanisms underlying osteolysis and potential therapies. *Arthritis research & therapy*, 9(1):S6, 2007.

[33] Ehsan Askari, Paulo Flores, Danè Dabirrahmani, and Richard Appleyard. A review of squeaking in ceramic total hip prostheses. *Tribology International*, 93:239–256, January 2016.

[34] Stephen M. Tai, Selin Munir, William L. Walter, Simon J. Pearce, William K. Walter, and Bernard A. Zicat. Squeaking in Large Diameter Ceramic-on-Ceramic Bearings in Total Hip Arthroplasty. *The Journal of Arthroplasty*, 30(2):282–285, February 2015.

[35] Ondrej Jirousek. Nanoindentation of human trabecular bone – tissue mechanical properties compared to standard engineering test methods. In Jiri Nemecek, editor, *Nanoindentation in Materials Science*. InTech, October 2012.

[36] Gladius Lewis and Jeffry S. Nyman. The use of nanoindentation for characterizing the properties of mineralized hard tissue: State-of-the-art review. *Journal of Biomedical Materials Research*, 87B(1):286–301, April 2008.

[37] P. K. Zysset. Indentation of bone tissue: a short review. *Osteoporosis International*, 20(6):1049–1055, June 2009.

[38] Jae-Young Rho, Liisa Kuhn-Spearing, and Peter Zioupos. Mechanical properties and the hierarchical structure of bone. *Medical Engineering & Physics*, 20(2):92–102, March 1998.

[39] B. Viswanath, R. Raghavan, U. Ramamurty, and N. Ravishankar. Mechanical properties and anisotropy in hydroxyapatite single crystals. *Scripta Materialia*, 57(4):361–364, August 2007.

[40] Saeed Saber-Samandari and Kārlis A. Gross. Micromechanical properties of single crystal hydroxyapatite by nanoindentation. *Acta Biomaterialia*, 5(6):2206–2212, July 2009.

[41] J.D. Almer and S.R. Stock. Micromechanical response of mineral and collagen phases in bone. *Journal of Structural Biology*, 157(2):365–370, February 2007.

[42] C. Edward Hoffler. An Application of Nanoindentation Technique to Measure Bone Tissue Lamellae Properties. *Journal of Biomechanical Engineering*, 127(7):1046, August 2005.

[43] Sabine Bensamoun, Zaifeng Fan, Ilharreborde Brice, Jae Young Rho, and Marie-Christine Ho Ba Tho. Assessment of mechanical properties of human osteon lamellae exhibiting various degrees of mineralization by nanoindentation. *Journal of Musculoskeletal Research*, 11(03):135–143, September 2008.

[44] Philippe K Zysset, X Edward Guo, C Edward Hoffler, Kristin E Moore, and Steven A Goldstein. Elastic modulus and hardness of cortical and trabecular bone lamellae measured by nanoindentation in the human femur. *Journal of Biomechanics*, 32(10):1005–1012, October 1999.

[45] C.E. Hoffler, K.E. Moore, K. Kozloff, P.K. Zysset, M.B. Brown, and S.A. Goldstein. Heterogeneity of bone lamellar-level elastic moduli. *Bone*, 26(6):603–609, June 2000.

[46] Donald T. Reilly, Albert H. Burstein, and Victor H. Frankel. The elastic modulus for bone. *Journal of Biomechanics*, 7(3):271–275, May 1974.

[47] Simin Li, Emrah Demirci, and Vadim V. Silberschmidt. Variability and anisotropy of mechanical behavior of cortical bone in tension

and compression. *Journal of the Mechanical Behavior of Biomedical Materials*, 21:109–120, May 2013.

[48] Franco Marinozzi, Andrea Marinozzi, Fabiano Bini, Francesca Zuppante, Raffaella Pecci, and Rossella Bedini. Variability of morphometric parameters of human trabecular tissue from coxo-arthritis and osteoporotic samples. *Annali dell'Istituto Superiore di Sanità*, (1), March 2012.

[49] Franco Marinozzi, Fabiano Bini, and Andrea Marinozzi. Evidence of entropic elasticity of human bone trabeculae at low strains. *Journal of Biomechanics*, 44(5):988–991, March 2011.

[50] Franco Marinozzi, Fabiano Bini, Alessandro Quintino, Massimo Corcione, and Andrea Marinozzi. Experimental Study of Diffusion Coefficients of Water through the Collagen: Apatite Porosity in Human Trabecular Bone Tissue. *BioMed Research International*, 2014:1–8, 2014.

[51] C. H. Turner and D. B. Burr. Basic biomechanical measurements of bone: a tutorial. *Bone*, 14(4):595–608, 1993.

[52] D. R. Carter and W. C. Hayes. Fatigue life of compact-bone-i. effects of stress amplitude, temperature and density. *Journal of Biomechanics*, 9(1):595–608, 1993.

[53] M. Pithioux, P. Lasaygues, and P. Chabrand. An alternative ultrasonic method for measuring the elastic properties of cortical bone. *Journal of Biomechanics*, 35(7):961–968, July 2002.

[54] X Neil Dong and X Edward Guo. The dependence of transversely isotropic elasticity of human femoral cortical bone on porosity. *Journal of Biomechanics*, 37(8):1281–1287, August 2004.

[55] Ziheng Wu, Timothy C. Ovaert, and Glen L. Niebur. Viscoelastic properties of human cortical bone tissue depend on gender and elastic modulus. *Journal of Orthopaedic Research*, 30(5):639–699, May 2012.

[56] Zaifen Fan and Jae-Young Rho. Effects of viscoelasticity and time-dependent plasticity on nanoindentation measurements of human cortical bone. *Journal of Biomedical Materials Research Part A*, 67A(1):208–214, September 2003.

[57] Naoki Sasaki and Atsushi Enyo. Viscoelastic properties of bone as a function of water content. *Journal of Biomechanics*, 28(7):809–815, July 1995.

[58] Elijah Garner, Roderic Lakes, Taeyong Lee, Colby Swan, and Richard Brand. Viscoelastic Dissipation in Compact Bone: Implications for Stress-Induced Fluid Flow in Bone. *Journal of Biomechanical Engineering*, 122(2):166, 2000.

[59] Stephen C. Cowin. Bone poroelasticity. *Journal of biomechanics*, 32(3):217–238, 1999.

[60] Melissa L Knothe Tate. "Whither flows the fluid in bone?" An osteocyte's perspective. *Journal of Biomechanics*, 36(10):1409–1424, October 2003.

[61] Theo H. Smit, Jacques M. Huyghe, and Stephen C. Cowin. Estimation of the poroelastic parameters of cortical bone. *Journal of biomechanics*, 35(6):829–835, 2002.

[62] W. J Parnell and Q. Grimal. The influence of mesoscale porosity on cortical bone anisotropy. Investigations via asymptotic homogenization. *Journal of The Royal Society Interface*, 6(30):97–109, January 2009.

[63] Etienne Malachanne, David Dureisseix, Patrick Canadas, and Franck Jourdan. Experimental and numerical identification of cortical bone permeability. *Journal of Biomechanics*, 41(1):721–725, 2008.

[64] Dajun Zhang, Sheldon Weinbaum, and Stephen C Cowin. On the calculation of bone pore water pressure due to mechanical loading. *International Journal of Solids Structures*, 35(34-35):4981–4997, 1998.

[65] Vittorio Sansalone, Joanna Kaiser, Salah Naili, and Thibault Lemaire. Interstitial fluid flow within bone canaliculi and electro-chemo-mechanical features of the canalicular milieu: A multi-parametric sensitivity analysis. *Biomechanics and Modeling in Mechanobiology*, 12(3):533–553, June 2013.

[66] T. Lemaire, E. Capiez-Lernout, J. Kaiser, S. Naili, and V. Sansalone. What is the importance of multiphysical phenomena in bone re-modelling signals expression? A multiscale perspective. *Journal of the Mechanical Behavior of Biomedical Materials*, 4(6):909–920, August 2011.

[67] Maurice A. Biot. General Theory of Three-Dimensional Consolidation. *Journal of Applied Physics*, 12(155), 1941.

[68] Maurice A. Biot. Theory of propagation of elastic waves in a fluid-saturated porous solid. II. Higher frequency range. *The Journal of the acoustical Society of america*, 28(2):179–191, 1956.

[69] R. De Boer. Highlights in the historical development of the porous media theory: toward a consistent macroscopic theory. *Applied Mechanics Review*, 49(-):201–262, 1996.

[70] Rodney Hill. Elastic properties of reinforced solids: some theoretical principles. *Journal of the Mechanics and Physics of Solids*, 11(5):357–372, 1963.

[71] RM Bowen. Theory of mixtures. *Continuum Physics, Vol. III, Mixture and EM Field Theories*, -(-):1–127, 1976.

[72] Stephen C. Cowin and Luis Cardoso. Mixture theory-based poroelasticity as a model of interstitial tissue growth. *Mechanics of Materials*, 44:47–57, January 2012.

[73] Stefan Scheiner, Peter Pivonka, and Christian Hellmich. Poromicromechanics reveals that physiological bone strains induce osteocyte-stimulating lacunar pressure. *Biomechanics and Modeling in Mechanobiology*, 15(1):9–28, February 2016.

[74] Joseph D. Gardinier, Chris W. Townend, Kei-Peng Jen, Qianhong Wu, Randall L. Duncan, and Liyun Wang. In situ permeability measurement of the mammalian lacunar–canalicular system. *Bone*, 46(4):1075–1081, April 2010.

[75] E. Rohan, S. Naili, R. Cimrman, and T. Lemaire. Multiscale modeling of a fluid saturated medium with double porosity: Relevance to the compact bone. *Journal of the Mechanics and Physics of Solids*, 60(5):857–881, May 2012.

[76] J.M. Crolet, B. Aoubiza, and A. Meunier. Compact bone: Numerical simulation of mechanical characteristics. *Journal of Biomechanics*, 26(6):677–687, June 1993.

[77] C. Hellmich and F. Ulm. Microporodynamics of bones: Prediction of the "frenkel–biot" slow compressional wave. *Journal of Engineering Mechanics*, 131(9), 2005.

[78] C. Hellmich, D. Celundova, and F. Ulm. Multiporoelasticity of hierarchically structured materials: Micromechanical foundations and application to bone. *Journal of Engineering Mechanics*, 135(5), 2009.

[79] C. Morin and C. Hellmich. A multiscale poromicromechanical approach to wave propagation and attenuation in bone. *Journal of Engineering Mechanics*, 54(5):1251–1269, 2014.

[80] V. I. Arnold. *Geometrical Methods in the Theory of Ordinary Differential Equations.* Springer edition, 1988.

[81] Alain Bensoussan, Jacques-Louis Lions, and George Papanicolaou. *Asymptotic Analysis for Periodic Structures.* Elsevier edition, 1978.

[82] G A. Pavliotis and A. M. Stuart. *Multiscale Methods: Averaging and Homogenization.* Springer edition, 2007.

[83] Sanchez-Palencia E. General introduction to asymptotic methods. *Homogenization Techniques for Composite Media. Lecture Notes in Physics*, 272(-):–, 1987.

[84] J. L. Auriault and D. Caillerie. Quelques remarques sur les méthodes d'homogénéisation. *Revue Française de géotechnique*, -(49):43–50, 1989.

[85] A. Zaoui. Continuum micromechanics: Survey. *Journal of Engineering Mechanics*, 128(8):808–816, 2002.

[86] L. Dormieux, Molinari A., and D. Kondo. Micromechanical approach to the behavior of poroelastic materials. *Journal of the Mechanics and Physics of Solids*, 50(10):2203–2231, 2002.

[87] M.M. Ameen, R.H.J. Peerlings, and M.G.D. Geers. A quantitative assessment of the scale separation limits of classical and higher-order asymptotic homogenization. *European Journal of Mechanics - A/Solids*, 71:89–100, September 2018.

[88] Ekkehart Kröner, editor. *Statistical Continuum Mechanics*, volume 0. Springer Vienna, 1971.

[89] Henri Darcy. Les fontaines publiques de la ville de Dijon: Détermination des lois d'écoulement de l'eau à travers le sable., 1856.

[90] Didier Lasseux and Francisco J. Valdés-Parada. On the developments of Darcy's law to include inertial and slip effects. *Comptes Rendus Mécanique*, 345(9):660–669, September 2017.

[91] Donald A. Nield and Adrian Bejan. Mechanics of Fluid Flow Through a Porous Medium. In *Convection in Porous Media*, pages 1–35. Springer, 2017.

[92] H. C. Brinkman. A calculation of the viscous force exerted by a flowing fluid on a dense swarm of particles. *Flow, Turbulence and Combustion*, 1(1):27, 1949.

[93] W. S. Almalki and M. H. Hamdan. Investigations in Effective Viscosity of Fluid in a Porous Medium. *International Journal of Engineering Research and Applications*, 6(4):41–51, April 2016.

[94] K. Kusuzaki, N. Kageyama, H. Shinjo, H. Takeshita, H. Murata, S. Hashiguchi, T. Ashihara, and Y. Hirasawa. Development of bone canaliculi during bone repair. *Bone*, 27(5):655–659, 2000.

[95] W.-P. Breugem. The effective viscosity of a channel-type porous medium. *Physics of Fluids*, 19(10):103104, 2007.

[96] Haidong Liu, Prabhamani R. Patil, and Uichiro Narusawa. On Darcy-Brinkman Equation: Viscous Flow Between Two Parallel Plates Packed wit Regular Square Arrays of Cylinders. *Entropy*, 9:118–131, 2007.

[97] J.A. Kolodziej. Influence of the porosity of a porous medium on the effective viscosity in Brinkman's filtration equation. *Acta Mechanica*, 75(1-4):241–254, 1988.

[98] D. A. Nield. The limitations of the Brinkman-Forchheimer equation in modeling flow in a saturated porous medium and at an interface. *International Journal of Heat and Fluid Flow*, 12(3):269–272, 1991.

[99] Andrew Edward Anderson. Computational modeling of hip joint mechanics. page 222.

[100] G Bergmann, G Deuretzbacher, M Heller, F Graichen, A Rohlmann, J Strauss, and G.N Duda. Hip contact forces and gait patterns from routine activities. *Journal of Biomechanics*, 34(7):859–871, July 2001.

[101] Georg Bergmann, Alwina Bender, Jörn Dymke, Georg Duda, and Philipp Damm. Standardized Loads Acting in Hip Implants. *PLOS ONE*, 11(5):e0155612, May 2016.

[102] W. A. Hodge, R. S. Fijan, K. L. Carlson, R. G. Burgess, W. H. Harris, and R. W. Mann. Contact pressures in the human hip joint measured in vivo. *Proceedings of the National Academy of Sciences*, 83(9):2879–2883, 1986.

[103] Philipp Schneider, Matias Meier, Roger Wepf, and Ralph Müller. Towards quantitative 3d imaging of the osteocyte lacuno-canalicular network. *Bone*, 47(5):848–858, November 2010.

[104] Auckland K. Distribution of body fluids: local mechanisms guarding interstitial fluid volume. *Journal of Physiology*, 79(-):395–400, 1984.

[105] Jean-Louis Auriault, Claude Boutin, and Christian Geindreau, editors. *Homogenization of Coupled Phenomena in Heterogenous Media*, volume 0. Springer Vienna, 2009.

[106] George Elmer Forsythe and Wolfgang R Wasow, editors. *Finite-difference methods for partial differential equations.*, volume 0. NY: Wiley, 1960.

[107] L Debernard, L Robert, F Charleux, and Bensamoun S. Analysis of thigh muscle stiffness from childhood to adulthood using magnetic resonance elastography (mre) technique. *Clinical Biomechanics*, 26:836–840, September 2011.

[108] Emil H van Haaren, Babette C van der Zwaard, Albert J van der Veen, Ide C Heyligers, Paul IJM Wuisman, and Theo H Smit. Effect of long-term preservation on the mechanical properties of cortical bone in goats. *Acta Orthopaedica*, 79(5):708–716, January 2008.

[109] Bryan Kaye. The Effects of Freezing on the Mechanical Properties of Bone. *The Open Bone Journal*, 4(1):14–19, June 2012.

FOLIO ADMINISTRATIF

THESE DE L'UNIVERSITE DE LYON OPEREE AU SEIN DE L'INSA LYON

NOM : PERRIN   DATE de SOUTENANCE : 10/12/2018

Prénoms : Eléonore

TITRE : Multiscale poroelastic modeling of bone

NATURE : Doctorat   Numéro d'ordre : AAAALYSEIXXXX

Ecole doctorale : MEGA (n°162)

Spécialité : Mécanique

RESUME :
Total Hip Arthroplasty is nowadays one of the most performed orthopedic surgery and is representing a major health and economic issue. Bone is a complex material showing a hierarchical and porous structure, but also a natural ability to remodel itself thanks to specific cells, which are sensitive to fluid flows. Based on these characteristics, a multiscale numerical model has been developed within this thesis in order to simulate the bone response under external mechanical solicitations. The developed model relies on the homogenization technique for periodic structures based on an asymptotic expansion. It simulates cortical bone as a homogeneous structure. The first application of the developed model is the case of the loading of a finite volume of bone, allowing for the determination of an equivalent poroelastic stiffness. Focusing on two extreme fluid boundary conditions (impermeable walls and atmospheric pressure), the analysis of the corresponding structural response provides an overview of the fluid contribution to the poroelastic behavior, impacting the stiffness of the considered material. To validate the developed model, both a numerical and an experimental validation are realized. The numerical validation consists in the variation of parameters such as material properties or boundary conditions to estimate the accuracy of the model tendencies. Regarding the experimental validation, a cubic trabecular bone sample, extracted from a human hip and put under a compressive load, has been used. Increasing the load applied on the top of the bone specimen, the displacement is extracted, allowing to computation of the equivalent strain-stress curve. The equivalent stiffness of the bone specimen calculated numerically is then compared with the one from the experiments. A good agreement between the curves attests the validity of the developed numerical model, accounting for both the solid matrix and fluid contributions.

MOTS-CLÉS : Bone modeling, homogenization technique, poroelasticity, multiscale modeling

Laboratoire (s) de recherche : LaMCoS (INSA-LYON) – DIMA (La Sapienza, University of Rome)

Directeur de thèse: Benyebka BOU-SAÏD, Francesco MASSI

Président de jury :

Composition du jury :

CHABRAND Patrick – Professeur – Université Aix-Marseille – Rapporteur
SANSALONE Vittorio – Professeur – Université Paris-Est – Rapporteur
CICONE Traian – Profesorul – Universitatea Politehnica Bucureşti – Examinateur
MEZIANE Anissa – Maître de Conférences – Université de Bordeaux – Examinatrice
BOU-SAÏD Benyebka – Professeur – INSA-LYON – Directeur de thèse
MASSI Francesco – Professore Associato – Università di Roma « La Sapienza » – Directeur de thèse